Master thesis : Multimodal analysis of the bone-tendon interface

Auteur : Benmoussa, Chahineze
Promoteur(s) : Ruffoni, Davide
Faculté : Faculté des Sciences appliquées
Diplôme : Master en ingénieur civil biomédical, à finalité spécialisée
Année académique : 2017-2018
URI/URL : http://hdl.handle.net/2268.2/5414

Master thesis

Nano-Scale Dynamic Mechanical Analysis of the Interface between Achilles Tendon and Calcaneus Bone in a rat model

MASTER BIOMEDICAL ENGINEERING

CHAHINEZE BENMOUSSA

Jury:

EPPE Gauthier
MALHERBE Cédric
GERIS Liesbet
DELAUNOIS Yann

Supervisor:

RUFFONI Davide

Graduation Studies conducted for obtaining the Master's degree in Biomedical Engineering in the Faculty of Applied Sciences - University of Liège

ACADEMIC YEAR 2017-2018

I. Abstract

Ensuring the transmission forces between muscles and bones with a low rate of failure, tendon-to-bone attachment called entheses have a crucial role in the musculoskeletal system. This complex biomaterial structure joins two dissimilar tissues having a Young's modulus mismatch of two orders of magnitude. Current research about entheses has been focused on the study of its structure and composition, much less have been done on the mechanical properties.

Despite their efficiency, medical issues can happen at entheses or surrounded tissues. Repair and healing after injuries are problematic in the long term, failure rate is high. This may be in part due to lack of knowledge about the heterogeneous mechanical properties of the tissue to be repaired.

This master thesis focus on nano-scale mechanical properties of the interface between Achilles' tendon and calcaneus bone. Histological investigations and dynamic mechanical analysis (DMA) based on nanoindentation were performed on rat models.

The histological pictures obtained after sample preparation at the CHU Liège reveal the well-aligned collagen fibres structure in tendons and interdigitations between tendon and bone at the insertion site. The gradient of collagen fibres alignment from tendon to bone is believed to absorb deformation energy. Interdigitation are believed to increase the surface contact, reducing local stress and increasing surface toughness.

Nanoindentation was performed to measure the mechanical properties of bone, cartilage, tendon, periosteal interface and enthesis interface. Due to their compliance and viscoelastic behaviour, soft tissues are not easily studied by this technique. The development of the sample preparation and DMA protocols took a big part of the master thesis. Indeed, the surface roughness of the samples must be lower than 10 $\%$ of indentation penetration depth. The roughness was measured by scanning probe microscopy using a Berkovich tip prior each indentation. The indentation was performed on the area having roughness lower than 30 nm^2. This was not possible when indenting tendon or the interfaces, as they always showed higher roughness. By using DMA, the impact of high roughness is expected to be reduced.

DMA use oscillating tip going deeper in the sample during the indentation. This technique allows to measure both elastic and viscoelastic properties as function of the tip penetration depth. Interestingly, elastic properties (storage modulus) decreased with indentation depth more in bone than in tendon. Conversely, viscoelastic properties (tan delta) were practically not influenced by depth.

Comparing the results obtained on bone, cartilage and tendon, the viscoelastic behaviour is gradually increasing when going from tendon to bone. The opposite was true for storage modulus which decreased from bone to tendon.

As hypothesised, periosteal interface has abrupt storage modulus transition in opposition to enthesis interface having gradual transition. This two closed but distinct regions have different functions. Periosteal fibrocartilage facilitates the sliding of the tendon on the bone surface. Enthesis allows a proper load transfer from the tendon to bone, and so gradual mechanical properties transition are present to reduce stress concentration and failure risks. Transition occurs in thicker area for entheses ($\sim$ 350 μm) than for periosteal interface ($\sim$ 100 μm).

II. Acknowledgements

The long and instructive journey that was Biomedical Engineering studies reach its end by this master thesis. From the University of Mons to the University of Liège, I have acquired the knowledge, the maturity and the willing to bring my contribution to the scientific and working world. All this would not have been possible without the support of several people that I would like to thank by these few words.

Foremost, I would first like to thank my professor and thesis advisor Dr. **Davide Ruffoni** for giving me the taste of Biomechanics. His door was always open to supervise and comment my work whenever it was necessary. He also taught me the use of the nanoindenter with a lot of patience and carefulness.

I would also like to thank Prof. **Philippe Compère** and his PhD student Mr. **Yann Delaunois** for their biological guidance in the sample preparation and the first supervision during the polishing. Without their expertise and input, the thesis would not have been successfully conducted.

In another hand, I would like to express my gratitude to Prof. **Alain Colige**, Ms. **Lola Vanoorschot** and Ms. **Aurore LECAT** for their histology education and trust in my work. Their support and enthusiasm make me feel comfortable and implicated in the analyses.

I would like to thank Prof. **Gauthier Eppe** and Prof. **Cédric Malherbe** for their time and the Raman spectroscopy theory explanations, the presentation of the equipment and their usage even if my thesis had followed another path that the one planned.

My best regards to Ms. **Laura Zorzetto** and Ms. **Cristina Gatti**, the two super Italian girls who gave me their knowledge, know-how and advice with the lab equipment and the experiments.

To Dr. **Luc Duwez**, Dr. **Jean-Paul Cheramy-Bien**, Dr. **Pierre Drion** and Dr. **Jean-Francois Kaux** for the sample supply with the respect of the Ethical Guidance.

A special thanks to the Prof. **Philippe Fortemps**, Head of Engineering Innovation Management Unit and Full Professor at the University of MONS, without whom engineering would still be a mystery to me. His listening and relevant advice gave me the force to continue my learning. Also, I would like to thank the Prof. **Liesbet Geris** who gave me the opportunity to continue my learning in a promising field.

Thank you **Arnaud Ega** for the long rereading night spent on all these pages. Thank you **BEST Liège** for all the smileys and laughs you gave me through your immeasurable kindness and fun, you are a real breath of fresh air between too many projects, lessons and exams. Work Hard, Play Harder!

Finally, I must express my very profound gratitude to my family and my dear friends **Théodore Di Pietro** and **Laure Piret-Gérard** for providing me with unfailing support and continuous encouragement throughout my years of study and through the process of researching and writing this thesis, in good as in the less good moments. No words can reveal how much you mean to me!

Contents

1. Introduction

Bone - soft tissue interfaces did not reveal all their secrets yet. Ensuring the forces transmission between muscles and bones with a low rate of failure, entheses have a crucial role in the musculoskeletal system. This complex biomaterial structure joins two dissimilar tissues having a Young's modulus mismatch of two orders of magnitude. Research about entheses has been focused on the study of its structure and composition. Much less have been done on the mechanical properties.

Even if the medical issues happen more on the surrounded tissues than on the entheses, the repair and healing are not correctly achieved. Understanding the organisation and the composition of this particular structure will help the regeneration and surgical attachment, but will also be a source of inspiration for biomimetic materials.

This master thesis, divided into five main chapters, focus on Achilles' tendon to bone insertion in rats. The first chapter is an overview of entheses, surrounded tissues and encountered clinical disorders. Short presentation of the techniques used to study the entheses and the main goals come next. The second chapter presents the sample preparation and methodology for histology and nanoindentation. Results are described in the next chapter, starting with histological pictures and interpretation, followed by the nanoindentation. The samples have been investigated by quasi-static and dynamic indentations on bone, cartilage, tendon and enthesis interface. Periosteal interface has also been studied by dynamic indentations. The fourth chapter discusses the results and limitations of our methods. The last chapter concludes this thesis by discussing the main results and giving indications for future works.

1.1 Entheses

The insertion area of soft tissue (tendon and ligament) into bone, called enthesis, is studied in this master thesis. This complex structure of composite biomaterials over a very small region of about 500 μm induces stress transfers between two dissimilar materials with different Young's modulus E: bone ($\sim$ 20 GPa) and soft tissue ($\sim$ 0.5-2 GPa) [1]. Entheses of tendons ensure the transmission of the contractile forces provided from the muscles to bones by compensating the differing elastic moduli between these two types of tissues. However, large gap between material properties creates stress concentration at the interface, increasing chances of failures under simple uniaxial loading. The study of this particular phenomenon with unexpected properties is clinically relevant and also inspiring for biomimetic purposes, even if the literature on entheses is not as abundant as for their surrounded materials (bones and soft tissues).

Bone

Bone composition, structure and functions have been investigated for years. The main functions of bone are motions and organs protection. The specific hierarchical structure, starting from protein matrix

reinforced by mineral crystals at nano-scale to collagen fibres assembly forming lamellae at macro-scale represented in the fig. 1.1, and the composition describe in the table 1.1 make bone stiff and though at the same time. Bone can be found under compact form (cortical, 80 % of the total skeletal mass) or spongy form (trabecular, 20%) depending on the porosity degree [2].

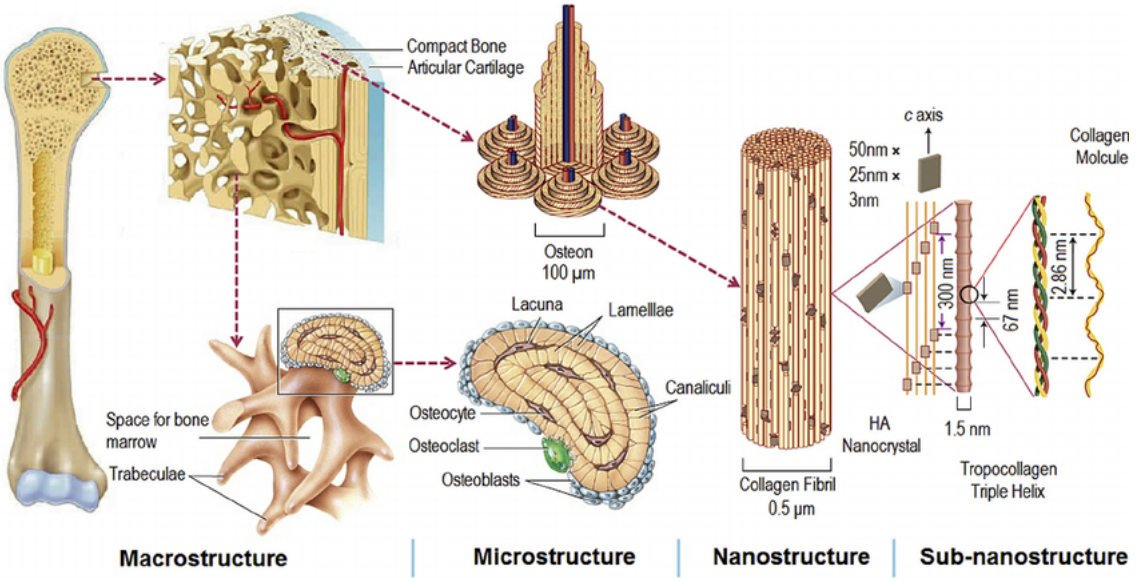

Figure 1.1: Cortical and Trabecular Bone hierarchical structure, showing the collagen fibres and mineral platelets organisation [3].

Phase	Composition	Roles
Inorganic (60%)	hydroxyapatite mineral platelets	rigidity and hardness
Organic (30%)	collagen fibres, proteins and cells	elasticity and toughness/ Ca and P source
Aqueous (10%)	Water	lubrication and viscoelastic properties

Table 1.1: This table resumes bone composition and functions according to their phase, express in relative weight amount [%]. Ca and P mean Calcium and Phosphorous.

Tendon and ligament

Soft tissues as tendons and ligaments are connective tissues joining the whole musculoskeletal system together by linking muscle to bone (tendon) or bone to bone (ligament). Tendons transmit efficiently muscular forces to the bones allowing bone motions. Ligaments provide joint stability, allowing or restricting specific motions.

Soft tissues are also well hierarchically structured with collagen fibrils at nano-scale and fascicles at milli-scale (fig. 1.2). The collagen fibrils are connected to each other by proteoglycans, allowing further tissue stretching by shear transmission. The tendon structure is similar to the ligament structure. The degree of alignment of fibrils and fascicles is close but not identical in the two soft tissues, the ligaments fibrils present more waviness than tendon fibrils. Also, in ligaments, the fascicles are not always parallel to the main orientation [2]. The soft tissues are mainly composed of water (65 % of wet weight), trapped in the proteoglycans matrix. The other components are presented in the table 1.2.

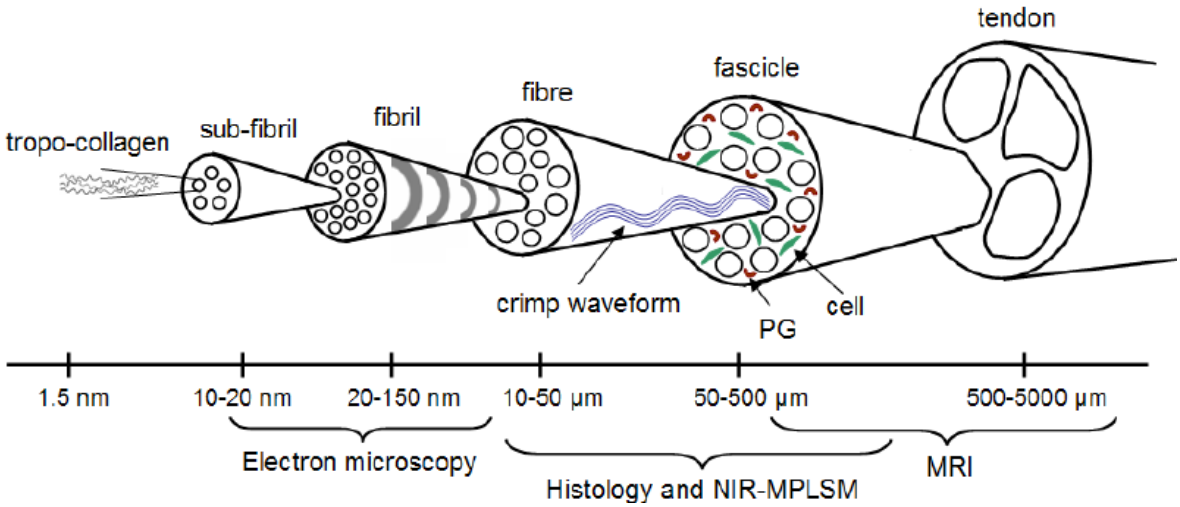

Figure 1.2: Tendon hierarchical structure, from tropo-collagen (1.5 nm diameter) to tendon (0.5-5 mm diameter) passing by fibre and fascicle [4].

.

Dry Composition	Collagen	Elastin	Proteoglycans and Glycoproteins
Tendon	75-85	1-3	1-2
Ligament	70-80	1-15	1-3

Table 1.2: Tendons and ligaments compositions expressed in relative $\%$ dry weight.

Cartilage

Cartilage is a tissue covering the ends of long bones, protecting bones at the joints by creating a sliding surface, friction and absorbing chocs. Three main types of cartilage are encountered: hyaline cartilage (covering joint surfaces), fibrocartilage (tendon/ligament to bone attachment and menisci) and elastic cartilage (nose tip, larynx). Cartilage structure, divided into 3 layers (fig. 1.3), is an avascular tissue looking like a sponge. It has 2 main phases: liquid (interstitial water and ions) and solid matrix. Cartilage is composed of 2-3 $\%$ chondrocytes, specific cartilage cells, and of 98 $\%$ extracellular matrix (table 1.3).

Composition	in relative $\%$ wet weight
Water	70-80
Collagen	10-20
Proteoglycan	4-7

Table 1.3: Extra-cellular cartilage matrix composition express in relative $\%$ wet weight [6].

Enthesis

Tendons, ligaments and bones can be found under different shapes and sizes in the body, thus as the entheses [7]. Entheses may be classified into two types: fibrous or fibrocartilaginous according to the tissue present at the skeletal attachment site [7].

- Fibrous entheses are attached directly or indirectly to the bone depending on the presence of periosteum. This membrane, composed of two layers, is a thin and dense vascular connective tissue enveloping the bones except at the surfaces of the joints. The two layers are: 1. Fibrous external layer with fibroblasts 2. Osteogenic internal layers with osteoblasts and Sharpey's fibres. This type

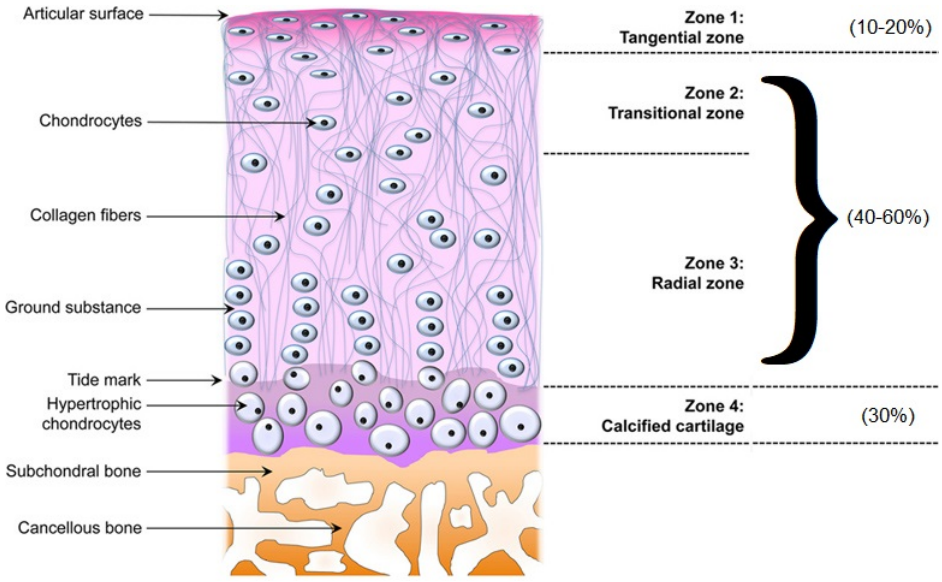

Figure 1.3: Cartilage composition and structure, which is divided into 3 mains zone: superficial tangential zone, middle zone and deep zone being respectively 10-20 , 40-60 and 30 % of the cross section. Adapted from [5].

of enthesis can be found at the deltoid tendon attachment to the humeral head. Periosteal fibrous enthesis can become a bony fibrous enthesis with age [7].

- Fibrocartilaginous entheses are directly attached to (un)calcified cartilage, without periosteum. This type of enthesis is more common with a gradual and continuous transition. This type of enthesis can be found in bony attachments of the femoral side of the medial collateral ligament and Achilles' tendon attachment to the calcaneus bone.

Fibrous entheses are composed of four zones:

Zone	Composition
I	Delicate connective tissue (ligament or tendon)
II	Densely-packed parallel collagen fibres
III	Loose connective tissue merging with the osteogenic layer of the cartilage or periosteum
IV	Bone

Table 1.4: Composition of the four fibrous entheses zones [7].

Fibrocartilaginous entheses are composed of four layers with several components described in the table 1.5.

Zone	Tissue	Main Components
I	Tendon/Ligaments	Fibroblasts, linearly arranged collagen type I
II	Uncalcified fibrocartilage	FCC, types I, II and III collagen, aggrecan
III	Calcified fibrocartilage	FCC, mineralized fibrocartilage, type II collagen, type X, aggrecan
IV	Bone	Osteoblasts, osteocytes, osteoclasts, mineralized type I collagen

Table 1.5: Specific components found in the four regions characterising the fibrocartilaginous entheses [8]. FCC means Fibrochondrocytes.

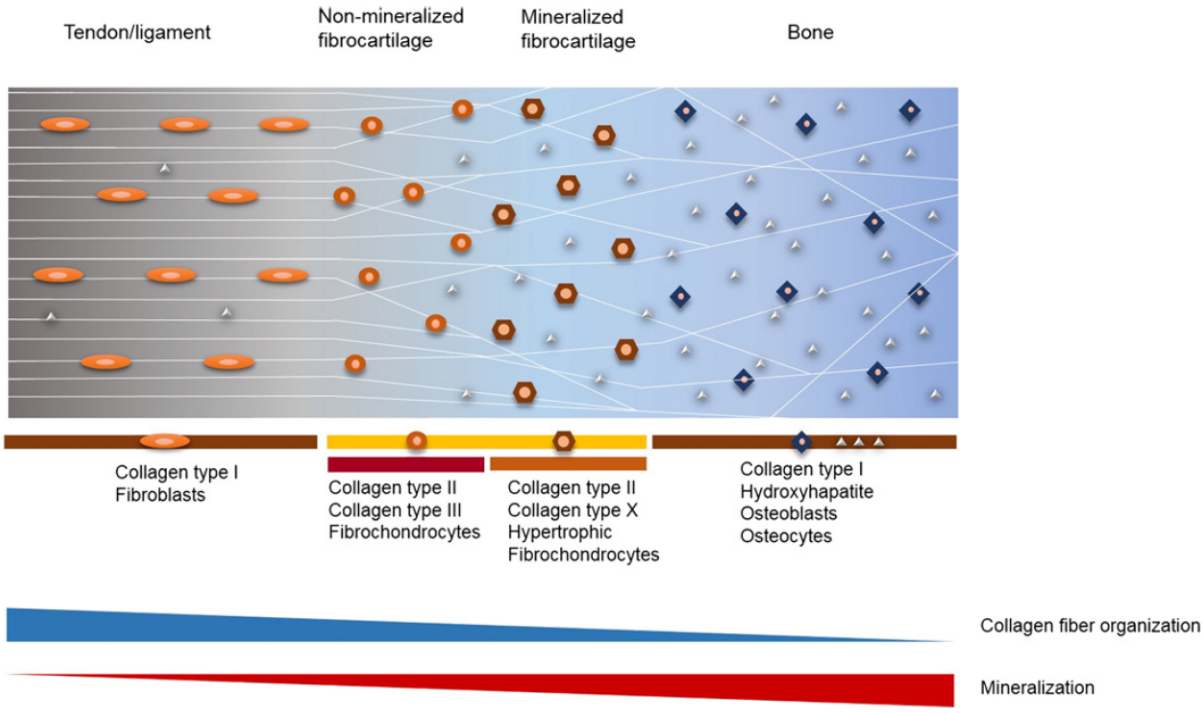

Figure 1.4: Structure and composition of fibrocartilaginous entheses. The four main zones are represented, with their components, collagen fibre organisation and mineralization gradient [9].

Histological investigations present the gradient in collagen orientation: the collagen fibres, well aligned to the main axis of the tendon, lose their organisation through the interface to finally be spread in several orientations in the bone. Such a decrease in orientation is believed to generate a local region at the interface being even more compliant than the tendon itself. This may act as an energy-absorbing layer [10]. 'Tidemark' has been also observed between the two fibrocartilage layers, being the calcification front. The tidemark shape seems to be wavy in order to increase the contact surface. The inspection of many entheses shows that tendons often slay out at their attachment sites to distribute forces on a greater area [7]. Moreover, histological studies point that the interfaces are not a flat surface. Interdigitations developed at the interface between the non-mineralized and the mineralized cartilage, leads to more stress than flat surface but increases surface toughness [8]. Other studies show a mineral gradation in the interface. Local mineral content produce stiffness transition between the two dissimilar tissues.

1.1.1 Achilles entheses

This thesis focus on Achilles entheses. We have decided to investigate only the insertion of Achilles' tendon into calcaneus bone by reason of limiting the movement complexity (fairly 1 degree of freedom).

Ankle anatomy includes several joints, bones, ligaments and tendons between the leg and the foot. Ankles play an important role in walking, running and jumping by allowing flexion of the foot, supporting body weight and providing balance, shock absorption, transferring ground reaction forces. The main bones of the ankle region are the tibia and fibula in the leg and the talus and calcaneus in the foot, represented on the fig. 1.5. Achilles' tendon attaches plantaris, gastrocnemius and soleus muscles into the posterior part of the calcaneus bone (heel bone) tuberosity. Achilles' tendon is the strongest and thickest tendon in the

body and is surrounded by a thin tissue, called the paratenon that allows the tendon to glide relatively to adjacent structures [11, 12].

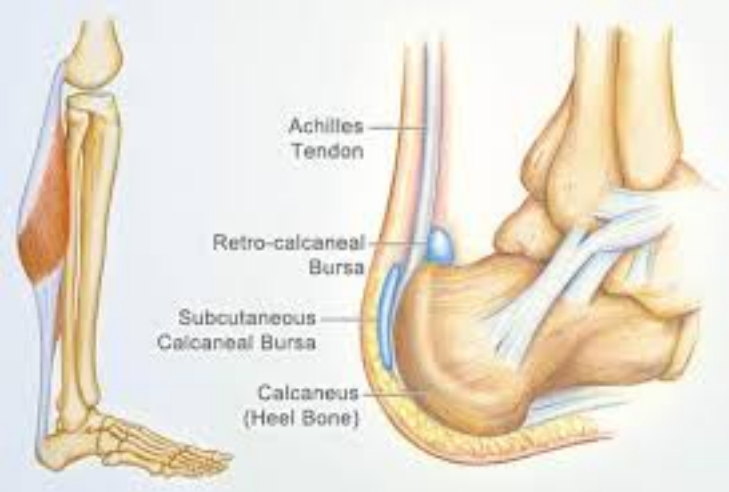

Figure 1.5: Ankle and Achilles' Tendon. The Achilles' tendon is attached to the back of the calcaneus bone [13].

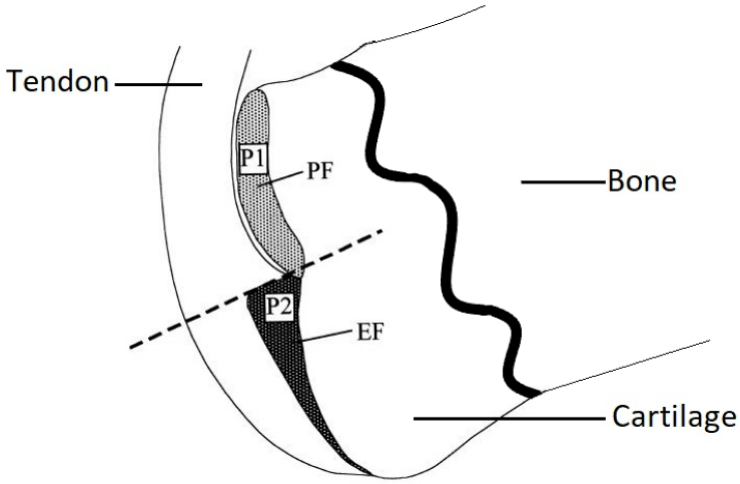

Figure 1.6: The Achilles' tendon in surrounded by bone, cartilage and tendon. The periosteal (PF) and enthesis (EF) fibrocartilage are hypothesised to act as two pulleys in series. EF protect the interface itself and PF protect the Achilles' tendon from friction with the calcaneus bone. Adapted picture from [14].

Two types of cartilage are found at the enthesis: periosteal cartilage and fibrocartilage. These two closed regions are known to have completely different biomechanical function and we assumed they will show different mechanical properties. The transition should be smooth for fibrocartilage entheses to decrease stress concentration. This feature may not be seen at the periosteal interface.

Anatomical and histological features of human and rat ankle joints are comparable, even if rats are quadrupeds. Rats use the same main solicitation during their gaits: ankle flexion [15].

1.1.2 Clinical disorders at entheses

As explained before, entheses are the junction between bone and soft tissue, having mismatch mechanical properties. Despite two orders of magnitude contrast in Young's modulus, entheses show an unexpected durability and can bear loads equivalent to multiples of the body weight as well as changes in the angle of the force application occurring over a broad range. The main role of the entheses is to dissipate stress away from the interface [7]. The four-zone structure create a gradient of mechanical stiffness that avoids traumatic injury, reducing the concentration of stress at the interface. The low number of injuries at the interface shows the efficacy of this structure, the failures happen more in bones or soft tissues [16].

Unfortunately, disruptions sometimes occur due to overload or injury. The entire enthesis, in particular the fibrocartilage, is characterized by the absence of blood vessels leading to a poor healing process. Disorders at entheses (enthesopathies) occur in conditions such as diffuse idiopathic skeletal hyperostosis (bone abnormally thick created by the periosteum overactivity) and the seronegative spondyloarthropathies (the patients have no antibodies in the blood serum, which lead to inflammatory rheumatism) [7]. Numerous common orthopaedic injuries require the repair of a ruptured tendon or ligament to its bony insertion. Depending on the severity of the injury and the age of the patient, 20–94% of repaired rotator cuff tears fail [8]. The current healing technique is to juxtapose tendon and bone. Regrettably, this juxtaposition creates a fibrovascular scar tissue rather than regeneration of a graded brocartilaginous transition, compromising the graft stability and long-term clinical results. The development of equivalent artificial tissues with the mechanical properties transition is difficult to produce. Cells feel the stiffness of the underlying and surrounding material and use this information to differentiate and grow in the preferred direction [17]. The reproduction of this ability is not achieved yet.

Lack of knowledge in this field makes them difficult to heal with a permanent solution. These clinical issues may be overcome with enough expertise of healthy enthesis composition, structure and natural healing process. They are also commonly seen as sporting injuries such as tennis elbow and jumper's knee. Also, bone avulsions (when a part of the bone is removed because of the tension) or tendon ruptures occur instead of enthesis failure.

Current approaches for interface regeneration include tissue engineering techniques, using cells, growth factors, biomaterials scaffold and mechanical stimuli to induce enthesis regeneration [8]. However, this approach is challenging because of the complex structural and cellular composition of the native interface [9]. No current solution has been highlighted to control the mineral distribution within the biomaterial or to induce gradient in orientation of the collagen fibres. Moreover, the biomaterial scaffold must have interdigitations at the interfaces, which increase the contact surface and reduce stress concentrations [14].

1.2 Histology

Histology, or microscopic anatomy, is the study of biological cells or tissues from a structural point of view. The structure and function of tissues are visualized with an optical or electron microscope. The reliability of the results depends on the preparation of high-quality samples. Histology is used as a diagnostic tool in clinical medicine and as descriptive tools in research.

Depending on the studied tissues and the final objective, the methodology varies. The samples are fixed to avoid tissues degeneration with chemical components. Samples containing bone are firstly decalcified in order to obtain good quality sections for observation under the microscope [18]. The difference in hardness in the sample leads to increase the difficulty of having a proper cut. The samples are dehydrated with several alcoholics baths and saturated with wax or resin substance before being embedded into a block. Theses substances are used to facilitate the cutting at room temperature without denaturation of the tissues. Paraffin embedding is the most used one. The block is sliced with a microtome to obtain slices thin enough to be visualized by the microscope, having one single layer of cells. The slices are mounted on a clean wet glass and dried. They are treated to dissolve the paraffin, stained with specific dyes depending on the tissues components and prepared for the microscope [19].

Fixing and Sectioning

To prevent the degradation of the nature and the morphology of tissues, the samples are fixed by several chemical components derived from aldehydes. The aldehyde group reacts covalently with amino groups and creates cross-link in proteins. The most widely used fixative for light microscopy is 4 $\%$ formaldehyde (formalin) to be compatible with the main dye used (haematoxylin and eosin, H&E stain) [20]. Fixation maintain tissue structure well but breaks amino groups. To avoid the total loss of secondary structure in proteins, alcohol is used to stop the fixation and do the dehydration progressively. This step induce small changes into the structure. If the sample is mineralized, decalcification is done with acids (for dense cortical bone) or ethylene diamine tetra-acetic acid (EDTA, for small amounts of calcium on the surfaces), before the dehydration with alcoholic baths, to ensure the good embedding and sectioning procedures. The decalcification is a critical step depending on the used solutions and at the time. Under-decalcification may induce tearing of the tendon at the insertion site during the cutting. Over-decalcification may cause an absence of nuclear staining.

The samples are cut in thin layers of typically 5 μm thick for light microscopy and 80-100 nm thick for electron microscopy. This is necessary to allow the light of a microscope to pass through the sample and have a net image without a mix of superimposed layers of cells.

To preserve the shape and the structure of theses sections, tissue sample must be supported in a hard matrix, so they are embedded in paraffin (light) or resin (electron) before being cut with a microtome or a diamond knife respectively. Since these components are immiscible with water, a medium is essential. The sample is dehydrated by removing progressively the water with alcohol (ethanol often), then it is removed by a hydrophobic medium (xylene) and the medium is substituted by the molten paraffin or resin during the infiltration of the sample.

The final step of fixation is the external embedding. The sample is placed in the liquid embedding material and is then hardened by cooling at room temperature. Hard blocks containing the sample is ready to cut with a blade in microtome. The cutting orientation can be chosen, vertical sectioning is the common used. The slices are mounted on a microscope slide.

Staining

Staining is employed to give both contrast to the tissue as well as highlighting particular features of interest. H&E stain are the most commonly used light microscopical stain in histology. Haematoxylin, a basic dye, stain nuclei blue due to an affinity to nucleic acids in the cell nucleus; eosin, an acidic dye, stains the cytoplasm pink. H&E-stained section is examined first, before deciding whether additional tests or staining procedures is required. The stained slices mounted on glass slide are then prepared to be visualised by the microscope with the goal of analysing the pictures.

1.3 Nanoindentation

Nanoindentation is a technique developed in the 1970s widely used to measure surface properties [21]. The size of the indenter probe being very small (few microns) allow property measurements at micro- and nano-scale, perfect for surface characterisation. This technique allows investigations of mechanical properties. Since this is surface properties measurements, the sample surface must be exposed, clean and with a correct low roughness [22].

Embedding & Polishing

Common sample preparation for nanoindentation includes dehydration and resin embedding to facilitate the manipulation. Epoxy or PMMA resin is mainly used for their easy of use, their good physical adherence, their mechanical properties and their conservation conditions. However, the resin must be conserved and prepared in good conditions. Indeed, the resin must always be at room temperature (never below 18 °C), otherwise the resin does not polymerise properly. Also, the homogeneity of the pure resin hardener mix must be obtained by vigorous agitation but without being too violent otherwise stress can modify the reticulation and air bubbles are trapped in the embedding material. The room humidity and mix proportion have consequence as well, having too much humidity, too much or too less hardener in the mix induce issues during the curing, resulting to glue-like viscous liquid [23].

The surface roughness is a critical parameter in indentation. In order to obtain smooth and flat surfaces, with minimal damages on the sample, two main techniques are used: polishing or microtome cut. Several studies used silicon abrasive papers and polishing suspension to obtain proper roughness [24, 25, 26, 27]. This paper type is often used for soft polymers or biological samples to remove the superficial material without producing a big deformation in the sample itself.

Interesting, the embedded samples must be studied without significant delay after their preparation. Indeed, Gibson and al. demonstrate that, after 6 months of storage, the elastic modulus of the embedded tissue may increase significantly, whereas the hardness appears to be less affected by increased storage time [21].

Another method to reduce the surface roughness is to cut the sample by a microtome. This instrument use glass, sapphire or diamond blade producing samples slice of a thickness about 50 nm to 100 μm. However, glass blades do not suit to cut bones. Several microtome types are available in the market:

sledge, rotary, vibrating microtome or even cryomicrotome. Xu and al. show that microtome sectioning have flattered surface and create less damage than polishing samples [28].

Scanning Probe Microscopy (SPM)

SPM is an imaging technique using a sharp tip to raster scan a surface. The SPM family is very diverse, with different methods specialising in different surface properties. The two most commonly used techniques scanning tunnelling microscopy, using tunnelling voltage, and scanning force microscopy, using contact force [29]. Several scanning modes are available: Forward scanning, Reverse scanning or Forward and Reverse scanning. The last one has the particularity to evaluate the surface modification during the scanning. Indeed, these two scanning lines must be identically to represent their passages. If they are not, this shows that the tip motion deteriorates the surface.

The recorded values are displayed as a heat map (usually black and white or orange colour scale), creating a roughness evaluation picture. These data are important to validate the quality of the surface roughness in order to accept the indentation.

Indentation

Nanoindentation is a technique able to measure several mechanical properties at micro- and nano-scale as the elastic modulus and the hardness. During the nanoindentation test, the probe is driven into the sample surface and then withdrawn, a defined function to extract material properties, recording both depth of penetration and applied loads. The most used model is the method developed by Oliver and Pharr (1992) [30]. This model determine the mechanical properties with these two information and the geometry of the tip. It is based on four simplifying assumptions:

1. perfect geometry of the indenter
2. negligible adhesive and frictional forces
3. specimen is treated as infinite half-space
4. material is linear elastic, isotropic and incompressible

The tip projected contact area ,which describes the contact area of the tip at a specific contact depth is defined by the following equation:

$$A = C_0 \, h_c^2 \tag{1.1}$$

where C_0 is a constant depending on the tip type and h_c is the contact depth represented on the fig. 1.7.

The contact depth can be found with:

$$h_c = h_{max} - \mathcal{E} \, \frac{P_{max}}{S} \tag{1.2}$$

where h_{max} is the Maximal Depth reached during the test, P_{max} the Maximal Load, S the Stiffness of the unloading curve. $\mathcal{E}$ is a constant factor equal to 0.75 accounting the deflection of the surface at the contact perimeter. The value of the contact depth is between the final depth and the maximal depth.

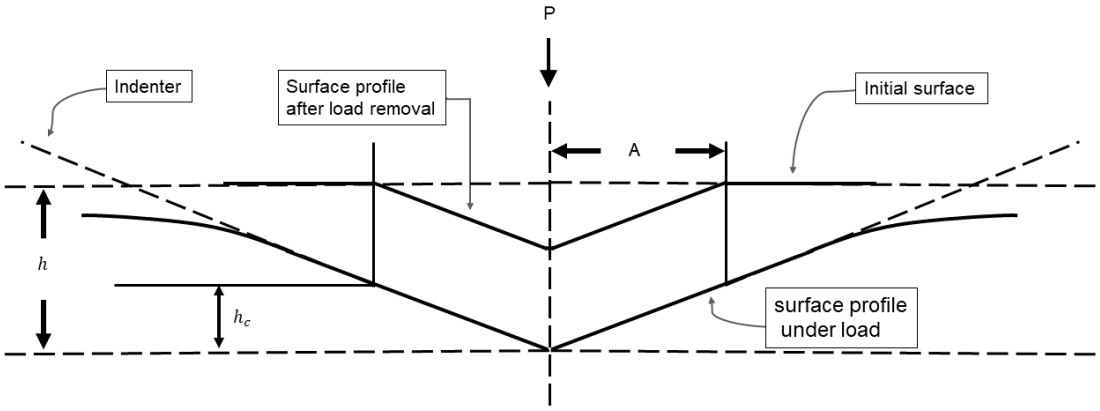

Figure 1.7: Schematic of tip surface contact during the indentation, taken from [31].

Different probe tip geometries are used in indentation, from sharp to spherical tip, depending on mechanical aspects investigated. Sharp tips are often used to analyse elastic properties for dehydrated, highly mineralized tissues such as bone and calcified cartilage or metals. Spherical tips are useful for viscoelastic properties research of soft tissues and polymers. Tips are mainly made out of very stiff materials, such as diamond or sapphire [32]. The tip cleanness is not negligible. Indeed, debris collection on the tip modify the projected contact area, the contact depth and may influence the measured forces and so the deduced property values.

As the projected contact area plays an important role in the mechanical properties computing, it must be determined accurately. Standard nanoindentation testing procedures relies on a known tip area function, A_c. The contact area calibration is effected by the production of several quasi-static indents by applying a varying load, and so a varying contact depth, to the material with known reduced modulus (typically, fused quartz). The Stiffness calculated from the unloading curve is used to determine the indent area by the following relationship [33]:

$$A_c = \frac{\pi \ S^2}{4 \ \beta^2 \ E_r^2} \tag{1.3}$$

Where β is a geometric constant with a value that is close to 1. The series of $A_c(h_c)$ are fitted to the polynomial form:

$$A_c = C_0 \ h_c^2 + C_1 \ h_c + C_2 \ h_c^{1/2} + C_3 \ h_c^{1/4} + C_4 \ h_c^{1/6} + ... \tag{1.4}$$

The C_i constant values depend on the tip type. This relationship represent ideal and perfectly sharp tip, and may deviate with time and use. Since h_c are really small, this expression can be approximate with the equation 4.1 .

The Stiffness is represented by the following relationship and schematise on the fig. 1.8. This is the initial slope of the unload-displacement curve:

$$S = \frac{dP}{dh} \tag{1.5}$$

With these parameters from load-displacement curves and tip geometry, quasi-static nanoindentation

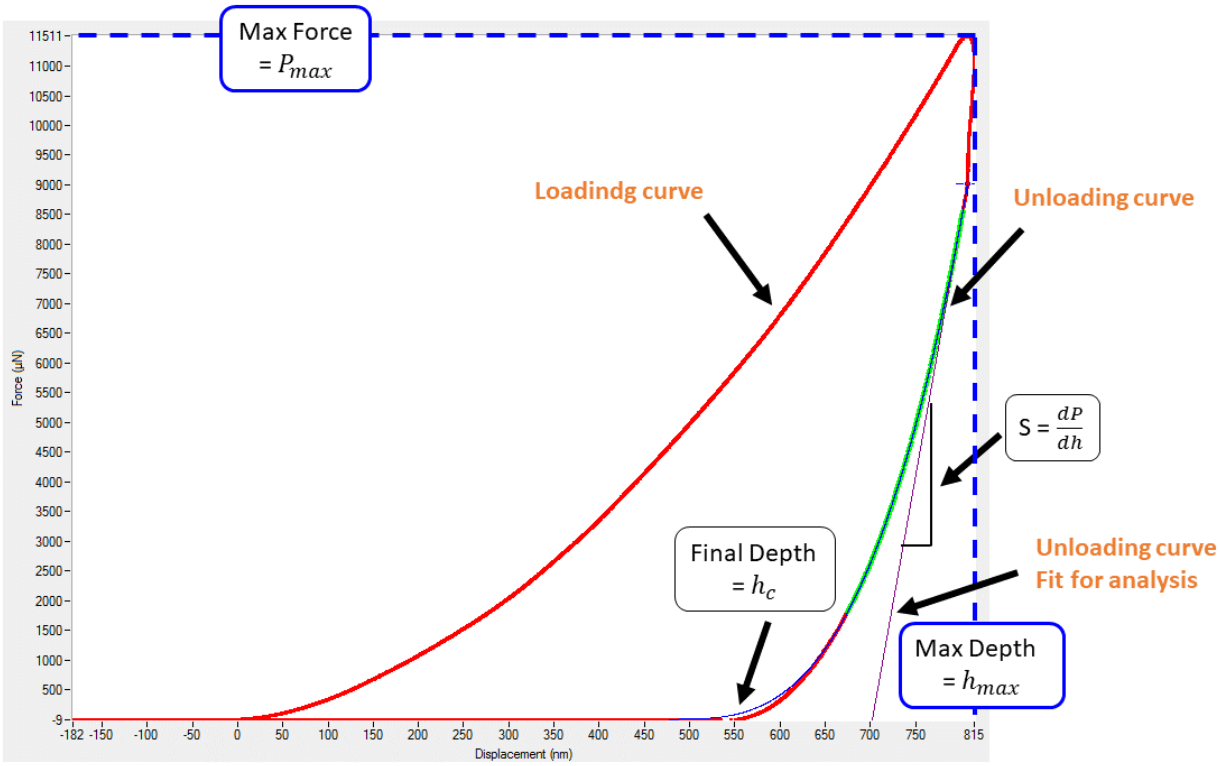

Figure 1.8: Schematic of loading-unloading indentation cycle with recorded parameters.

measure Elastic modulus E and Hardness H. The Reduce modulus E_r, representing the elastic deformation that occurs in both sample and indenter tip, is related to the Elastic modulus E_{sample}, the elastic deformation resistance of a material , with:

$$\frac{1}{E_r} = \frac{1-\nu_{sample}^2}{E_{sample}} + \frac{1-\nu_{indenter}^2}{E_{indenter}} \tag{1.6}$$

where ν is Poisson's ration, varying from 0 to 0.5 for most materials. For diamond indenters probe as ours, $E_{indenter}$ is 1140 GPa and $\nu_{indenter}$ is 0.07.

The Reduce modulus is defined as:

$$E_r = \frac{S}{2}\sqrt{\frac{\pi}{A(h_c)}} \tag{1.7}$$

The Hardness, measurement of material's strength by the ability to resist a localized plastic deformation, can also be determined by the analysis of the unload curve by this equation:

$$H = \frac{P_{max}}{A} \tag{1.8}$$

In some cases, reversible plastic deformation, creep, and viscoelasticity can make the extraction of elastic moduli very problematic [33]. Nanoindentation are typically conducted with load-time functions, which do not take into account viscoelasticity and time-dependent plasticity [34]. Whereas, most of biological samples present viscoelastic behaviour, having the consequence to induce creep behaviour. This creep behaviour is observed in the force–displacement curve as a "nose" in the unloading part, which can give rise to the appearance of a negative stiffness [30, 35]. As initial slopes of the unload curve is used to

determine the Elastic modulus in the Oliver and Pharr model, creep behaviour must be avoided. The trapezoidal load or displacement function, with a hold period at the maximum load, decreases the creep effect before the unloading.

Nevertheless, the Oliver-Pharr model hypothesises the pure elastic behaviour of the sample, which is not the case with the most of the biological material. The collagen fibres contained in bone, cartilage and soft tissues induce their viscoelastic and time-dependent nature. New models or technique must be investigated to have a better understanding of natural time-dependent properties in the microstructure.

A more recent technique for mechanical research is the Dynamic Nanoindentation. In dynamic mechanical analysis (DMA), more properties can be computed by the use of a small oscillatory force is imposed on the indenter. Indeed, DMA allows the viscoelastic study of the material at microstructural levels, leading to storage modulus, Loss modulus and tan delta thanks to the Complex modulus E^* in addition to the Elastic modulus and the Hardeness. DMA use the same tip type with an oscillated loading mode, measuring load, displacement and phase signals to calculate the elastic and viscous components. The properties are functioning of the oscillation frequency. storage modulus represents the stored energy, this is the elastic part; Loss modulus is the dissipate energy (usually under heat form), this is the vicious part. tan delta is the ratio between these two properties, correlated to the damping and humidity of the sample.

Zlotnikov and al. said that in this method, the sample is rastered using a piezoscanner and a tiny static force is applied to the nanoindenter tip at every node of the raster. Due to the smallness of the static force, the tip penetrates only a few nanometres beneath the surface of the sample [33]. DMA as two main advantages:

- practically pure elastic contact between the tip and the surface is realised with negligible amount of plastic deformation
- the contact area remains very small, less than 20 nm in size, thus providing an excellent lateral resolution

The well-known expressions for these properties are:

$$Complex : |E^*| = \frac{\sigma_0}{\epsilon_0} = E_s + E_l \tag{1.9}$$

$$Storage : E_s = \frac{\sigma_0}{\epsilon_0} \cos\delta \tag{1.10}$$

$$Loss : E_l = \frac{\sigma_0}{\epsilon_0} \sin\delta \tag{1.11}$$

$$Tan\ delta : tan\ \delta = \frac{E_l}{E_s} \tag{1.12}$$

Where σ_0 and ϵ_0 are respectively stress and strain amplitude and δ is the phase lag between the stress and strain.

The storage modulus represents the stiffness of a viscoelastic material and is proportional to the energy stored during a loading cycle. It is roughly equal to the elastic modulus for a single, rapid stress at low load and reversible deformations. The loss modulus is defined as being proportional to the energy dissipated during one loading cycle. It represents, for example, energy lost as heat, and is a measure of vibrational

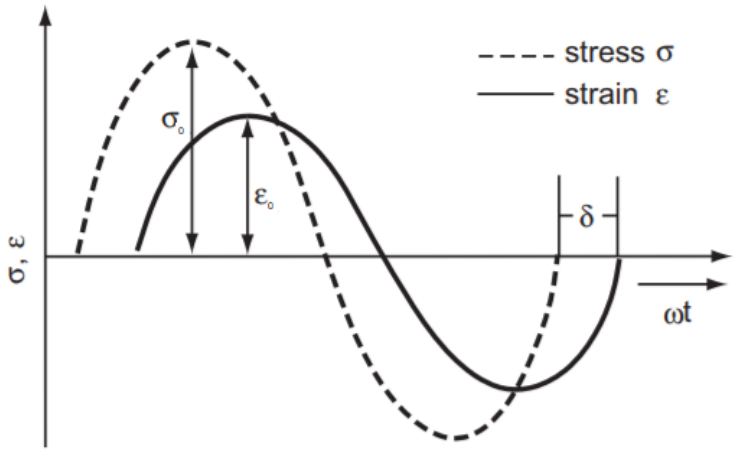

Figure 1.9: Sinusoidal tip oscillation and mechanical response of a linear-viscoelastic material adapted figure from [36].

energy that has been converted during vibration and that cannot be recovered. The phase angle δ is the phase difference between the dynamic stress and the dynamic strain in a viscoelastic material subjected to a sinusoidal tip oscillation, see fig. 1.9. The loss factor tan δ is the ratio of the loss modulus to storage modulus. It is a measure of the energy lost, expressed in terms of the recoverable energy, and represents mechanical damping or internal friction in a viscoelastic system. The loss factor tan δ is expressed as a dimensionless number. A high tan δ value is indicative of a material that has a high, nonelastic strain component, while a low value indicates one that is more elastic [36]. To determine these properties in nanoDMA, the theory say that these properties can be determined with nanoindenter parameters by:

$$E_s = (1-\nu^2) \frac{S}{2} \sqrt{\frac{\pi}{A}} \tag{1.13}$$

$$E_l = (1-\nu^2) \frac{D_s\,\omega}{2} \sqrt{\frac{\pi}{A}} \tag{1.14}$$

$$tan\ \delta = \frac{D_s\,\omega}{S} \tag{1.15}$$

with D_s is the harmonic contact damping and ω the angular frequency [37, 38, 21]. The results are mainly represented in terms of the storage modulus and Loss factor in the literature. Indeed, tan delta is considered as the fundamental measure of damping in a linear material and is not affected by the geometrical parameters [39].

Bones have been recently investigated through DMA and have promising results [34, 35, 40, 41, 42, 43]. However, soft materials can contemporaneously store and dissipate applied mechanical energy, and so the transformation between the measured instrumental response and actual sample properties obtained from an indentation measurement is more difficult to interpret than that for more traditional engineering materials, such as metals or ceramics. Thus, these materials present a major challenge to the application of this technology [44].

Despite the fact that several studies used nanoindentation for mechanical properties at tissue level, Rodriguez and al. investigated the bone properties by nanoindentation and said that they depend not only on the sample itself, but also on the hydration state, probe geometry and data analysis method [40]. So, we must take care of the experimental and analytical options when we want to compare the values of different studies.

Dry vs Hydrated samples

Bone and soft tissues are mainly composed of water. The hydration plays an important role in organic tissues by interacting within the collagen and minerals, leading to viscoelastic behaviour. However, the water rule in mechanical properties is poorly understood [45].

For a practical aspect, a lot of studies investigate dry samples to have better control on the surface properties. Indeed, the surface roughness of wet biological samples is known to be greater than the roughness of dry specimens [35]. Dehydration and altered hydrogen bonding cause an increased of the stiffness. The Young's modulus can increase by a factor 2 from a wet to dehydrated state [45]. Pathak and al. said that studies of bone specimens report increases in indentation moduli of 11% to 28% after dehydration, with further increases after embedding and this trend is even more marked in demineralized and unmineralized tissues [35].

New trends investigate indentation in wet condition to be closer to physiological conditions. The hydrated sample preparation may have several parameters to set. The selection of fluid nature must be taken seriously, in the same proportion as the hydration process. The sample can be kept moisturised or dehydrate followed by rehydration. This last technique does not significantly affect the whole mechanical properties in bone [35].

Here is a list of some preparation type prior indentation:

- natural hydration by unfreezing the sample
- droplets deposit on the sample surface
- irrigation system with microfluidic chip
- hydration from the edges using gauze
- hydration from the edges using foam
- fluid immersion
- DMA with tip oscillation in liquid medium

1.4 Goals

Previous studies have highlighted the highly complex tissue composition and organisation at the interface; much less is known about the corresponding local variations in mechanical properties.

The goals of this master thesis are to investigate the nano-scale mechanical properties at the interface between bone and tendon by using nanoindentation. Two interfaces have been investigated: fibrocartilage interface and periosteal cartilage interface.

The specific goals of this thesis are to :

1. develop a protocol for sample preparation for histology
2. perform histology at tendon-bone interface to visualise collage fibres and the insertion
3. develop a protocol for sample preparation for nano-scale dynamic mechanical analysis (nanoDMA) based on nanoindentation
4. perform nanoDMA at tendon-bone insertion
5. compare mechanical gradients at two different interfaces (enthesis and periosteal interface)

Since anatomical and histological features of human and rat ankle joints are comparable, we choose to start our investigation on rat samples [15].

2. Materials and Methods

During this thesis, several aspects of the Bone-Tendon complex has been investigated. The aim of nanoindentation is to study the mechanical response to the pure and transitional tissues in order to determine their evolution along the interface. Structural investigations were performed with histology to determine the collagen organisation in the tendon near the interface.

The preparation and analyse processes are divided into several steps, represented in the following diagram:

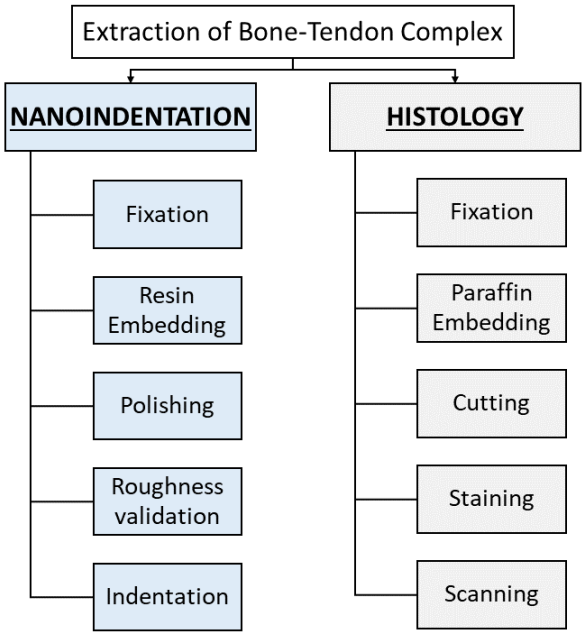

Figure 2.1: Methodology followed during this thesis. The Bone-Tendon Complex was extracted from rats and then prepared for histology and nanoindentation separately.

The first step is the extraction of the Bone-Tendon complex from the rats' legs for both analyses. For the nanoindentation, the samples were fixed, dehydrated and embedded in an epoxy resin in order to facilitate the manipulations, to create a reproducible environment and control the roughness with a polishing procedure. The surface roughness is critical for the nanoindentation. Indeed, the divers properties are evaluated with the projected contact area, the maximum load and the displacement. The contact area cannot be determined accurately with a large roughness. Donnelly and al. said that indentations with contact depths an order of magnitude larger than local surface roughness are thought to be sufficiently deep to avoid a strong effect of roughness on the measured properties. Then static and dynamic indentation were performed to measure the mechanical properties through the interface and at several locations where only bone, tendon or cartilage were present.

For the histology, the samples were also fixed and embedded but in paraffin. Here again, dehydration is the first step to ensure an adequate embedding. Then, thin slices were cut with a microtome to allow optical microscopy as the final step. After being cut, the slices were stained to increase the visibility of several components during the scanning.

2.1 Extraction procedure

Sprague-Dawley rats coming from the University Hospital of Liege (CHU) - tower 3: Pathology- animal house were sacrificed with the collaboration of Dr *Drion Pierre*, *Luc Duwez* and *Cheramy-Bien Jean-Paul* in the framework of other studies which have received ethical approval according to the Ethics Guidelines of the University of Liege.

After being euthanized with a natrium pentobarbital solution, the fresh rat legs were cut under the knee by the doctors and conserved into ethanol. For each leg I have removed the feet, the skin and the flesh with a surgical kit. The bone was exposed and the tendon was extricated from the attachment point. Achilles' tendon and calcaneus bone were extracted with precautions and carefulness. Special attention was paid to remove the other surrounded tissues as other tendons and adipose tissues.

(a) Rat's leg without skin

(b) During the extraction

(c) Tendon-Bone Complex

Figure 2.2: Tendon-Bone Complex Extraction from the entire leg to sample

The samples were put individually into ethanol 70% at room temperature to fix and preserve the sample from tissue deterioration. Indeed, we want to minimise the impact of ambient air containing microorganisms and pollutants, physical and chemical stresses. The different parameters to set during the fixation depends on the nature of the examined biological samples, on the penetration velocity and on the thickness of biological samples. In our cases, the fixation was done at the same time as the dehydration in alcoholic bath with the advice of *Yann Delaunois*.

2.2 Sample preparation for histology

Fixation & Embedding

The samples were placed in a solution of paraformaldehyde 4% completed with PBS at 1h/mm thick (generally 2 days). Formic acid was added to the decalcification during a minimum of 2 weeks. The

samples were then placed in several ethanol baths to stop the fixation and do the dehydration. The ethanol 100% was replaced by isopropanol for budget reason. To be cut in thin slices, the sample has to be embedded in paraffin. Since the paraffin and the ethanol are not miscible, intermediary baths of xylene were used. The procedure for the baths is the following:

- 1 night ethanol 70%
- 1 hour ethanol 70%
- 1 hour ethanol 95%
- 1 hour ethanol 95%
- 1 hour isopropanol 100%
- 1 hour isopropanol 100%
- 1 hour xylene
- 1 hour xylene
- 1 night paraffin solution at 56-60°C

The bath changes were performed under ventilated fume hood with respect to the chemical precaution. After this procedure, the inner pores of the samples were full of paraffin, they were prepared to be in a paraffin block. For each sample, the mould was filled with melt paraffin. The sample was placed carefully on the wanted orientation with warm forceps. To ensure the position and the stability of the sample by solidifying the paraffin, the mould was placed on a refrigerated plate. A labelled cassette was placed on top of the sample. Hot paraffin was added until the face of the plastic cassette was covered. The block was cooled during 15-30 minutes and then extracted from the mould. Before cutting the block, it was placed face down on crushed ice during at least 1 hour to prevent rip.

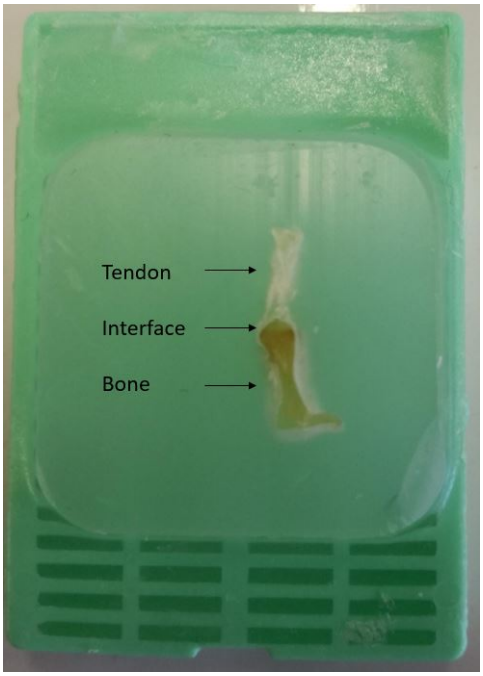

Figure 2.3: Sample in paraffin bloc.

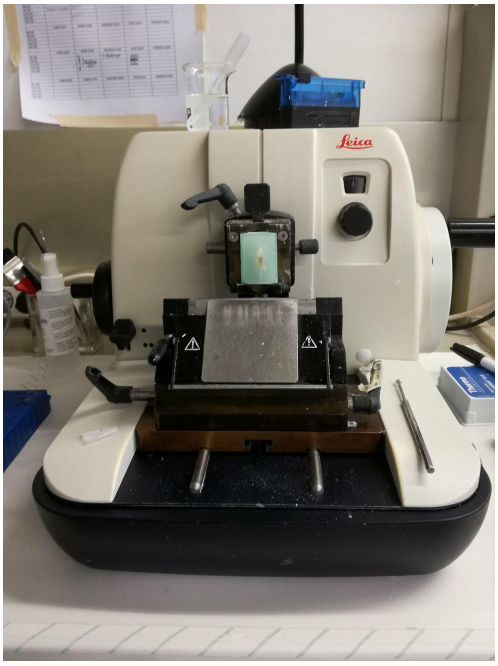

Figure 2.4: Microtome.

Cutting

A new blade and the block were placed on the microtome Leica RM2125 RTS and are positioned to be in contact. The block was roughed by 20 m sections and 0° angle and then cut by 5m sections for 5-10 slices and put again on the ice for 10 minutes before a new cutting. Deionised water was dropped on clean glass slide and a slice was placed on it. The slide is placed on a warming plate to help the stretching of the slice in order to obtain a flat tissue without folds. The excess of water was removed with a blotting paper. The slide was dried one night and put in an oven 1 hour at 50°C.

Staining

To increase the visibility, the tissues were stained with main dyes whose preparations are the following:
Haematoxylin: colour the nuclei in dark purple

- 50 ml stock solution (1 % eosin in AD2x (desionised water))
- 150 ml AD2x
- 8 droplets glacial acetic acid

Eosin: colour cytoplasmic components in pink/red

- Dissolution 50g potash alum in 40ml AD
- Addition 1g crystallised haematoxylin
- Addition 0.2g potassium iodate and 200ml glycerin
- Heating until boiling
- Cooling to room temperature and addition 400ml AD

Because the dyes are prepared in aqueous solution, the slices have to be rehydrated by xylene dewaxing, successive alcoholic baths and deionised water being careful not to touch the slices:

- 8 min Xylene IA
- 4 min Xylene IIA
- 2 min Isopropanol 100 A
- 2 min Ethanol 95 A
- 2 min Ethanol 70 A
- 2 min AD2x
- 8 min Haematoxylin
- 8 min Under a thin stream of cool water
- 1 min Eosin
- 2 min Under a thin stream of cool water
- 1 min Ethanol 70 B
- 1 min Ethanol 95 B
- 1 min Isopropanol 100 B
- 1 min Xylene IIB
- 1 min Xylene IB

Scanning

The slide is put well horizontally. A droplet of Eukitt is put on the slice and then covered with a cover glass by being careful to eliminate any air bubble. The slides dry 2 hours under the hood and are ready for the digital microscope NanoZoomer 2.0-HT.

Figure 2.5: Dying table used to stain the tissues prior the scanning in order to bring contrast and highlight specific features. The tissues are visualised with blue nuclei and pink cytoplasm.

2.3 Sample preparation for indentation

2.3.1 Fixation and embedding

The samples were fixed and embedded into a Epoxy resin EpoThin 2® (Buehler, Germany). Since we have decided to embed samples, we must work on dry condition. The dehydration is a non-skippable step because most of the resin used in embedding process are a-polar, so water has to be completely removed from the sample. If water remains in the sample, the resin does not create cross-link and become hard resulting in a sample stuck in semi-liquid glue.

Firstly, we used the following method:

Fixation and dehydration

- 1 day in 5 ml of 70% v/v ethanol at room temperature
- 1 day in 5 ml of 80% v/v ethanol at room temperature
- 1 day in 5 ml of 90% v/v ethanol at room temperature
- 1 day in 5 ml of 100% v/v ethanol at room temperature

Preparation of the resin

- Put 5 ml of hardener + 10 ml of resin in separated syringes
- 2’ Mixing into the syringes by a connector
- 2’ Mixing into a beaker

Embedding

- Filling the mould with the prepared resin and the sample
- 1 night drying at room temperature

The fixation and dehydration started in 5 ml of 70% v/v ethanol at room temperature. The complete dehydration happened in 4 days with 4 successive ethanol baths with increasing concentration at 70, 80, 90 and 100% for 24 hours each (with a maximum of 3 hours delay). The gradual concentration avoid any brutal change in the tissue structure and configuration.

EpoThin 2 is a low viscosity exopy resin, having good properties: low shrinkage, good physical adherence, good infiltration into pores and transparent. This resin was also used by several studies including the one conducted by Rho J. Y. [26]. To prepare the resin, 5 ml of EpoThin 2 Hardener and 10 ml of EpoThin 2 Resin were taken separately with a syringe. With a connector, the hardener was pressed into the resin and mixed 10 by movement back and forth until the colour was homogeneous. The mixture was put in a beaker and stirred for 2 min with a wood pic. The bottom of the cylindrical clean and dry mould was filled with the mixture, the sample was then placed in the desired orientation and the mould was filled entirely. The curing lasted at least 1 night at room temperature.

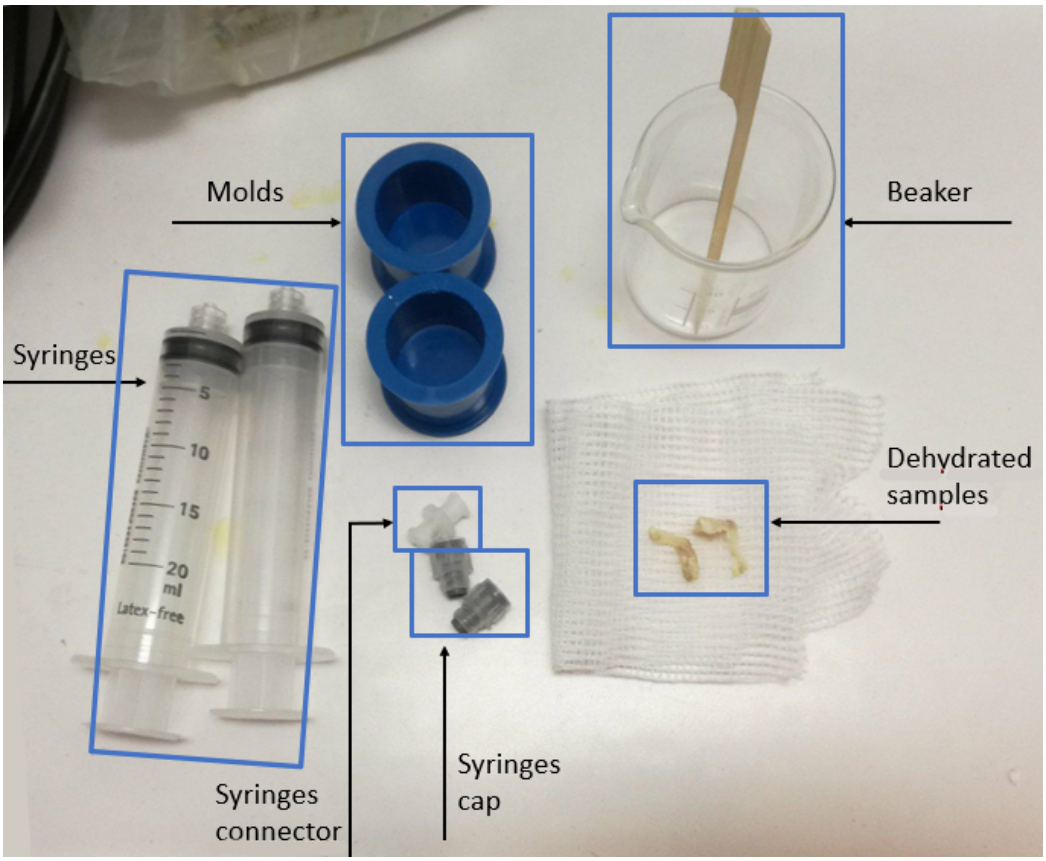

Figure 2.6: Embedding materials used with Epothin 2 resin and hardener

Unfortunately, we discovered the resin was not hard in the sample leading to the degradation of the surface during the scanning done to determine the surface roughness. After a meeting with Mr. *Philippe Compère*, we change the method and implement an impregnation step during the embedding. Without this step, the inner pores and the spaces between the fibres of the Bone-Tendon complex are still full of water or ethanol, inducing issues during the curing/ hardening. To overcome this, we discuss the right protocol and with his expertise, the new method used was the following:

Fixation and dehydration

- 10' in 5 ml of 30% v/v ethanol at room temperature
- 10' in 5 ml of 50% v/v ethanol at room temperature
- 10' in 5 ml of 70% v/v ethanol at room temperature (Can stay more time)
- 10' in 5 ml of 90% v/v ethanol at room temperature
- 10' in 5 ml of 100% v/v ethanol at room temperature
- 10' in 5 ml of 100% v/v ethanol at room temperature

Substitution Ethanol by solvent

- 30' in 5 ml of acetone
- 30' in 5 ml of acetone

Preparation of the resin

- Put 5 ml of hardener + 10 ml of pure resin in separated syringes
- 2' Mixing into the syringes by a connector
- 2' Mixing into a beaker

Impregnation of resin

- 90' in solution of 2/3 acetone - 1/3 resin
- 90' in solution of 1/2 acetone - 1/2 resin
- 90' in solution of 1/3 acetone - 2/3 resin

Embedding

- Filling the mould with the resin and the sample
- Put the filled mould under vacuum
- 3 days in an oven at 60°C

The fixation and dehydration started in 5 ml of 30% v/v ethanol at room temperature (even if the sample was preserved into ethanol 70% The complete dehydration lasted 60 minutes with 6 successive ethanol baths at 30, 50, 70, 90 and twice 100% of 10 minutes. The dehydration had to be done carefully because the resin doesn't polymerase in the presence of water. The first three steps can be substituted by 70% v/v ethanol bath.

The resin is not miscible with alcohol so it must be substituted with a solvent. Acetone is the common solvent used in biological studies. The sample was impregnated three times by a solution of acetone and resin monomers at different concentrations to fill the inner pores and holes. The resin preparation was the same as above.

Then the embedding procedure was pursued by putting the resin in the bottom of a dry and clean mould. The sample placed in the desired orientation is surmounted by the resin and was placed under vacuum during around 20 minutes. The air inlet was opened each time bubbles appeared on the top of the resin. The mould was then completely filled with resin and placed three days to polymerase in an oven at 60°C. This temperature does not alter the morphology of the fixed cells.

In each case, the embedded sample was later extracted from the mould and conserved at room temperature. The resin excess was removed with a low speed saw (IsoMet^{TM}).

Initially, Raman Spectroscopy was planned with the goal of comparing the two obtained maps (mechanical properties and composition). To be accurate, a corner is cut with the same low speed saw to have a landmark and help the mapping match. The indentation positions were collected with this referential: (0,0) = Corner, X-axis = smaller side, Y-axis = longer side.

2.3.2 Polishing and cleaning

The bone and the tendon surface must be a plane surface with a maximal roughness of 50 nm to allow nanoindentation displacement of 5 μm without any issue. To reach this condition with minimal sample damage, a polishing was done with a polisher (MetaServ^{TM} 250, BUEHLER®) with several grids and suspensions (all from BUEHLER®) used between 2 and 10 minutes each, according to the manufacturer recommendations, *Mr. Compère* and *Yann Delaunois* advice as well as the observation of the surface with an optical microscope of magnification between 1 and 5.

The samples were maintained by manual forces on the abrasive paper of 150 or 100 rpm with a continuous water flow. The surface was inspected with a stereomicroscope before using the next abrasive paper. Indeed, the surface scratches must have the same orientation, size and depth (which much decrease with the used of the different papers).

- Trim the resin: CarbiMet^{TM} S [P400] at 150 rpm
- Expose the Bone-Tendon complex surface: CarbiMet^{TM} S [P800] at 150 rpm
- Polishing Step 1: MicroCut^{TM} S Disks [P1500] at 150 rpm
- Polishing Step 2: MicroCut^{TM} S Disks [P2500] at 150 rpm
- Polishing Step 3: MicroCut^{TM} S Disks [P4000] at 150 rpm
- Polishing Step 4: VerduTex + MetaDi^{TM} Monocrystalline Diamond Suspension 3 μm at 100 rpm
- Polishing Step 5: MicroCloth + MetaDi^{TM} Monocrystalline Diamond Suspension 1 μm at 100 rpm
- Final Polishing: MasterTex + MasterPrep^{TM} Polishing Alumina Suspension 0.05 μm at 100 rpm

The CarbiMet^{TM} S [P800] was not delivered at the beginning of this thesis, we used the CarbiMet^{TM} S [P400] to expose the surface during this time, even if the polishing was hardly controlled to remove the right amount of resin and bone. The steps 4 and 5 were not made for the first samples also for delivery reasons. They were replaced by VerduTex + running water and the final polishing was done with a soft tissue and the Alumina suspension.

Finally, the samples were cleaned ultrasonically in a deionized water bath for 5 minutes with a frequency of around 40 Hz to remove the eventual debris from the polishing procedure. The surface of the samples were not touched after this step to avoid any oils deposition and degradation. A magnet is glued on the other side of the resin to secure the fixation on the nanoindenter stage. The samples were stored at ambient temperature until the testing time. The samples were cleaned with soft tissue before each manipulation at the nanoindenter.

2.3.3 Surface Roughness measurement

The surface roughness is a critical parameter for the nanoindentation, the validity of the points depends on it. To analyse the surface, we used Scanning Probe Microscopy (SPM) done with a Berkovich tip of the Bruker® Hysitron TI 950 TriboIndenter Nanoindenter on a 20x20 μm^2 square. The Berkovich tip has a standard radius of 150 nm. A forward and reverse scanning was done, paying attention to the similarity of both the scanning lines. Indeed, mismatch between the two means a modification of the sample surface during the scan.

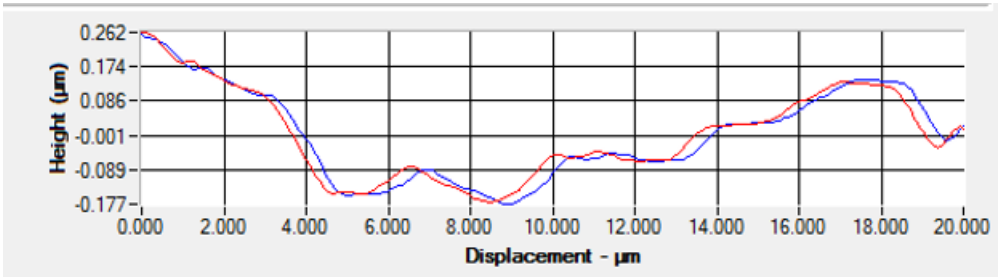

Figure 2.7: Forward (blue) and Reverse (red) surface analysis on bone showing no surface deterioration since the two lines are closed to each other.

Before indenting, the 20x20 μm^2 square was analysed to determine the best 10x10 μm^2 square projected area. This size was chosen to ensure no effect from previous indentations. The tip projected area is around 5x5 μm^2. Thus, if we want to indent on the right side of the SPM square and the left side of the next point on the right, there is still at least 8 μm between them both.

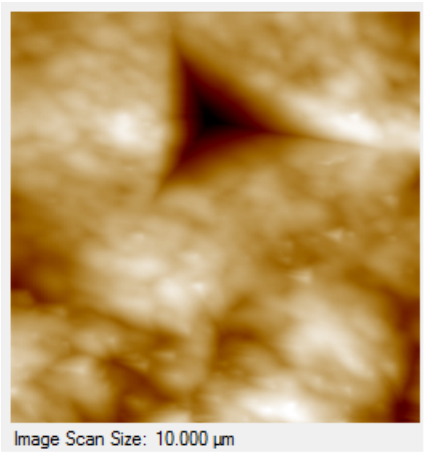

Figure 2.8: Tip imprint giving the projected contact area.

We consider the roughness as good if the Root Mean Square (RMS) average is below 15 nm^2 and Peak-to-Valley (PtV) below 65 nm. The roughness is acceptable if the RMS is below 30 and PtV below 100. RMS is the main parameter taking into account. The points having a roughness higher than these values have not been taken into account. The indentation was done on several lines where the following square centres were spaced by 20 μm

RMS $[nm^2]$	PtV $[nm]$	Condition	colour code
$15 \leq X$	$65 \leq X$	Good	Green
$15 < X \leq 30$	$65 < X \leq 100$	Acceptable	Orange
$X < 30$	$X < 100$	Bad	Red

Table 2.1: Roughness validation condition and colour code

2.4 Nanoindentation

Nanoindentations were performed using a Nanoindenter Bruker® Hysitron TI 950 TriboIndenter. We used a Berkovich tip for its well-defined tip geometry and its good measurement of modulus and hardness on hard polymers and most bulk materials. Berkovich tip is perfect for bone indentation but a bit less for soft tissues. Indeed, viscoelastic behaviours are well represented with spherical tip. However, since we have dehydrated and the sample, this tip is completely acceptable. This pyramidal probe with a sharply pointed tip has the following projected contact area:

$$A = C_0 \, h_c^2 \tag{2.1}$$

where C_0 is a constant equal to 24.5 for the Berkovich tip and h_c is the contact depth.

The instrument was calibrated each day by the calibrations functions and when the software was launched. The tip was cleaned by using fused quartz indentation.

To ensure the stability of the sample during the indentation, a magnet was glued on the resin bottom and the sample was dropped on the magnetic stage. The indentations point was spaced by 20 μm, to avoid the influence of the precedent point. The penetration depth was around 1 μm, which is below 10% of the sample thickness and the surface roughness.

2.4.1 Quasi-static indentation

Quasi-static nanoindentation analysis is based on an assumption of fully elastic recovery without consideration of viscoelasticity and time-dependent plasticity. The final indentation procedure was obtained by trial and errors on the tendon. Indeed, indentation in soft tissues is challenging due to the nature of the sample, the creep effect and the difficulty to obtain smooth surface. After some tests on the tendon, the most difficult material to study in this thesis, we decide to indent with a displacement-controlled procedure with a trapezoidal displacement function.
This function is divided into three phases, each last 10 seconds:

1. Gradual displacement increasing
2. Plateau at the peak displacement of 800 nm
3. Gradual displacement decreasing

Tests were performed on pure bone, pure mineralized cartilage, pure tendons and through the interface, at room temperature (21 °C, controlled to within ± 1 °C using a constant reheat system) in closed room to avoid any temperature change or noisy vibration.

The data were firstly analysed by the Nanomechanical Testing Software- Hysitron TriboScan ®. Roughness, depth and Elastic modulus were investigated.

Unfortunately, the results obtained in the tendon region were not of good quality because of the roughness and the shape of the load-displacement curve. To overcome this issue, we decided to follow our investigations by Dynamic Mechanical Analysis (DMA). Oscillated penetration may reduce the bad roughness influence during the Continuous Stiffness Measurement (CMX).

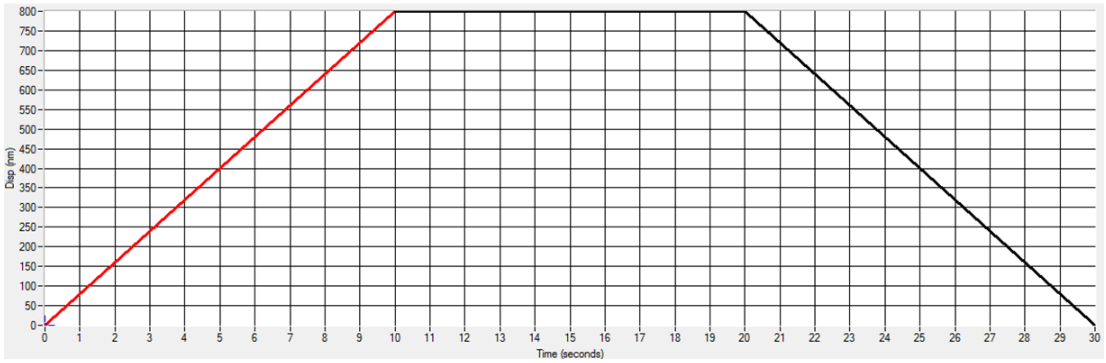

Figure 2.9: Trapezoidal quasi-static displacement control function composed of three segments of 10 s each with peak displacement at 800 nm. The data acquisition rate is 200 pts/s.

2.4.2 Dynamic Indentation

Dynamic mechanical analysis (DMA) involves applying an external, usually sinusoidal, oscillatory load to the indentation tip during a static indentation, and monitoring the phase lag between displacement and load measurement to ascertain the materials' dynamic properties [41]. Dynamic method (often called Continuous Stiffness Measurement CMX) has the benefits to be able to probe the mechanical response to submicrometer spatial resolution both laterally across the surface and through the thickness, reducing the roughness impact on the results accuracy and be able to measure time-dependent properties [44].
Two sources of uncertainty can be encountered with dynamic indentation. The first one is a thermal drift which is compensated by the calibration. The second source comes with Pile-up or sink-in phenomena in relation to material behaviour. To our knowledge, there is no general method that bypasses this problem. We assume no such behaviour when the tip enters in contact with the surface.

To establish a protocol, several parameters were investigated such as the oscillation frequency, the preload force, the peak force and they begin displacement amplitude in order to obtain indent displacement amplitude firstly below 3 $nm \pm 0.5$ nm, then below 5 nm and finally below 10 nm going from bone to the tendon. The parameters setting was done to minimise strongly the influence of uncertainties linked to the displacement measurements. If a point has a displacement amplitude above 10 nm, it was excluded.

To obtain that, we firstly modified the Peak force at 5000, 6000, 7000 or 10000 μm. The optimum is 6000 μm. The oscillation frequency varied from 180 to 240 Hz by 20 steps, no significant changes were observed so we kept the initial default value of 220 Hz.

The critical parameter was the begin displacement amplitude (BDA). This parameter modifies the displacement amplitude. We investigated its influence on the tendon with BDA being at 12, 14, 15, 16, 18 and 20 nm.

2.4.3 Final dynamic indentation protocol

The final protocol includes optical picture of the region of interest where the indentation line will be done, roughness validation by SPM analysis and DMA by indentation on at least 11 points along a predefined line. Tests were also performed at room temperature in theses regions, namely bone, mineralized cartilage, tendons, enthesis interface and additionally periosteal interface.

The final DMA analysis was performed with a constant strain rate curve with the following parameters. Dynamic oscillation was superimposed over load histories that included an increasing load segment followed by a constant load segment with applied normal force ranging from 15 to 6000 μN. Harmonic frequency was set at 220 Hz. The displacement amplitude of oscillation was maintained below 10 nm, the recorded points above this value was rejected.

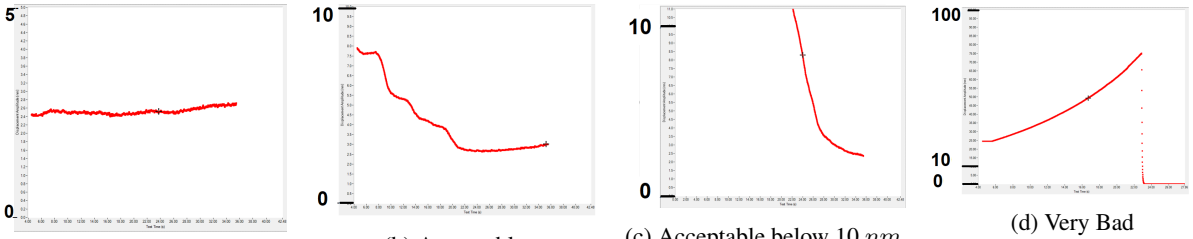

(a) Very Good (b) Acceptable (c) Acceptable below 10 nm (d) Very Bad

Figure 2.10: Evolution of the tip Displacement Amplitude during dynamic indentation (Displacement amplitude [nm]/time[s] graphs)

Enter parameters:

- Begin Displacement Amplitude = 15 nm
- Peak Force = 6000 μN
- Preload = 2 μm
- Oscillation Frequency = 220 Hz

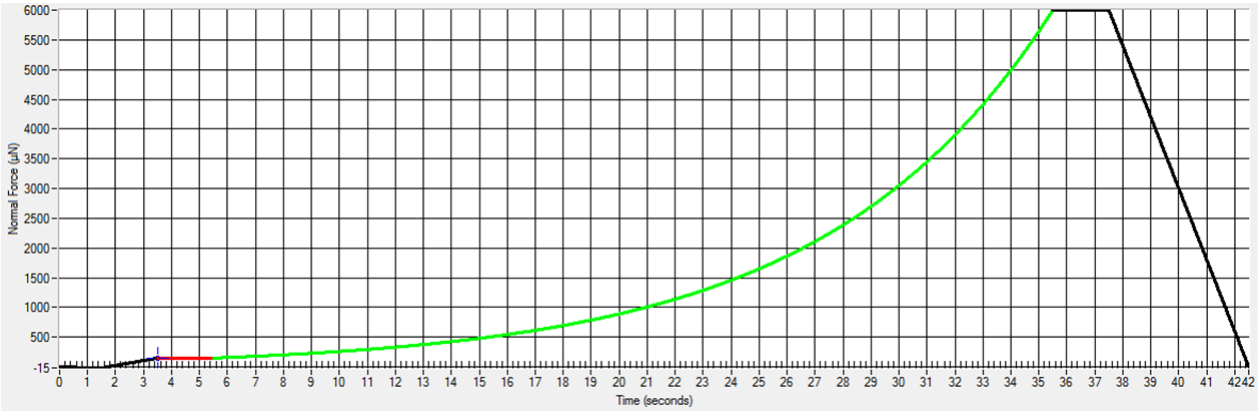

Figure 2.11: Constant strain rate dynamic mechanical analysis function, data acquisition rate = 100pts/s.

This test method provides a considerable amount of data. For each position, the data were processed with histogram analysis in order to obtain the frequency distribution characterised by means value and standard deviation. Those characteristics were analysed according to their spatial position to provide the properties evolution in the interfaces and to observe the tissues heterogeneity. The mechanical properties were also analysed along the penetration depth.

3. Results

In this section we describe the main results, focusing on the surface properties, the indentations and structural analysis. A colour code is used for each region:

Region	Associated colour
Bone	Green
mineralized Cartilage	Red
Tendon	Blue
Interface	Yellow
Resin	Grey

Table 3.1: Regions colour code

Several samples have been utilised: four in histology and 10 in resin preparation and indentation. Most of them were trials and used for the protocol investigation. The sample named S4 was studied with the final quasi-static method. Three samples, named D1, D2 and D3, were finally studied with the final procedure.

Bone, mineralized cartilage and tendon regions were investigated separately by nanoindentation. We then focus on two types of interfaces featuring a combination of those tissues.

3.1 Histology

The microtome cuts were difficult to perform because of the tendon tearing from the bone (fig. 3.1). After discussion with Prof. *Alain Colige*, this may be due to the decalcification protocol. Also, the sample cleaning was not perfect, some residual adipose tissues were still attached to the tendon.

On the following fig. 3.2, we can observe the insertion area, with the aligned linear collagen fibres on the tendon on the left part of the picture b and the bone on the right side.The interdigitation is more visible on the fig. 3.3.

The histological analysis was only partially successful. The several parts of the pictures obtained were not easily recognisable. From the macroscopic visualisation, the tendon is stretched in the same direction as the bone. However, we found the insertion site is not in the same direction and there are weird bony and adipose parts above the enthesis. For future works, longer decalcification or other decalcifying products should be used.

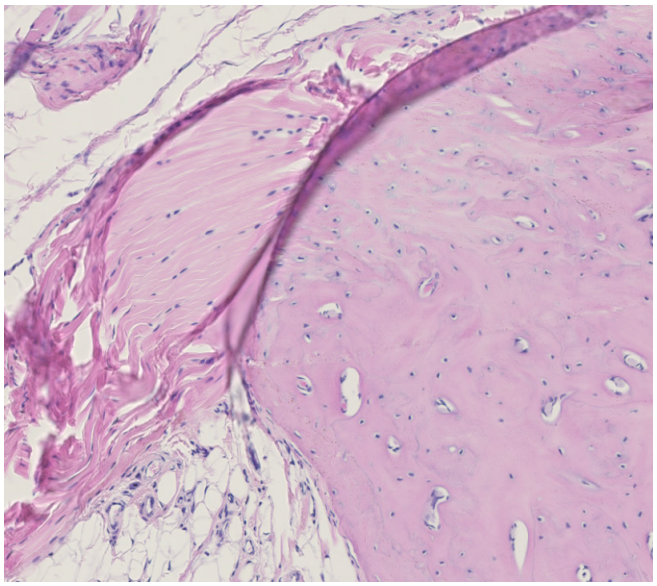

(a) Tendon is teared on the left part of the picture. The stain slice of tissues overlap itself in some parts.

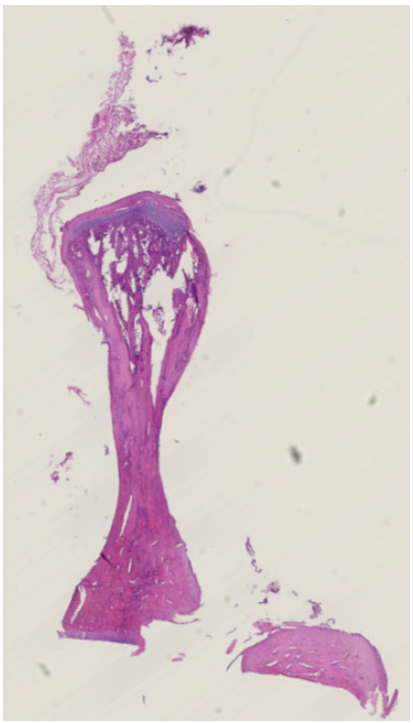

(b) The bone can be seen clearly but the tendon is less visible, teared and contaminated by adipose tissue

Figure 3.1: The difficulty of histology lies on the sample preparation. The decalcification was not optimal to produce good tissues slices without damage.

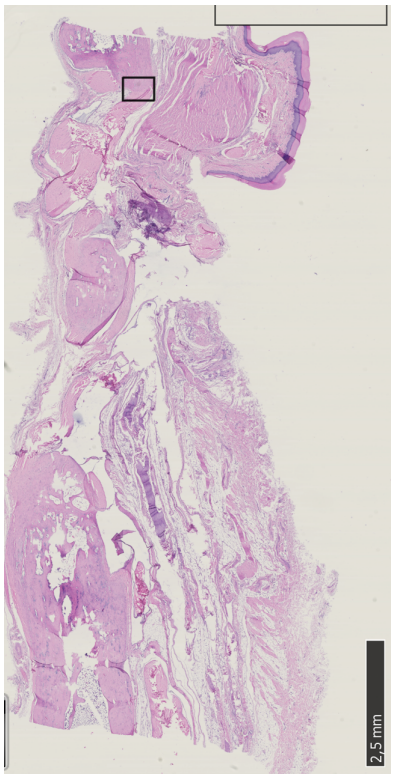

(a) Whole image obtain after scanning. The picture is contaminated by adipose and teared tissues.

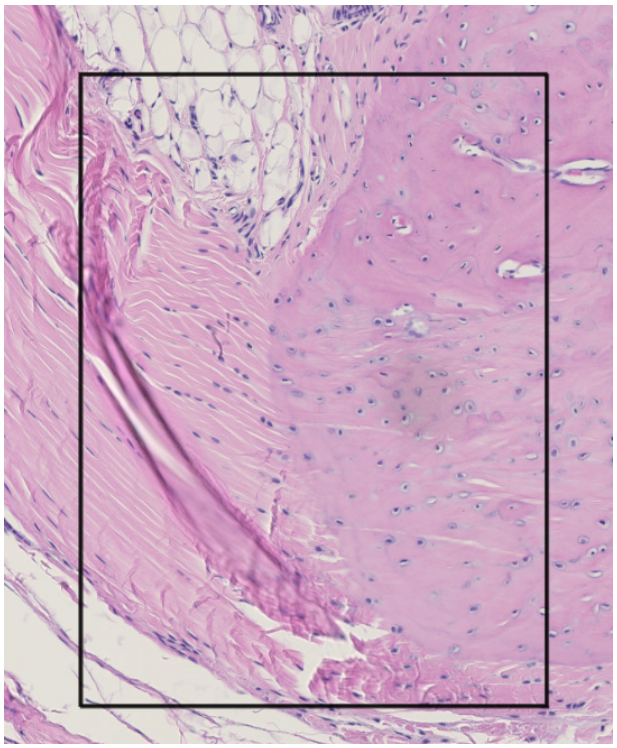

(b) Zoom at the enthesis. The left side shows the tendon and the right part shows the cartilage. The tidemark is visible at the centre, when the collagen fibres start to be disorganised.

Figure 3.2: The good images obtained by histology reveal the collagen fibres organisation gradation through the interface

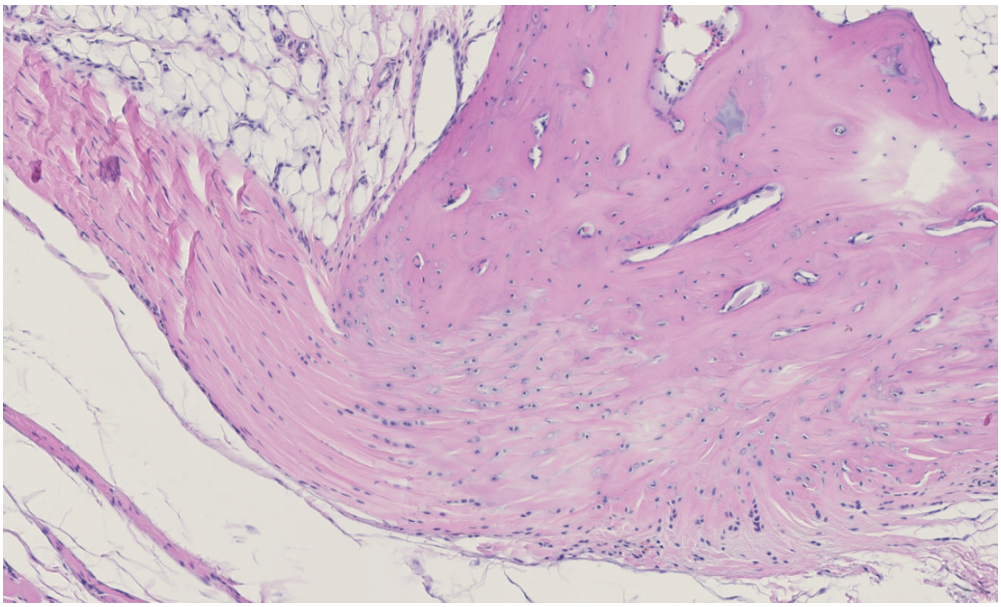

Figure 3.3: The enthesis interdigitation is visible, the tendon (with aligned collagen fibres slightly more transparent, on the left) enters the bone (dark pink). The fibres become less organised through the interface.

3.2 Surface Properties

At the beginning, we encounter embedding issues, leading to soft sticky glue liquid, which deteriorate the sample and make them impossible to analyse. The first issue was the presence of residues into the syringe connector. This old resin induces shear stress during the mixing, which may break the polymer chains. This was solved by cleaning the connector with a needle and using a new one. Also, the mixing with the wood pic was too vigorous creating the same issue. The second issue was the presence of air bubbles in the mix, which could be overcome with a vacuum pump. The homogeneity is pre-requise to have a good resin preparation and curing.

After having a sample embedded into a well mixed, cured and hard resin, the polishing was determining to the validity of the result. The manual polishing requires not damaged abrasive papers and force precision. Holes or scratches on the paper produce debris and deteriorate the sample surface. The applied force must be controlled to conserve flat surfaces with the right amount of removed material.

Nanomechanical testing corrects automatically the slope of the surface profile to determine the surface roughness precisely. To complete this analysis, we manually compute the depths along a line to validate our polishing routine.

Depths analysis: in pure bone, the surface has quite a perfect flat profile even when there is the surface is tilt. The depth varies principally between -0.4 and +0.4 μm. The mineralized cartilage follows the same trend as the bone: good roughness. In tendon, the roughness is much less correct with values variation higher than 4 μm. Through the enthesis interfaces, the roughness is quite linear in each region with changes in the transition and also worse in the tendon. There is a weird depth drop encountered at the

resin edges maybe due to a lower polymerisation rate of the resin at the sample border. The same effect seems to be also present at the periosteal interface. fig. 3.4 to fig. 3.9 show different depth lines and their analogous tilt-corrected lines. Other figures can be found in the appendix A.

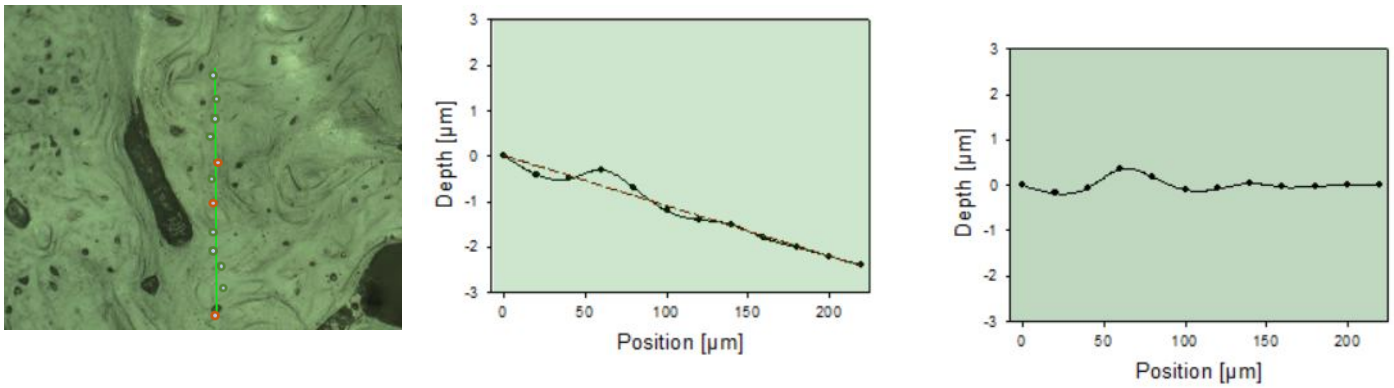

Figure 3.4: Optical picture (left side), Depth evolution (middle graph) and corrected depth evolution (right graph) on the sample D2, bone region.

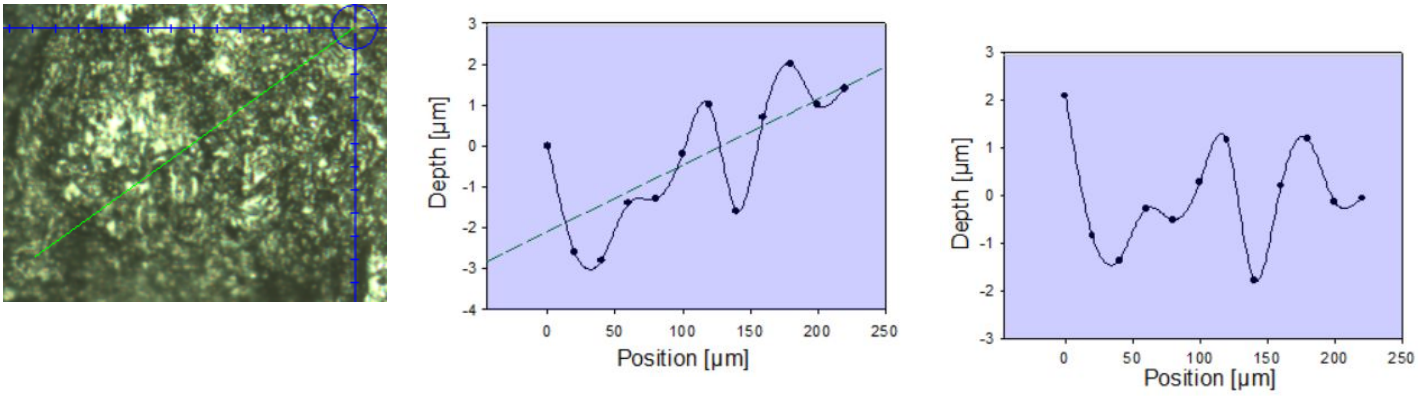

Figure 3.5: Optical picture (left side), Depth evolution (middle graph) and corrected depth evolution (right graph) on the sample S4, tendon region.

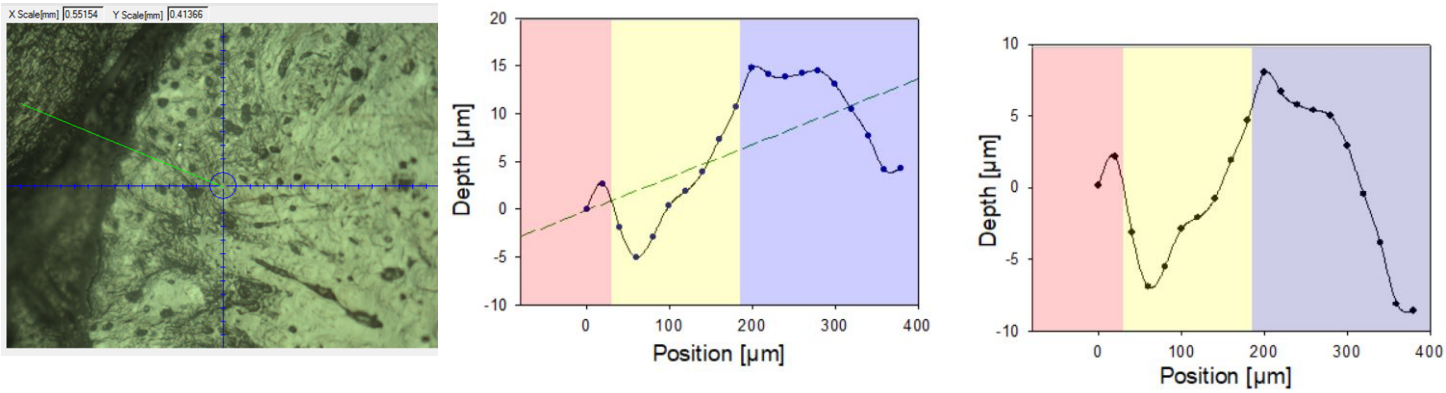

Figure 3.6: Optical picture (left side), Depth evolution (middle graph) and corrected depth evolution (right graph) on the sample S4, interface between enthesis fibrocartilage and bone.

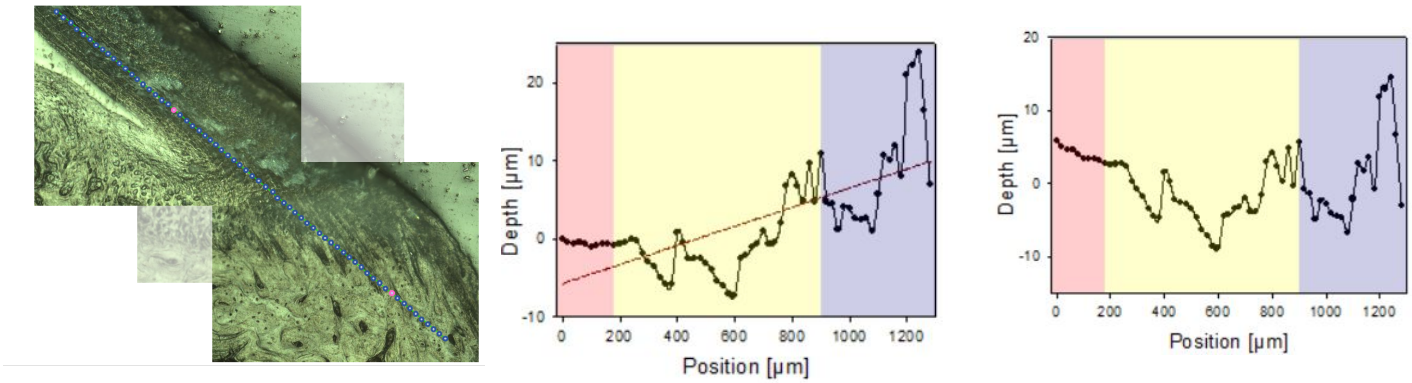

Figure 3.7: Optical picture (left side), Depth evolution (middle graph) and corrected depth evolution (right graph) on the sample D3, interface between enthesis fibrocartilage and bone.

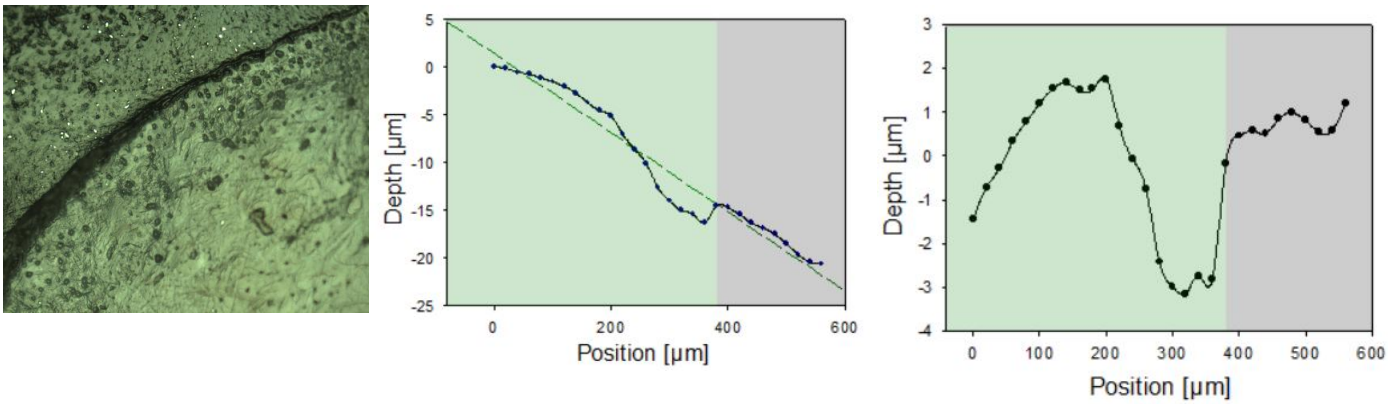

Figure 3.8: Optical picture (left side), Depth evolution (middle graph) and corrected depth evolution (right graph) on the sample S4, bone border to resin.

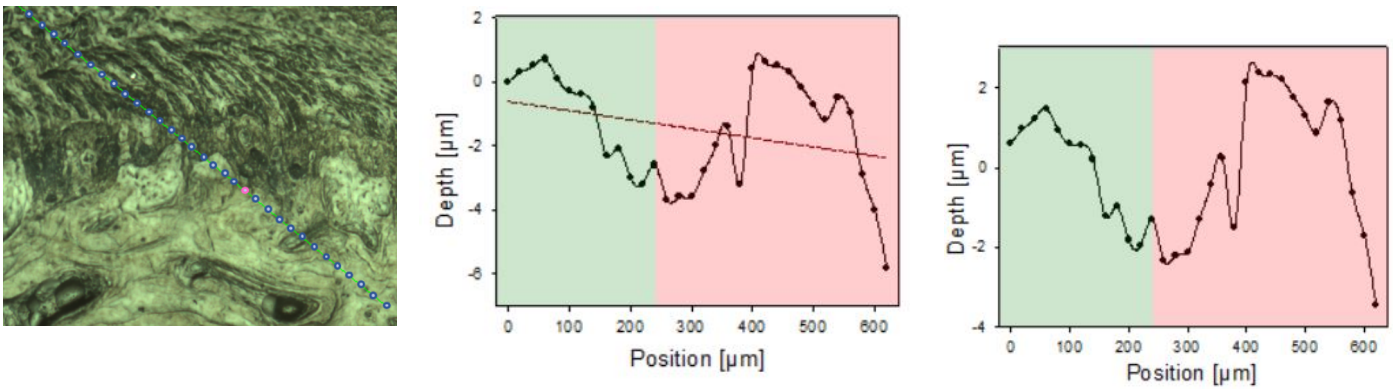

Figure 3.9: Optical picture (left side), Depth evolution (middle graph) and corrected depth evolution (right graph) on the sample D3, interface between periosteal fibrocartilage and bone.

SPM analysis: before each indentation, the surface was scanned by a SPM to validate the roughness of the area. The sample was placed on the stage and secure by a magnetic attraction. One linear zone was chosen to be investigated with at least 10 points. The SPM has several parameters as the tip velocity, the setpoint (force applied by the tip), the scan rate or the scan size. The scan size was chosen firstly at 10 μm^2 but this analysis square area was too small to define a good area and at the same time avoiding the influence of the surrounded points. Indeed, the tip has an approximated area of 5μm^2 and to avoid

any influence, the minimal distance between two points is around 8 μm. The scan size was then set at 20 μm^2, the analysis square are represented on the fig. 3.12. The tip velocity was at 40 $\mu m/s$ and the setpoint at 2 μN. These two parameters were modified during the protocol investigation to lower values (until 20 $\mu m/s$ and 0.01 μN respectively) in order to improve the SPM analysis quality in the tendon, but no change was observed. We hypothesise the resin was not hard enough in the tendon leading to the surface modification or debris collection on the tip. The new embedding protocol given by Mr. Compère did not improve this issue; the tip cleaning between each indentation line either.

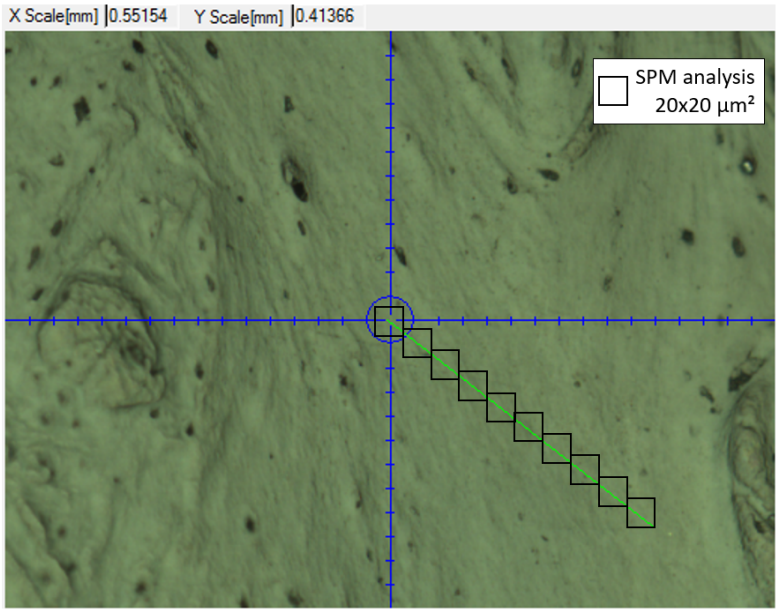

Figure 3.10: SPM analysis square on a bone line. The squares have an area of 20x20 μm^2 to avoid any influence from previous indent points

The roughness was mostly good in bone and acceptable in the cartilage. Since the SPM analysis was not correct each time, the roughness quality could not be confirmed but it seems to be worse than in the two other pure regions. Here also, the same observations were made in the interfaces: the roughness quality decreases from the bone to the tendon.

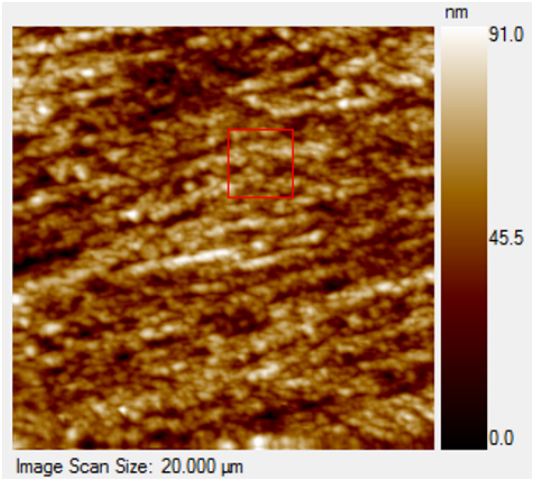

Figure 3.11: SPM analysis on bone, good roughness. Projected Area = 10.2 μm^2, RMS = 11.0 nm and PtV = 61.9 nm

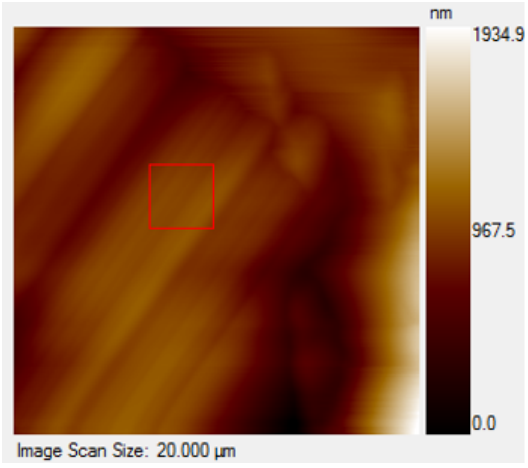

Figure 3.12: SPM analysis on tendon, bad roughness. Projected Area = 10.2 μm^2, RMS = 46.2 nm and PtV = 271.4 nm

3.3 Quasi-static Indentation

The quasi-static indentation gives Reduced modulus and Hardness from the unloading curve. A correct curve must start at a point very close to (0,0) for force and displacement, follow a smooth concave load curve and have a constant displacement value during initial unloading moment. The second indication is the most important. Bad curves are convex or present some steps. fig. 3.13 and fig. 3.14 are examples of good and bad force-displacement curves. Firstly, we indent using load control with a peak force of 800 μN on the sample, but the curves were not correct. We switch to a displacement control of 800 nm.

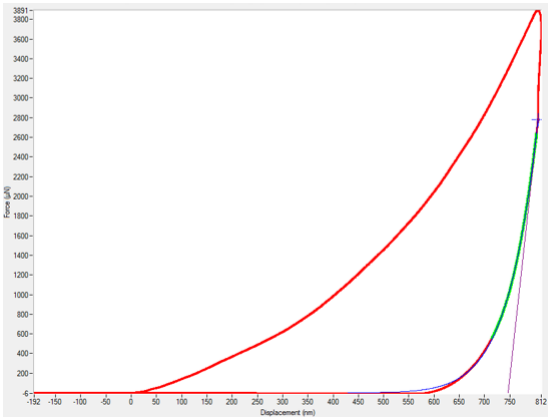

Figure 3.13: Shape of a good Force-Displacement curve.

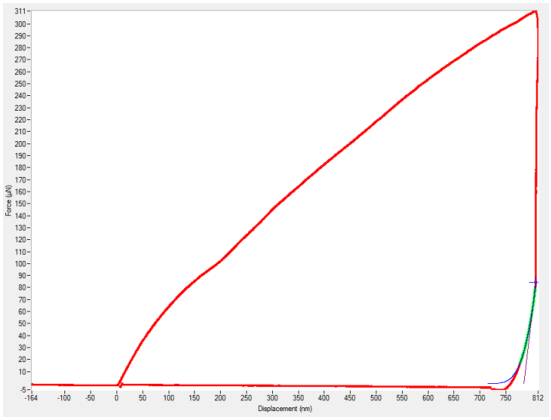

Figure 3.14: Shape of a bad Force-Displacement curve.

Some results displayed for the nanoindentation measurements are represented on the fig. 3.15. The Reduced modulus values are not too far from each other for each individual region containing only one type of tissue, with values closed to the ones measured on bulk samples that is 20 GPa for bone and 2 GPa for tendon.

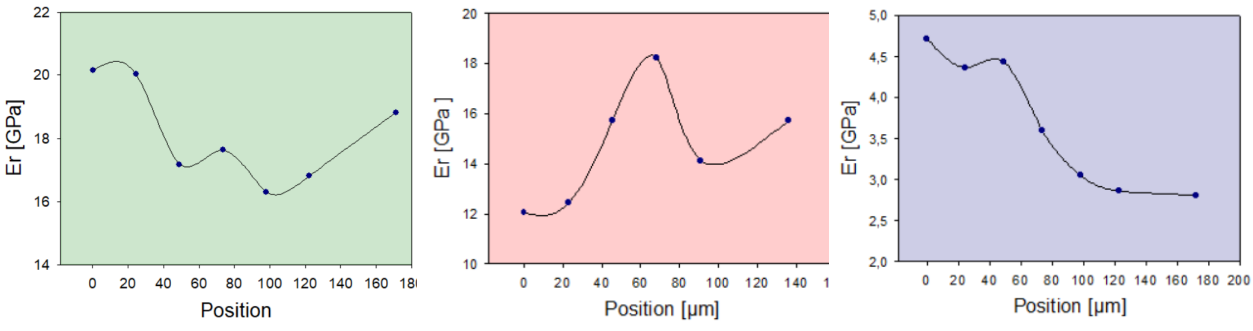

(a) Pure Bone (b) Pure mineralized Cartilage (c) Pure Tendon

Figure 3.15: Reduced modulus measured by QS indentation on the sample S4

The sample S4 indentation line of the enthesis interface starts in mineralized cartilage, as seen in the fig. 3.16. The tendon insertion is not really visible in the sample, maybe due to the first sample preparation, so it may be possible than the defined interface region is not the real one.

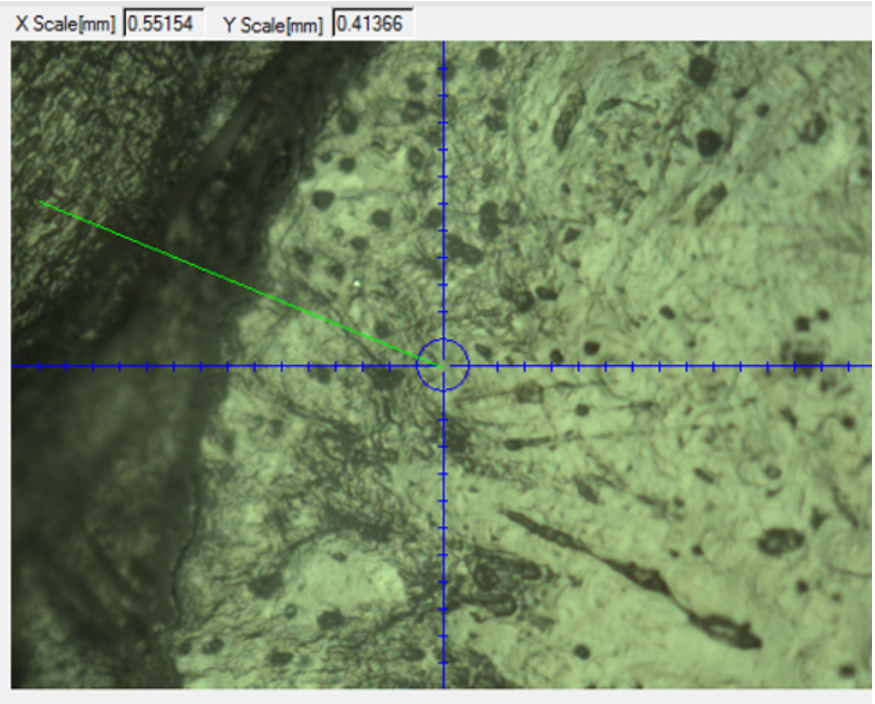

Figure 3.16: Enthesis interface sample S4, the indentation line start in cartilage and end in tendon

After selecting the indent line, the roughness was analysed. Most of the 28 points had a good or acceptable RMS. The average roughness was also measured but not taken into account, RMS is more affected by larger peaks [46].

There is a nice decreasing trend through the interface, going from 20 to reach 5 GPa. The measured values do not deviate a lot from the linear regression pattern, indicating nice gradual transition through the interface.

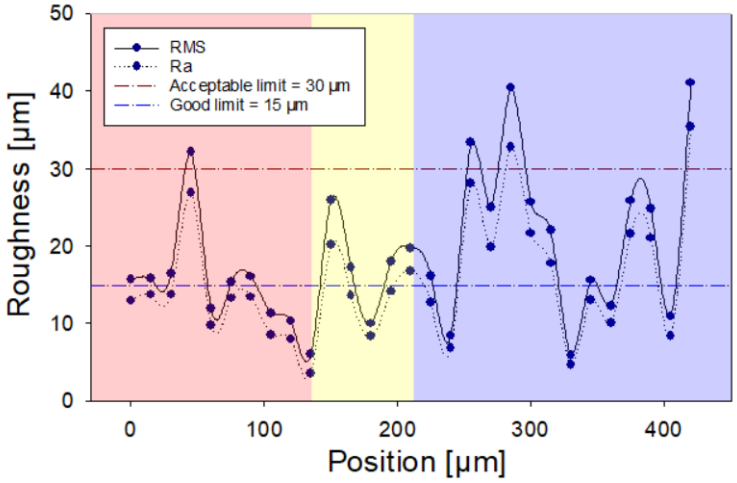

Figure 3.17: Roughness values and boundaries of Enthesis interface sample S4

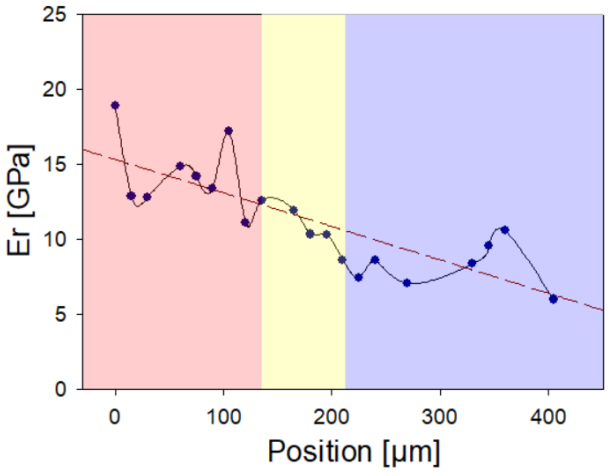

Figure 3.18: Reduced modulus of Enthesis interface sample S4

3.4 Dynamic indentation

Several indentations lines were performed on the samples, sometimes on the same sample. The table 3.2 and the table 3.3 represent the name of the line and the sample where the indentation was done.The results displayed of the Continuous Measurement (CMX) are storage modulus and tan delta.

Region	Sample	Indentation line	Region	Sample	Indentation line	Region	Sample	Indentation line
Bone	D1	A	Cartilage	D1	A	Tendon	D1	A
Bone	D1	B	Cartilage	D1	B	Tendon	D1	B
Bone	D2	C	Cartilage	D2	C	Tendon	D2	C
Bone	D2	D	\			\		

Table 3.2: DMA analysis: Individual region samples

Region	Sample	Indentation line	Region	Sample	Indentation line
Enthesis interface	D1	A	Periosteal interface	D2	A
Enthesis interface	D2	B	Periosteal interface	D3	B
Enthesis interface	D3	C	\		

Table 3.3: DMA analysis: Interfaces region samples

Several samples have been studied, the next sections will provide the main results and the one most representative indentation line. Firstly, the data were represented into properties (storage modulus and tan delta) histograms for each individual indent point. From these, we extracted the mean values and standard deviation and expressed it through the indentation line. Secondly, we examined the property evolution according to the penetration depth in the sample.

3.4.1 Bone dynamic mechanical analysis (DMA)

To have a better understanding of the data processing, this section give some results in the processing order. Firstly, we have made an optical picture of the region of interest, and analysed the roughness. Here in bone, the roughness was good for all 46 points except 3 acceptable points.

Figure 3.19: Bone B optical picture. The dots are separated by 20 μm. The dots colour represent the quality roughness, here they are green so the roughness is good. The points are close to the line without being on it each time, depending on the SPM analysis results.

Then, for each point, we have analysed the mechanical properties through their frequency distribution and through the penetration depth, example can be found in the fig. 3.20 and fig. 3.21. Attention was paid on the tip displacement amplitude. It was below $\sim 3\ nm$ for all the bone indentations. The frequency distribution of the storage modulus has several shapes on the different points and the tan delta form a Gaussian-like distribution around 0.04.

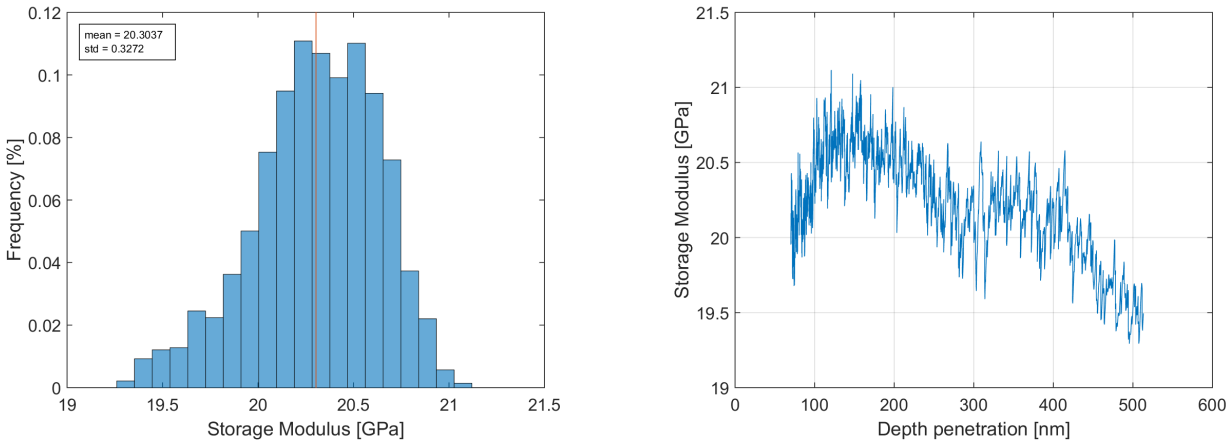

(a) Frequency distribution

(b) Property values depending on the depth indentation

Figure 3.20: Example of results obtained on one indentation point. On the left, the figure present the storage modulus frequency distribution. On the right, the figure is the storage modulus evolution in depth.

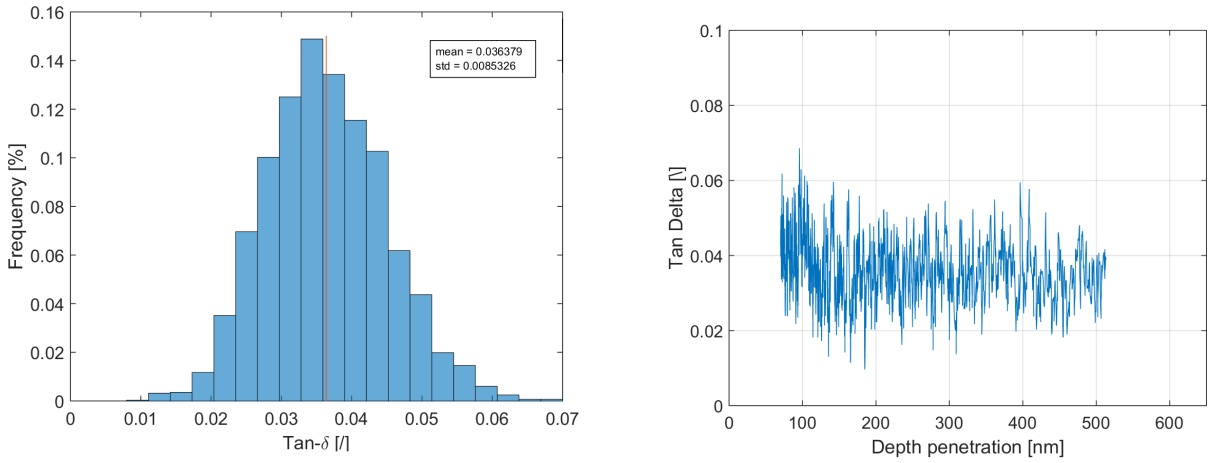

(a) Frequency distribution

(b) Property values depending on the depth indentation

Figure 3.21: Example of results obtained on one indentation point. On the left, the figure present the tan delta frequency distribution. On the right, the figure is the tan delta evolution in depth.

With the means and standard deviation values collected from the individual indentation points, the evolution of the properties through the indentation line was highlighted for bone. The data collected in each indentation line were merged to look at the distribution in the line.

All the individual depth curves were put together into the same figure in order to compare that general tendency. To have a better visualisation of the trend, these data were present under mean curve with error bars. The conclusion them gave allowed us to see a bone depth dependence with constant values from 350 nm. So, new frequency distribution was done with the data having penetration depth higher than 350 nm.

Bone A: The optical picture of the Bone A indent line shows a black dot being certainly a bone cell for the second indentation. The SPM analysis displays good roughness for all the points.

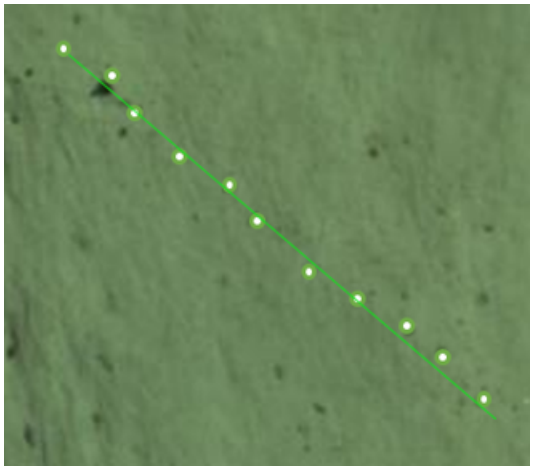

Figure 3.22: Bone A optical picture.

Individual points were analysed on the storage modulus and tan delta. All theses graph are available in annex document called "Data-DMA.pdf". Storage modulus has several distribution type. The first type is a low flat distribution except for maximal values around 24 GPa. For some points, the maximal value is not reached. In those cases, the distribution is more evenly distributed with higher frequency near 18 and 22 GPa with slightly higher frequency at $\sim$ 18.5, 20 or 21.5 GPa. The tan delta distribution look like Gaussian function with mean value at $\sim$ 0.04.

The average storage modulus does not change a lot depending on the point position, see the red curve on fig. 3.34. The second point is in a black dot (certainly cell), this does not show any influence in storage modulus and in tan delta.

The data collection of the whole indent line shows a bimodal distribution for storage modulus, from 18 to 22 GPa with high frequency and one small from 23 to 25 GPa, and a Gaussian distribution for the tan delta, mean value being 0.04.

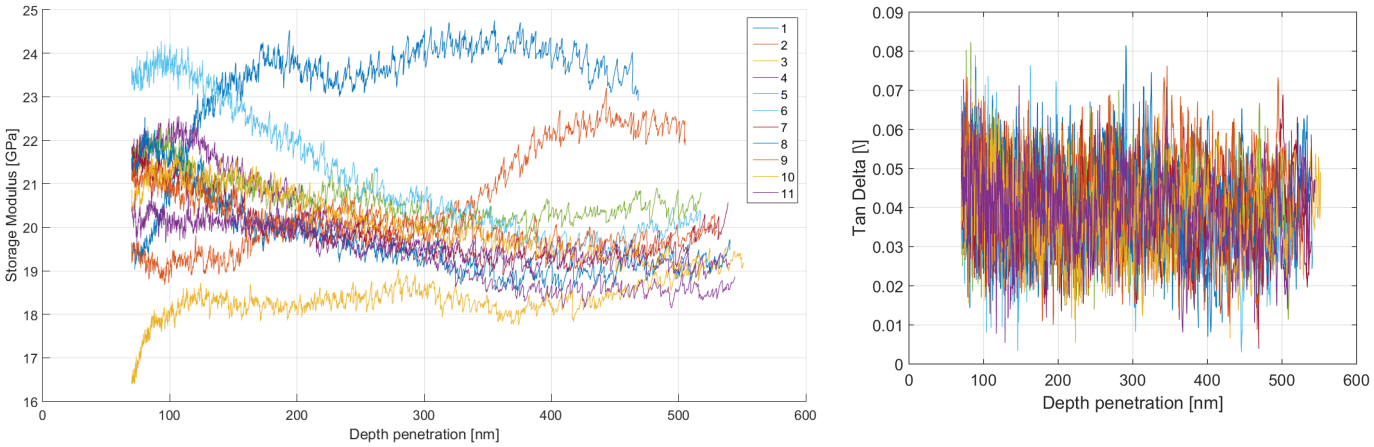

Figure 3.23: Bone A storage modulus and tan delta Depth dependence.

Regarding the depth influence on fig. 3.23, we observed that the storage modulus values are spread between 18 and 24 GPa at the surface contact and more closed at the final depth being at 500 nm depth from 18 to 21 GPa. The storage modulus evolution mainly decrease and stagnate from 350 nm. Concerning the tan delta, the main trend seems to be a constant value at $\sim$ 0.04 but the curve is composed of high and close oscillations. To have a better visualisation of the depth dependence, we looked at the average curve. The average storage modulus depth dependence presents the same decrease and stagnation after 350 nm on fig. 3.24. tan delta curve is more oscillating with a mean value of 0.0395.

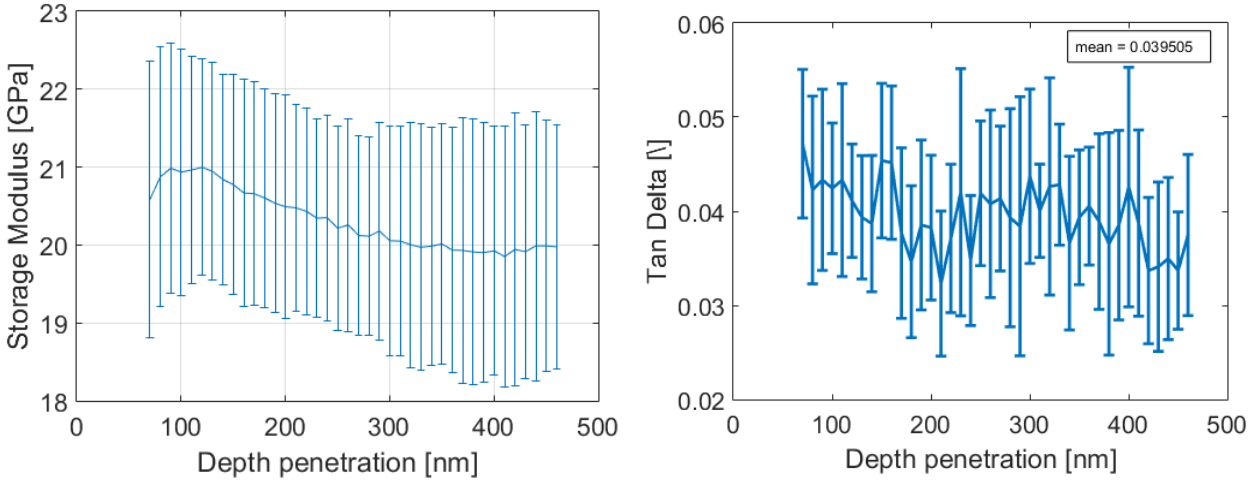

Figure 3.24: Bone A storage modulus and tan delta Average Depth dependence.

350 nm, cf fig. 3.25. Now the storage modulus follows a Gaussian curve between 18 and 21 GPa with mean value at 19.35 and some greater values at low frequency. The mean value for the tan delta Gaussian is 0.038.

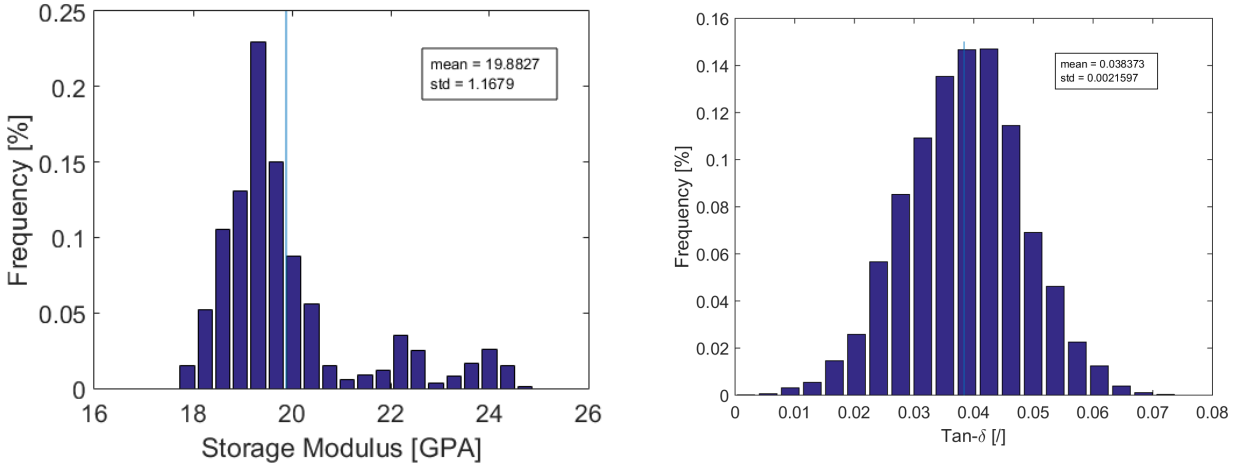

Figure 3.25: Bone A Frequency distribution of storage modulus and tan delta with data having penetration depth higher than 350 nm.

With these observations on the Bone A, we will focus on the optical picture of the indent points, the associated roughness, the property evolution depending on the point position, the line histogram, the average depth dependence and the new histogram with data having penetration depth higher than 350 nm for the other bone indents.

Bone B: The optical picture of the Bone B indent line represented on the fig. 3.19 shows a flat surface without any cell, cartilage, or other tissues than pure bone. The roughness is good for all the points.

The average storage modulus represented by the brown curve on fig. 3.34 are quite constant at ~ 20 GPa with low deviation. tan delta is also quite constant with main value around 0.04. The deviation here is really high, being at ~ 25 $\%$ of the mean value.

The data collection shows Gaussian distribution around 19.6 GPa with small frequency after 22 GPa and a tan delta Gaussian distribution around 0.039.

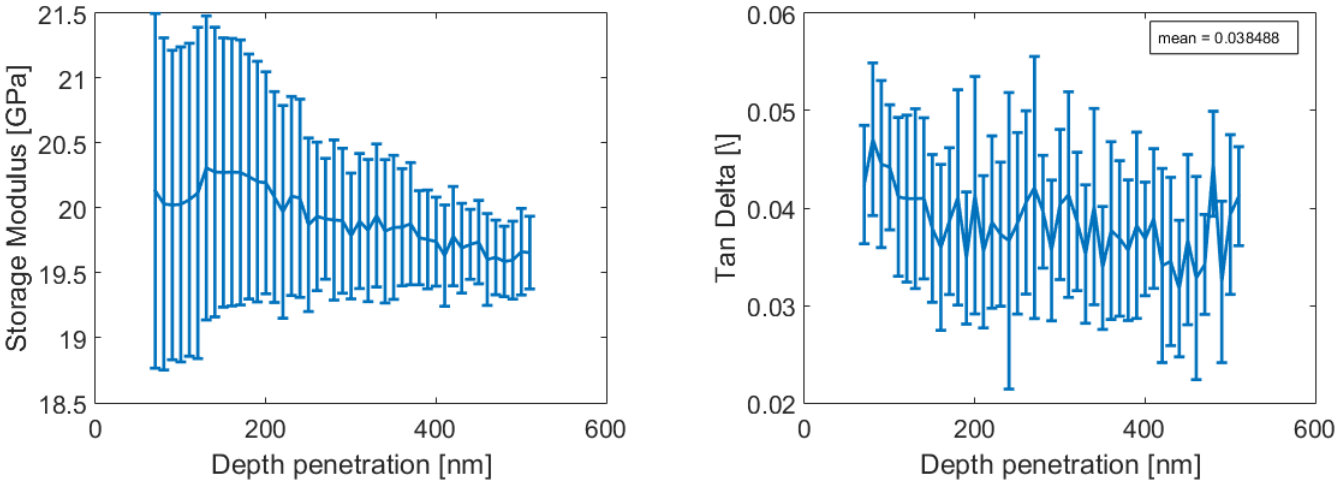

Figure 3.26: Bone B storage modulus and tan delta Depth dependence.

The property evolution through the depth follows the same trend as in Bone A: storage modulus values are well spread at the contact surface between 18 and 22 GPa and decrease to reach 19-20 GPa at 350 nm to the final indent measure at 550 nm. The average curve shows this lower deviation after 350 nm. The tan delta has a large dispersal between 0.02 and 0.06 with 0.0385 as main value for each penetration depth.

The new histograms display better Gaussian function with 19.7 GPa and 0.037 as mean values.

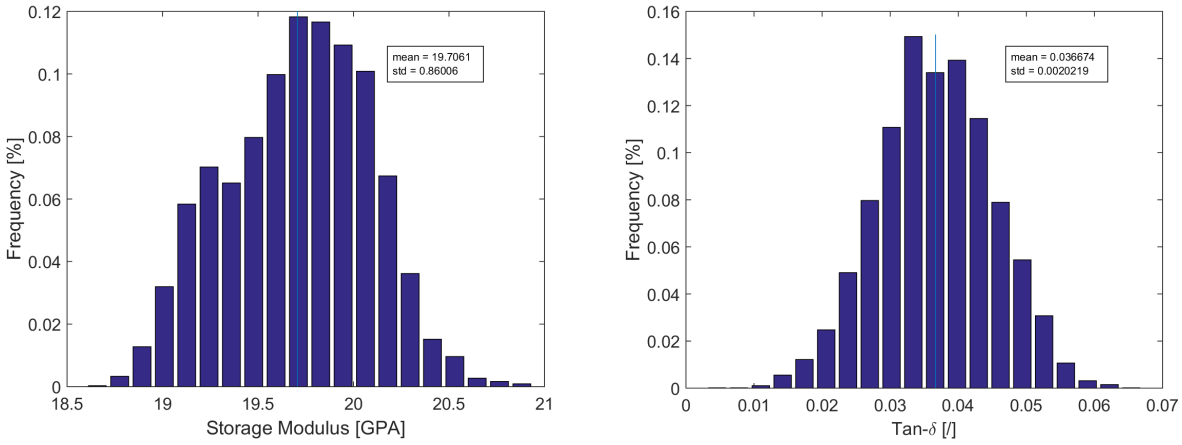

(a) Storage modulus (b) Tan delta

Figure 3.27: Bone B Frequency distribution with data having penetration depth higher than 350 nm.

Bone C: The optical picture of the Bone C indent lines shows proper pure bone surface. The roughness is good for all the points.

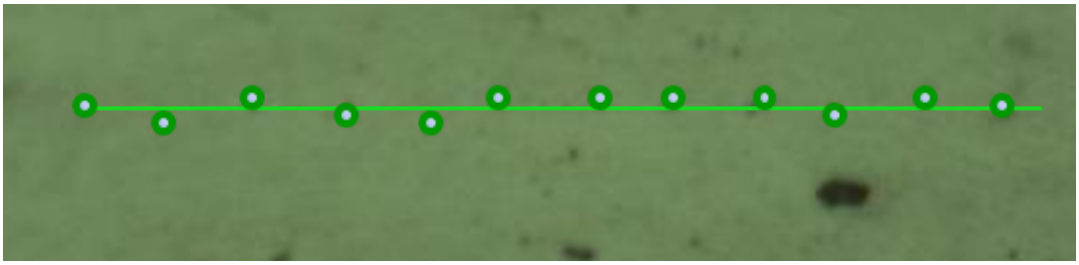

Figure 3.28: Bone C optical picture.

Storage modulus fluctuates between 16 and 20 GPa with pretty low deviations, see green curve on fig. 3.34. Tan delta is also quite constant with main value around 0.041. The deviation is still really high, being at ~ 25 %.

The data collection shows a large bell shape curve between 16 and 22 GPa with mean value equal to 18.3 GPa. Tan delta Gaussian distribution has 0.043 as mean value.

Here again, the depth dependence is shown with large spread between 15 and 23 GPa at the contact surface and smaller deviations starting from 350 nm depth reaching 17-18 GPa. The tan delta display here a slight decreasing trend from 0 to 350 nm with values from 0.045$\pm$ 0.02 to 0.041$\pm$ 0.02 . The deviation is fairly constant along the line.

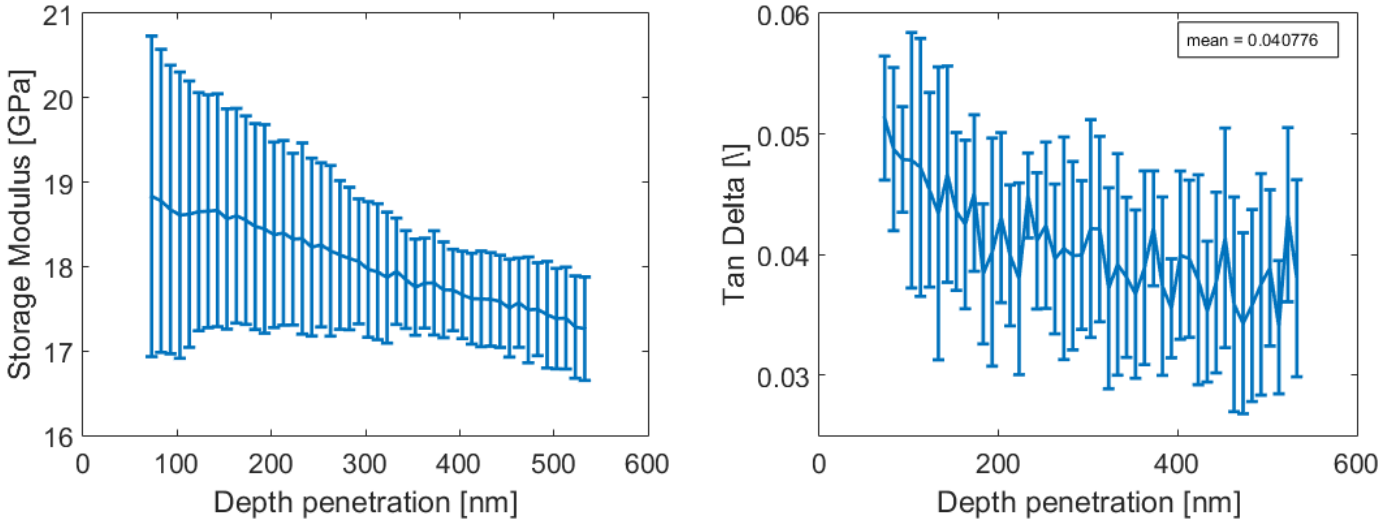

Figure 3.29: Bone C storage modulus and tan delta Depth dependence.

The new histograms show bell curve around 17.5 GPa and small frequency for smaller storage modulus values (below 17 GPa). The new tan delta distribution has the same shape but lower mean value, being at 0.038 instead of 0.041.

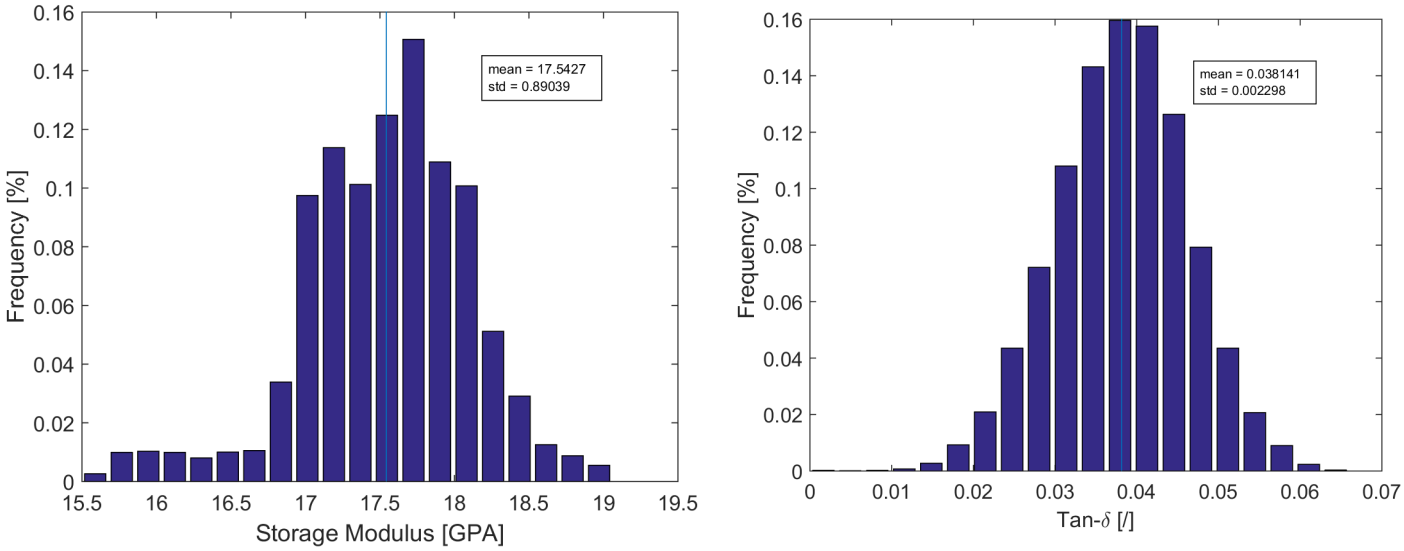

Figure 3.30: Bone C: storage modulus and tan delta Frequency distribution with data having penetration depth higher than 350 nm.

Bone D: The optical picture of the Bone D indent line is not as clear as the other ones, cf fig. 3.31. The bone seems to have been remodelled. Indeed, adult rats modify their bone composition in their lifetime and remodelled bone area has smaller the mineral content [47]. Of the 12 indent points, 9 have good roughness and 3 have acceptable roughness.

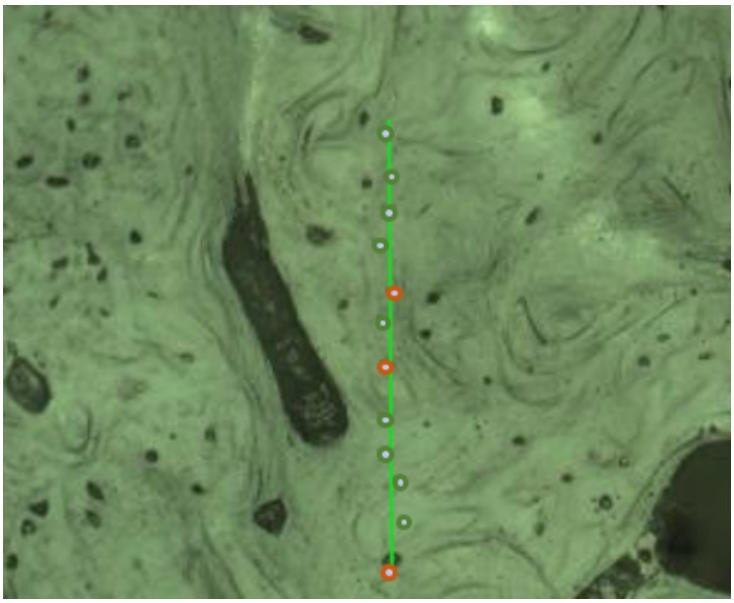

Figure 3.31: Bone D optical picture.

The storage modulus oscillates quite sharply between 16 and 18 GPa with higher deviation than the other bones along the indent line. Same observations are made for the tan delta as the other bones, blue curve on fig. 3.34.

The data collection show roughly a bell shape curve between 13 and 19 GPa and low frequency for values from 19 to 21 GPa. Tan delta Gaussian distribution has 0.044 as mean value.

Here, the depth dependence is not as pronounced as in the other bones. The indent measurements at the contact surface vary from 13 to 21 GPa to reach values between 14 and 16.5 and between 17 and 18 starting from 350 nm. Tan delta trends show a slight diminution from 0.05 to 0.038, with a $\sim 40\%$ dispersion rate.

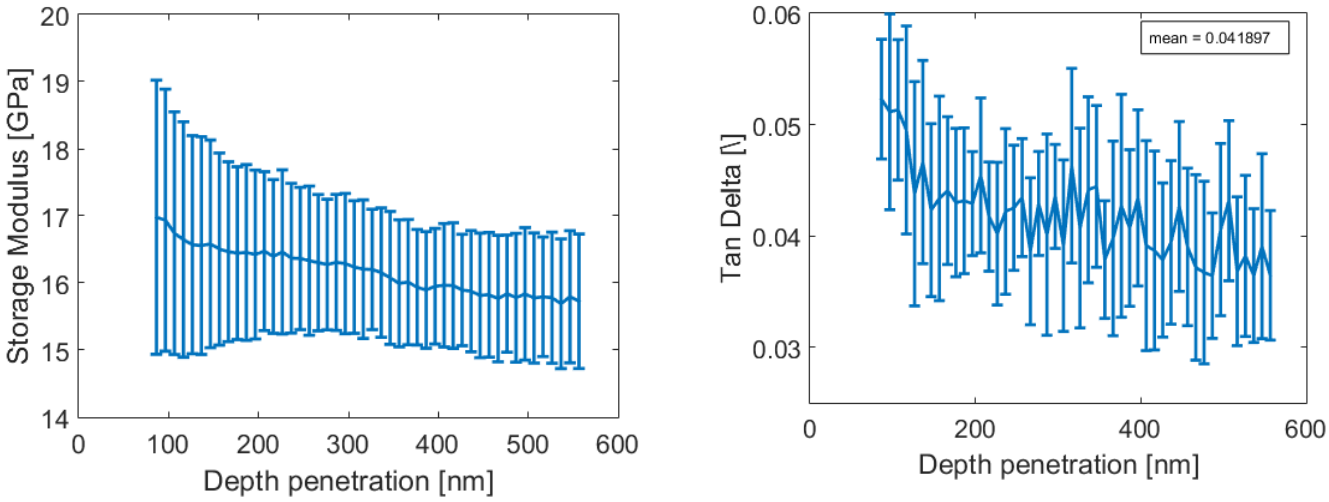

Figure 3.32: Bone D storage modulus and tan delta Depth dependence.

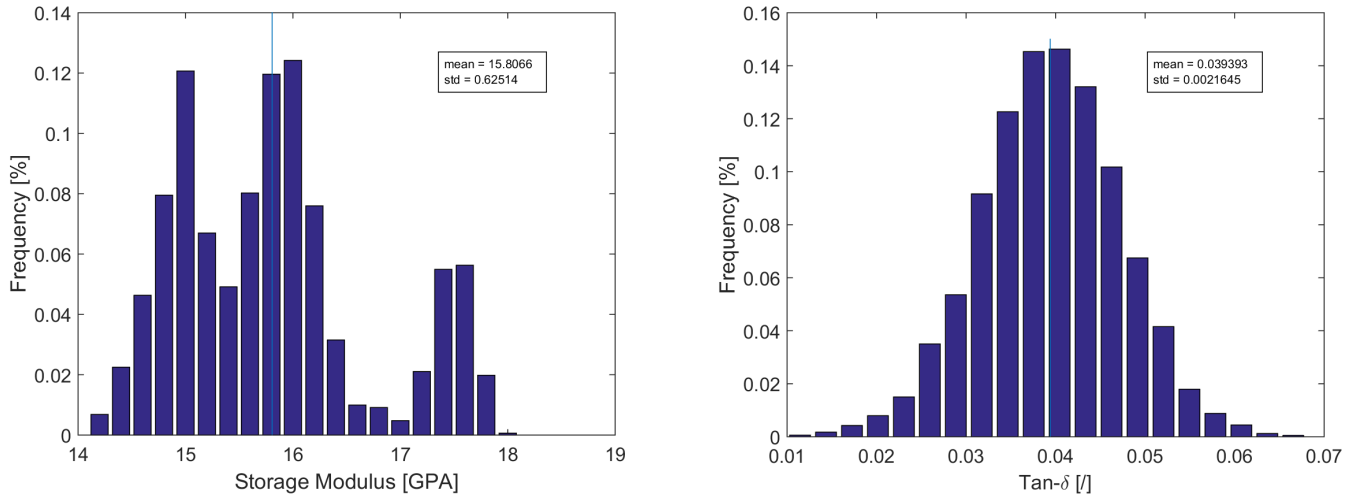

Figure 3.33: Bone D: Frequency distribution with data having penetration depth higher than 350 nm.

We kept the same depth limit to obtain the new histograms, even if the constant state was less marked by the decreasing part. The trimodal storage modulus distribution shows higher frequency at 15, 16 and 17.5 GPa. The tan delta Gaussian function is more flared at the bottom and has meant value equal to 0.039.

Bones: To sum up, the means and standard deviation obtained on the individuals histograms are represented on the fig. 3.34 according to their position in each indent line. The storage modulus and tan delta seem to be quite constant in an indent area with small fluctuations. Indentation in a hole or in a cell does not seem to influence the measurements. It was expected to get smaller elastic behaviour in cells. The first three lines are in pure mature bone, having storage modulus close to 20 GPa and tan delta close to 0.04.

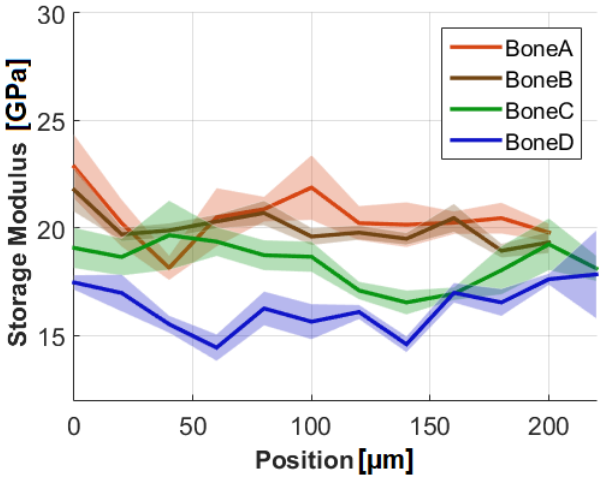

(a) Storage modulus

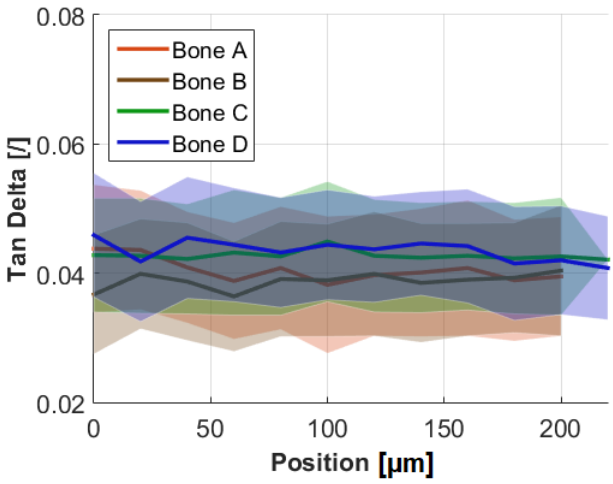

(b) Tan delta

Figure 3.34: Properties evolution on a bone indentation line, straight line represents the main values obtained by the histograms, the transparent part represents the standard deviation.

Bone	Storage modulus [GPa]		Tan delta [\]	
	mean	STD	mean	STD
A	19.88	1.17	0.0384	0.0022
B	19.71	0.86	0.0367	0.0020
C	17.54	0.89	0.0381	0.0023
D	15.81	0.62	0.0394	0.0022

Table 3.4: Bones Values from the new histograms.

3.4.2 Mineralized cartilage DMA

The optical pictures of the several mineralized cartilage show that the indent line for the Cartilage A is between subchondral bone and mineralized cartilage, having the consequence of not completely reflecting the mechanical cartilage properties. Since that, we have taken into account only the Cartilage B and C for the analysis. On 22 points, 19 have an acceptable roughness, 2 good roughness and 1 bad roughness. The same analysis protocol was performed as in bone. The tip displacement amplitude was also below ~ 3 nm for the cartilage indentations.

Cartilage B: The optical picture shows that the indent points 3, 5, 9 and 10 and in or close to a black dot (cell or blood vessels). The roughness is acceptable except for the first point having good roughness.

Figure 3.35: Cartilage B optical picture

Individual storage modulus frequency distribution shows that the points 7 and 11 have very high value, around 30 GPa, which is unrealistic in mineralized cartilage. We excluded those points. The other points exhibit values between 15 and 24 GPa, the holes do not seem to influence the storage modulus distribution, even if Sebastián Jaramillo Isaza showed lower elastic values when indenting on osteons [48]. Tan delta is represented mainly by a Gaussian function with a mean value being at ~ 0.04. Regarding the mean property evolution according to the point position on the indent line, they increase gradually: storage modulus from 19 to 25 GPa and tan delta from 0.038 to 0.05, see brown curves on fig. 3.41.

The data collection of all the line shows a large bell-shape distribution excepted high frequency for storage modulus at 20 GPa. The tan delta curve represents a Gaussian slightly shift with lower decreasing slope at the right of the mean being at 0.04.

Regarding the depth influence, there is no main tendency. The values at the contact surface are quite as spread as in depth, varying between 16 and 22 GPa. The evolution through the depth does not have clear trend: at some points the storage modulus increase by ~ 40 %, at some other values it goes down by ~ 20 %. However, curves show two clusters starting at 350 nm with values varying around 17 and 21 GPa, with more points near to the highest value. Looking at the average curve, the deviation is higher at the contact surface and quite constant after 350 nm. The tan delta varies at high frequency from 0.02 to 0.08 (main value=0.05) and then from 0.02 to 0.06 (main value=0.04) starting from 350 nm. The average curve does show the same feature but less pronounced.

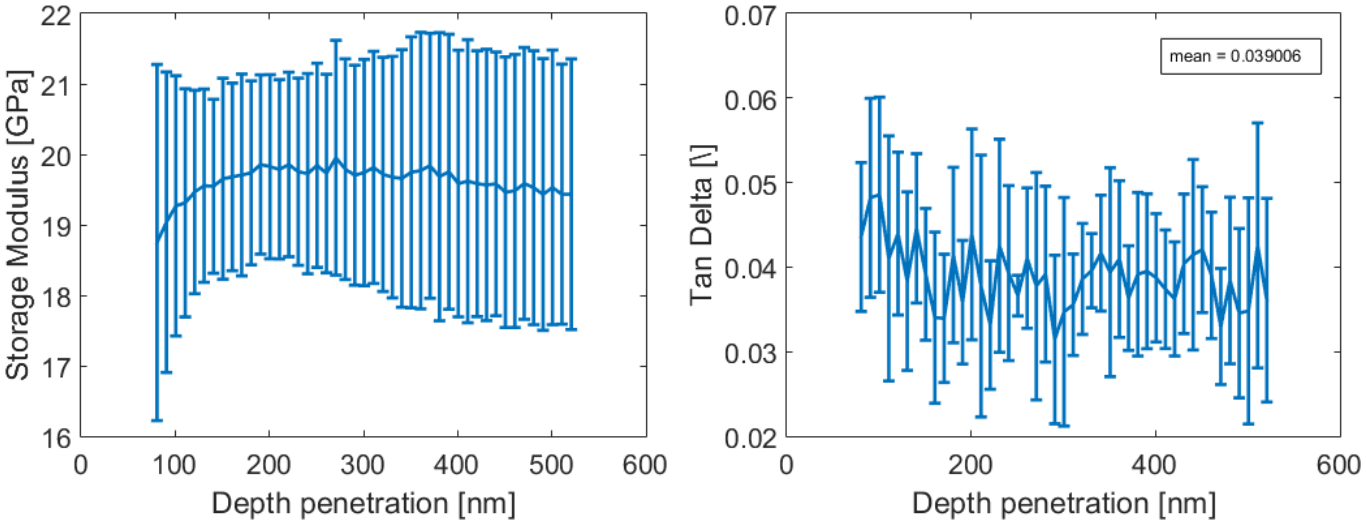

Figure 3.36: Cartilage B storage modulus and tan delta Depth dependence

The new frequency distribution along the whole line shows clearly a bimodal storage modulus distribution around 17 and 21 GPa. The mean value for the Gaussian tan delta function is at 0.037.

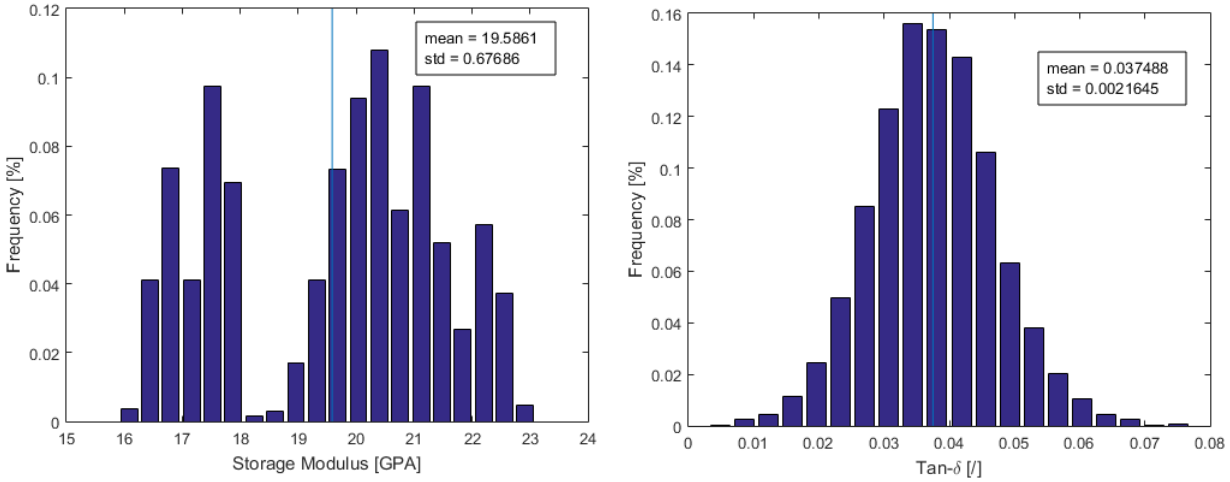

Figure 3.37: Cartilage B Frequency distribution with data having penetration depth higher than 350 nm

Cartilage C: The optical picture of the Cartilage C (fig. 3.38) shows indent points in pure mineralized cartilage, with the indent points 3, 7, 10 and 11 are in or close to a black spot. That roughness is acceptable except for location 5 (good) and location 9 (bad).

The storage modulus is spread mainly from 11 to 20 GPa more or less evenly depending on the indent point. The tan delta still follow the same distribution shape but have bit higher mean values. Regarding the property values according to the point position, they evolve is a saw-tooth path, from 8 to 18 GPa and from 0.04 to 0.05, see green curves on fig. 3.41. The comparison with the optical picture do not seem to show lower storage modulus value when the indent were performed into a black spot except for the location 10 having a storage modulus below 10 GPa.

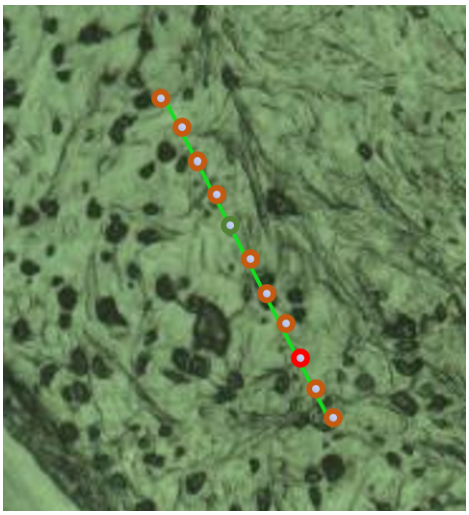

Figure 3.38: Cartilage C optical picture. The dots are separated by 20 μm. The dots colour orange represent the acceptable roughness, green and red respectively good and bad roughness

.

The data collection of the line does not show well-distributed function, the storage modulus values are mainly spread between 11 and 20 GPa with higher frequency at 12.5 and 18.5 GPa. The tan delta distribution is here again represented by a Gaussian function having 0.044 as mean value.

Regarding the depth influence, there is a diminishing trend. The contact surface indents form three clusters at 11, 15 and 18.5 GPa. The progression in depth distribute more evenly the storage modulus values between 12 and 16 GPa. No specific trend is noticed after 350 nm. However, the average curve shows a clear decreasing curve with equal deviation all along. Tan delta representation has the same observations as for Cartilage B with higher distribution.

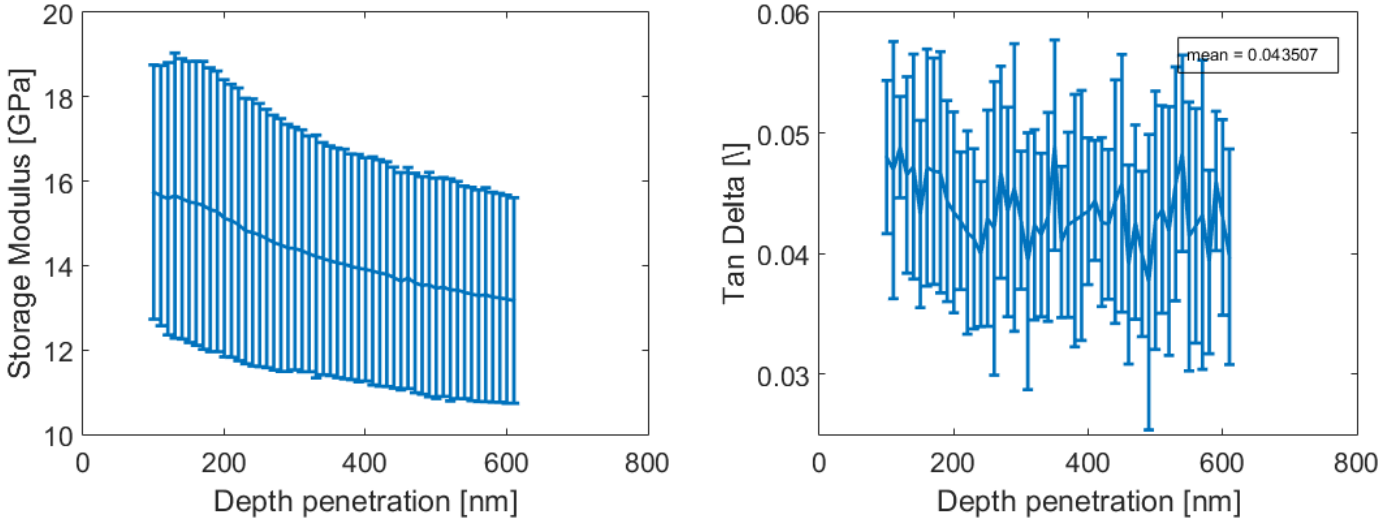

Figure 3.39: Cartilage C storage modulus and tan delta Depth dependence

The new frequency distribution along the whole line show two main clusters for storage modulus distribution around 13 and 16.5 GPa, the low value represents a single indentation curve. The mean value for the Gaussian tan delta function is at 0.043.

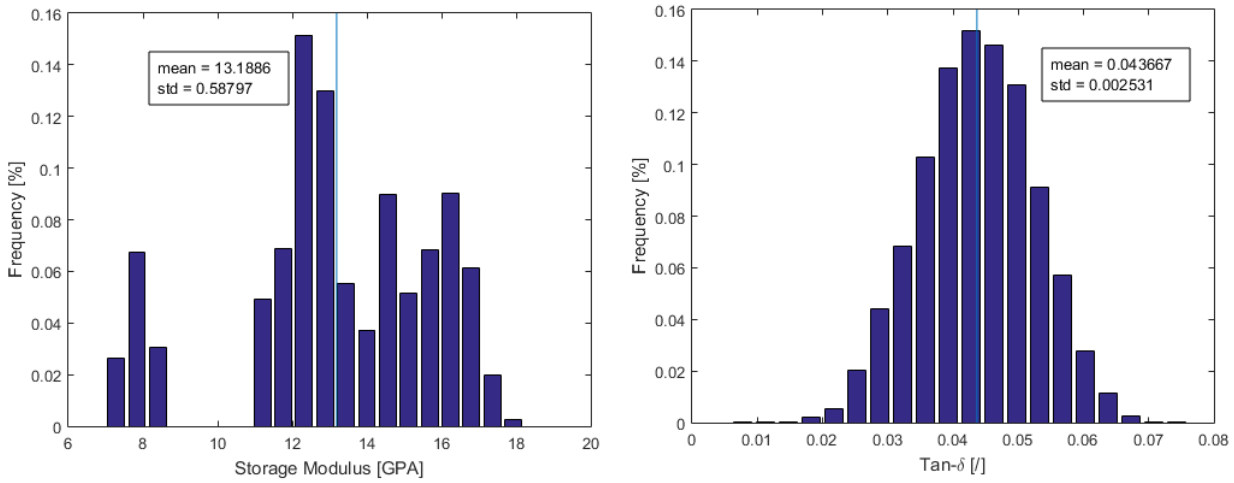

Figure 3.40: Cartilage C Frequency distribution with data having penetration depth higher than 350 nm

Cartilage: The means and standard deviation obtained on the individuals histograms are represented on the fig. 3.41 according to their position in each indent line. The storage modulus is lower in Cartilage C than in Cartilage B, but this seems normal since Cartilage B is between bone and cartilage. The values fluctuate more in pure cartilage, either for storage modulus than for tan delta.

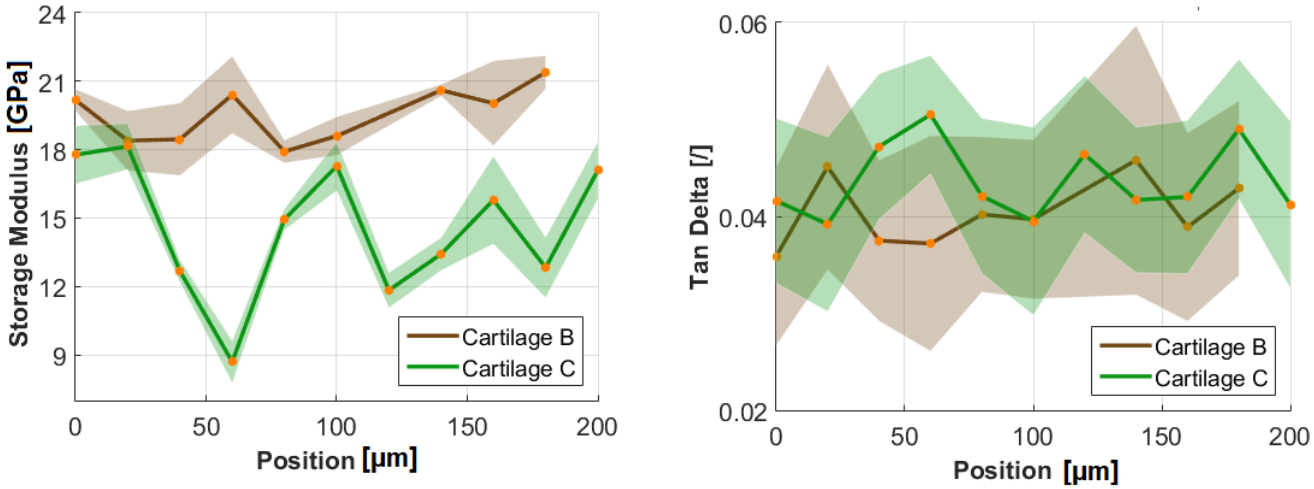

(a) storage modulus

(b) tan delta

Figure 3.41: Properties evolution on a cartilage indentation line, straight line represents the main values obtained by the histograms, the transparent part represents the standard deviation

Cartilage	Storage modulus $[GPa]$		Tan delta [\]	
	mean	STD	mean	STD
B	19.59	0.68	0.0375	0.0022
C	13.19	0.59	0.0437	0.0025

Table 3.5: Values from Cartilage B new histograms and Cartilage C old histogram

3.4.3 Tendon DMA

Some optical pictures of the tendon show white coloured clouds in some part that could be adipose tissue or resin residue. Also, the SPM analysis was not always concluding: the forward and reverse scanning mismatch, leading to a surface deformation due to tip rastering. As we cannot measure the surface roughness accurately, we cannot determine if the deformation is temporary or definitive. Since it was very difficult to obtain good or acceptable roughness in tendons (and also in enthesis and periosteal interface), we kept all the points and discredit the measurement having a tip displacement amplitude above 10 nm, whatever its penetration depth.

Most of indent points had good displacement amplitude (25/34 indent points including all the Tendon C points), but some had acceptable displacement amplitude (3/34) or really bad displacement amplitude could reach 100 nm and them drop to value below 10 (6/34), example can be found on the fig. 2.10.

Tendon A: 11 points were analysed in this first indentation line in the tendon. The points 5, 6 and 7 present really bad displacement amplitudes and weird results with storage modulus negative or greater than 1000 GPa values. They were excluded from the next analysis.

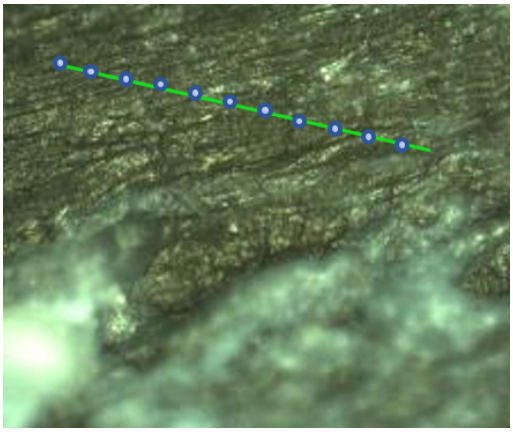

Figure 3.42: Tendon A optical picture. The dots are separated by 20 μm. The white part is adipose tissue or resin

.

Individual storage modulus frequency distribution shows even distribution except at the lowest values. This trend is not followed by the point 8 where the highest value (highest value in this particular histogram but low value compared to the main range) had the highest frequency and by the point 10 having higher frequency at third one $\sim$ 5.5 GPa and on the right side of the histogram $\sim 7GPa$. The storage modulus value range is from 0.5 to 11 GPa. Tan delta do not have the Gaussian curve shape for all the individual frequency distribution, some of them are more spread on the right side of the highest value, with mean values around 0.063 . The Gaussian curve shape has meant value around 0.043 . The data fusion does not highlight main values for storage modulus and tan delta.

Regarding the depth influence, the storage modulus follows exponentially decreasing by 50 $\%$, being more or less stable after 600 nm, except for 2 points which have increasing evolution but the indentation recording start at higher penetration depth. Also, we can observe than the indent tip went deeper with the decreasing initial storage modulus value recorded. The average curve show the clear decreasing tendency

with constant deviation. Regarding the tan delta, evolution are high frequency oscillations around 0.05 - 0.06 except for the two same points out of the trend as in the storage modulus representation. The average curve shows more constant behaviour than in bone or cartilage with a mean value at 0.053.

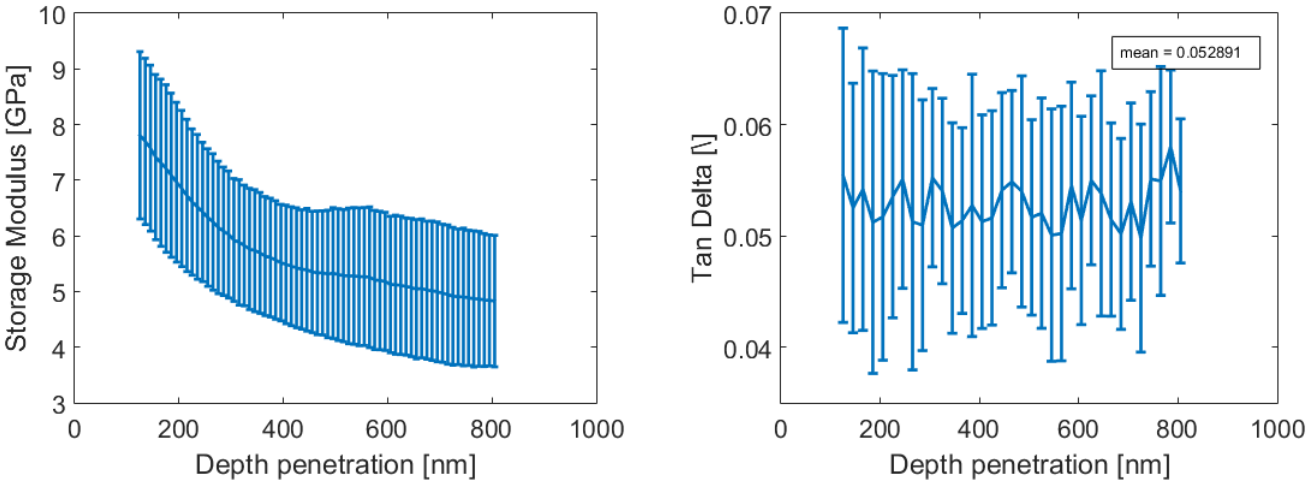

Figure 3.43: Tendon A Average Depth dependence, the two points having storage modulus below 2 GPa were excluded

The new frequency distribution along the whole indent line having penetration depth higher than 600 nm show flat distribution between 0.5 and 7 GPa with superior frequency at 3 GPa. Tan delta distribution shows low dispersion to the mean left side and low decreasing frequency to the right side, the mean being equal to 0.060

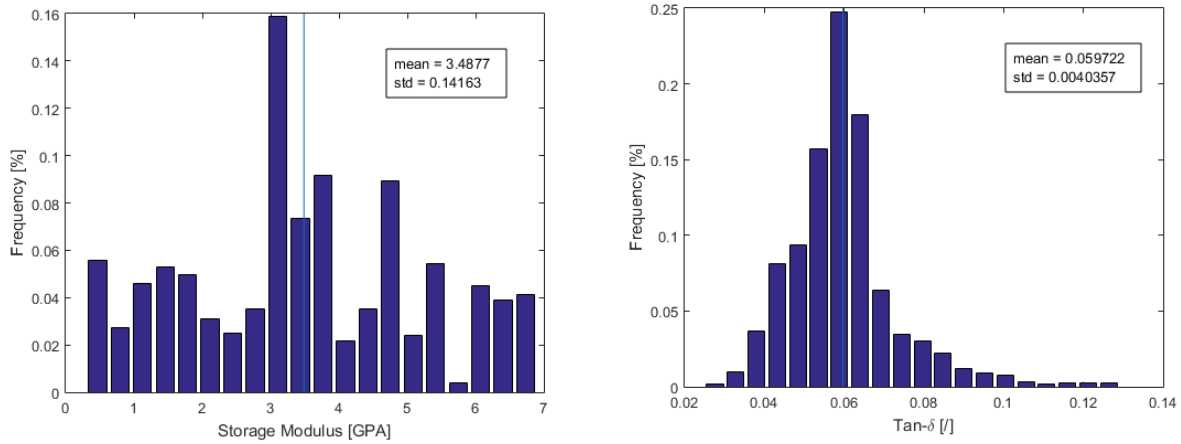

Figure 3.44: Tendon A Frequency distribution with data having penetration depth higher than 600 nm

Tendon B: Out of eleven indentation points, only one was not taken into account, due to unrealistic storage modulus value.

No main trend was observed in the individual histograms, either in storage modulus than in tan delta, even if tan delta presents more symmetrical behaviour.

Looking at the storage modulus depth dependence, the curves decline to bottom out at around 500-600 nm and increase gently after that point. The three curves having starting contact indentation after 1000 nm had bad displacement amplitude curves. Tan delta here again fluctuates closely to 0.05 between 0.02 and 0.06 .

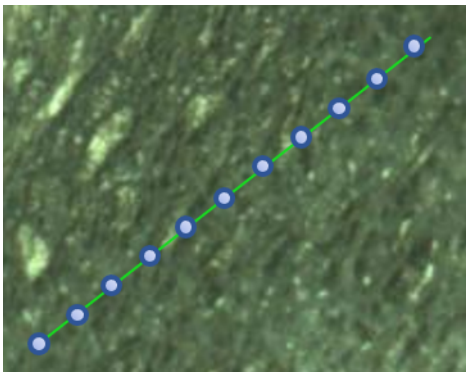

Figure 3.45: Tendon B optical picture

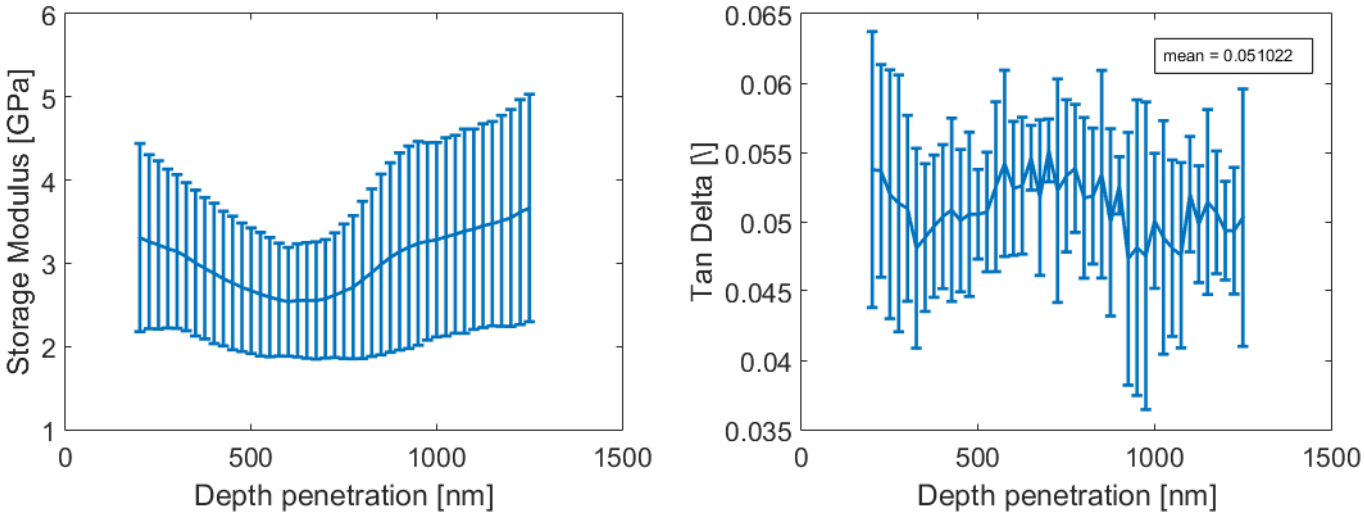

Figure 3.46: Tendon B Average Depth dependence, the two lines after 3000 nm were excluded

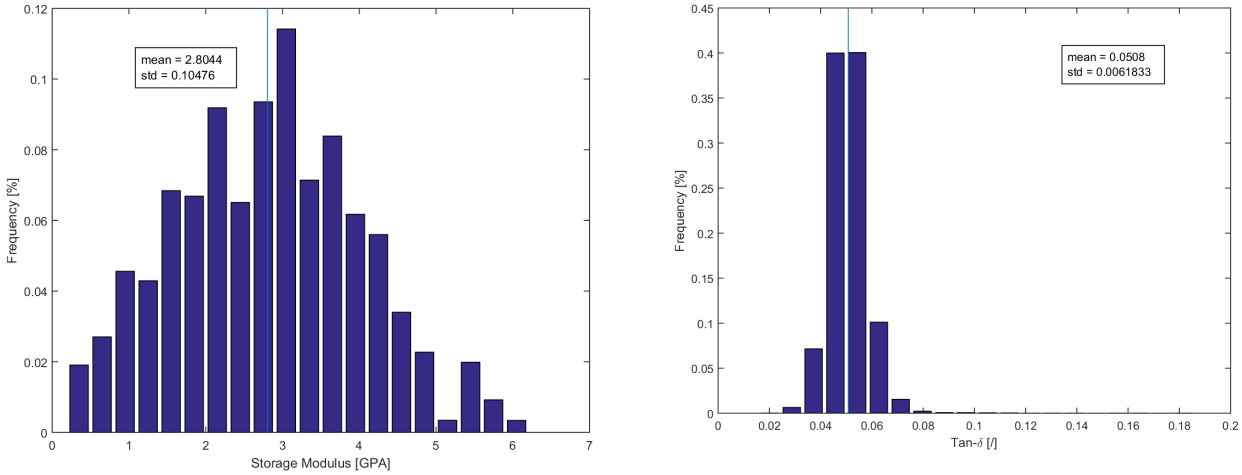

Figure 3.47: Tendon B Frequency distribution

Tendon C: The eleven points analysed in the Tendon C had good tip displacement amplitude during the indentations, being around 3 nm.

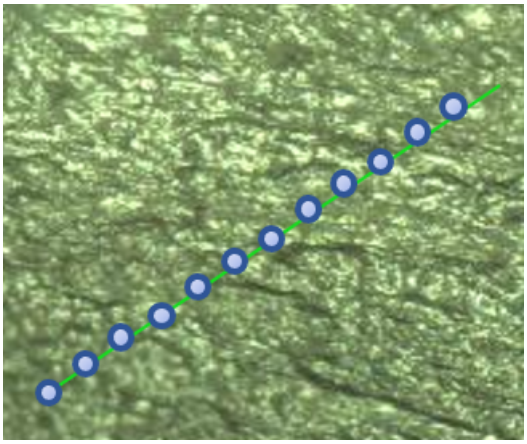

Figure 3.48: Tendon C optical picture

The storage modulus values range is between 3.5 and 22 GPa, no trends bring out from the individual frequency analysis. Those results are not expected for this region, tendon is known to have modulus $\sim$ 2 GPa. The depth dependence display a clear exponential decline from contact surfaces indents value (above 15 GPa) and slight decrease in the other locations. After 400 nm depth, all the lines go closer to 9 GPa, which it still seems very high for tendon. This trend is confirmed by the average curve, having higher deviation at the contact surface than in depth.

Regarding tan delta, the symmetrical Gaussian shape is again encountered with mean value around 0.054 in the histogram. The depth dependence shows also slight decrease through the depth with more constant behaviour after 400 nm. Tan delta decreases from 0.060 $\pm$ 0.005 to 0.055 $\pm$ 0.05 .

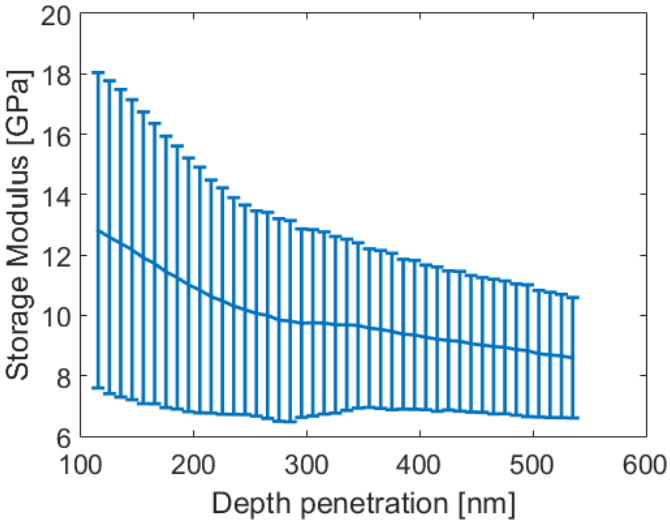

(a) Storage modulus

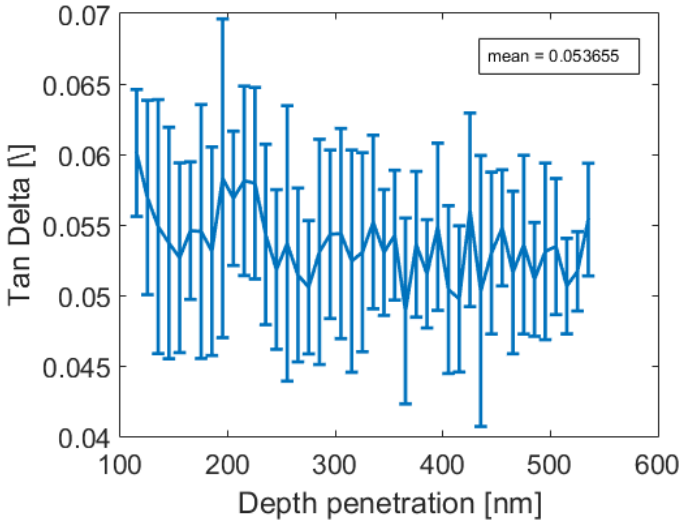

(b) Tan delta

Figure 3.49: Tendon C Average Depth dependence, the two lines below 2 GPa were excluded

Plotting data with higher depth than 400 nm expose storage modulus distribution from 4 to 11 with higher frequency around 8 GPa, the mean value is 7.59 GPa and tan delta Gaussian-like distribution around 0.053.

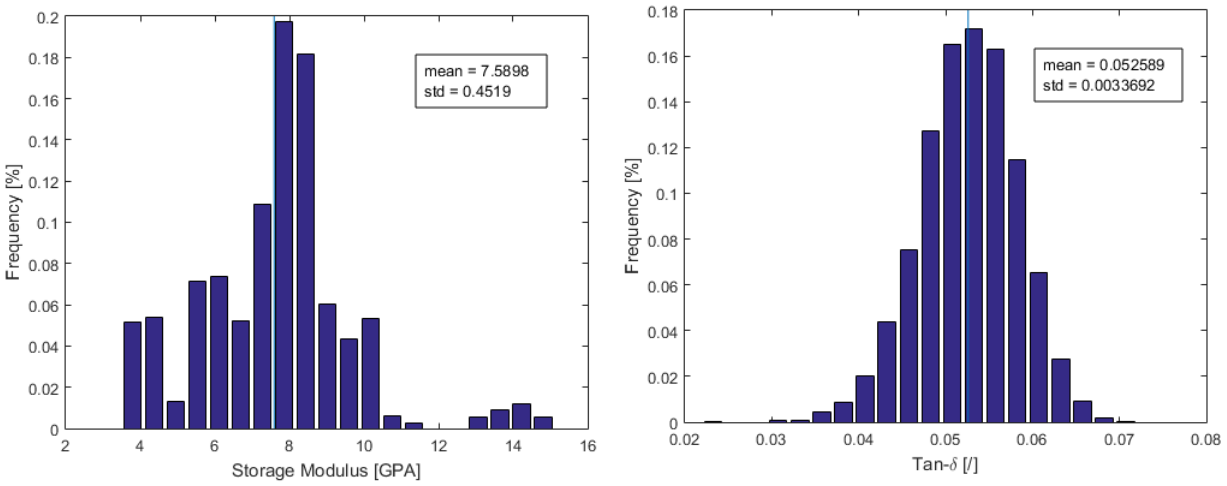

Figure 3.50: Tendon C Frequency distribution with data having higher penetration depth than 400 nm

Tendon: To sum up, tendons have more spread storage modulus values in frequency and thought the depth, with values between 0.5 and 19 GPa but the Tendon C seems to be less trustworthy than the two other. Tendon A and B have storage modulus values between 0.5 and 8 GPa in saw-tooth profile that could be caused by the fibres structure. About the tan delta, the values are between 0.04 and 0.07. The tan delta decrease when the storage modulus increase and inversely.

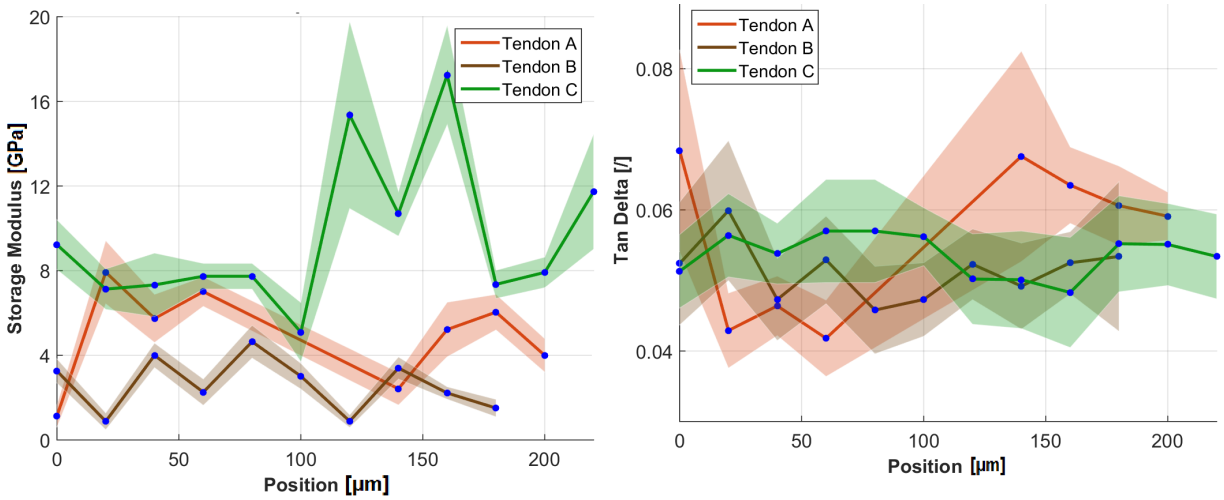

Figure 3.51: Properties evolution on a tendon indentation line, straight line represents the main values obtained by the histograms, the transparent part represents the standard deviation

Tendon	Storage modulus [GPa]		Tan delta [\]	
	mean	STD	mean	STD
A	3.49	0.14	0.0597	0.0040
B	2.80	0.10	0.051	0.0062
C	7.59	0.45	0.0526	0.0034

Table 3.6: Values from Tendon A, B and C histograms

3.4.4 Comparison

Bone, cartilage and tendon are three tissues with different composition and structure. To obtain a first draft of comparison, we looked at the Bone B, the Cartilage C and the Tendon B. The comparison of their storage modulus show three distinct ranges of values. The tendon has smaller values (less than 5 GPa) than cartilage (10-18 GPa) which have smaller average values than bone (19-21 GPa).

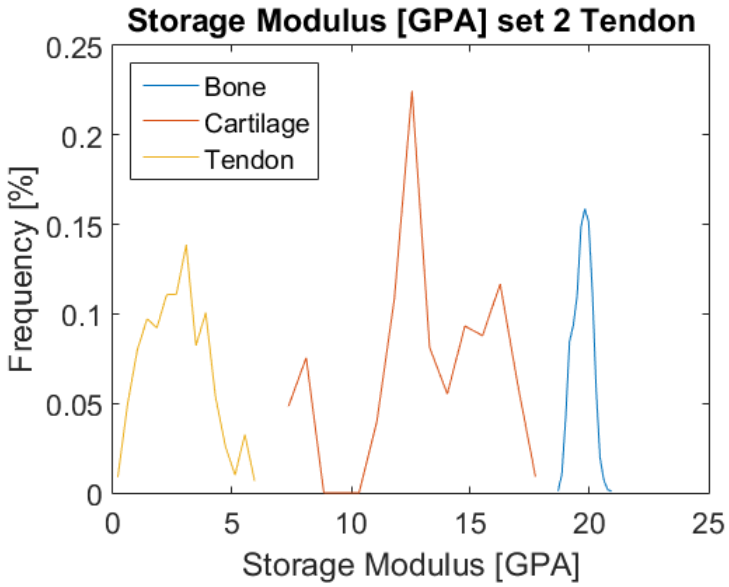

Figure 3.52: Storage modulus of Bone, Cartilage and Tendon. The lines presented are Bone B, Cartilage C and Tendon B. We think they represent more accurately their regions.

Concerning their tan delta, the values are closed with increasing average value from bone ($\sim$ 0.035) to tendon ($\sim$ 0.05)

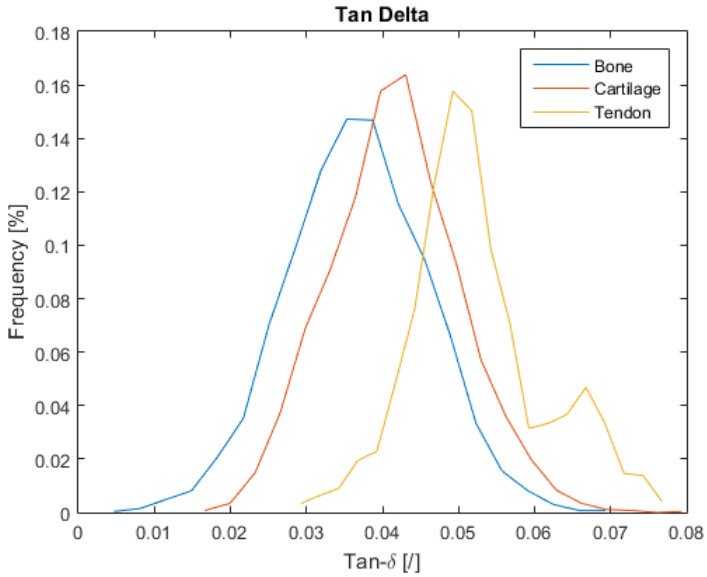

Figure 3.53: Tan delta of Bone, Cartilage and Tendon. The lines presented are the same that for fig. 3.52, namely Bone B, Cartilage C and Tendon B.

3.4.5 Enthesis interface DMA

This region was analysed in three samples but only the last one have great optical pictures with interdigitation and the right angle to see all the interface region.

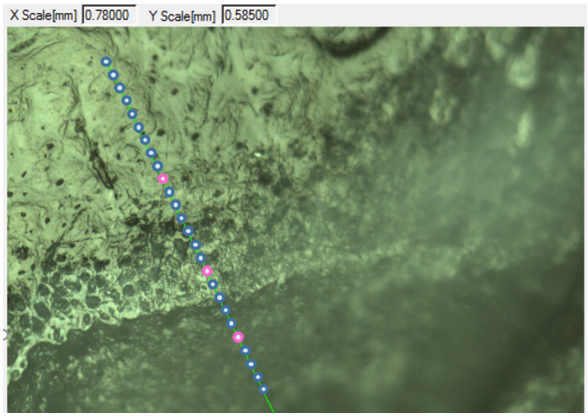

Figure 3.54: Enthesis interface A optical picture

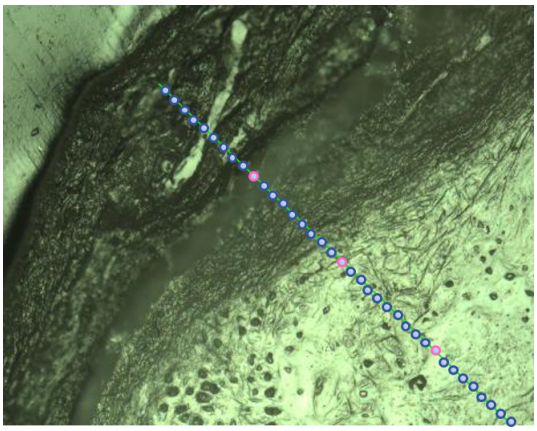

Figure 3.55: Enthesis interface B optical picture

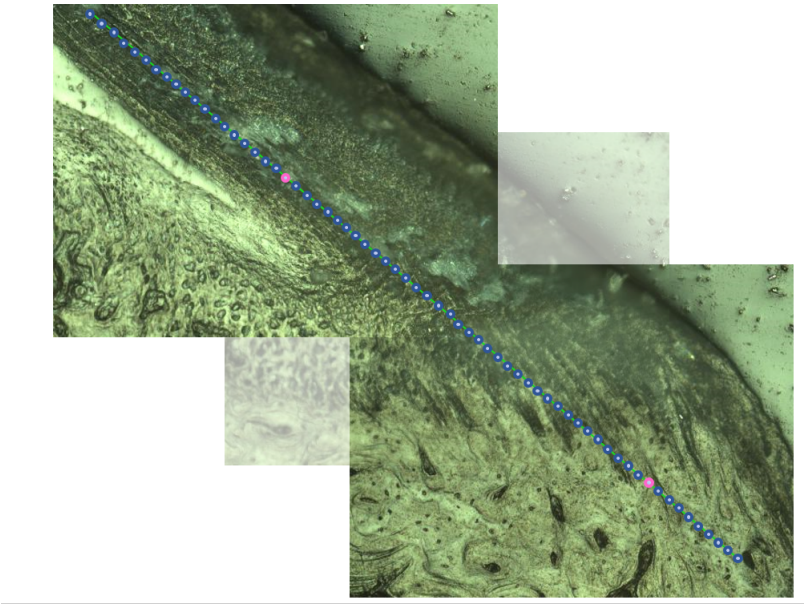

Figure 3.56: Enthesis interface C optical picture

The three interfaces shows a gradual storage modulus decrease from bone/cartilage to tendon. This trend is a bit less visible in the Interface C, because of the interdigitations going from location at 180 to 440 μm. Regarding the tan delta, it slightly increases through the interface from 0.04 to 0.06 and then reaches 0.04 in the tendon.

The depth dependence graphs show the same features as in pure tissues: storage modulus decreasing with the depth of initial values higher than 10 GPa and increasing or remain stable for initial values lower than 10 going deeper than the previous point. Concerning the tan delta, we still have the funnel shape graph.

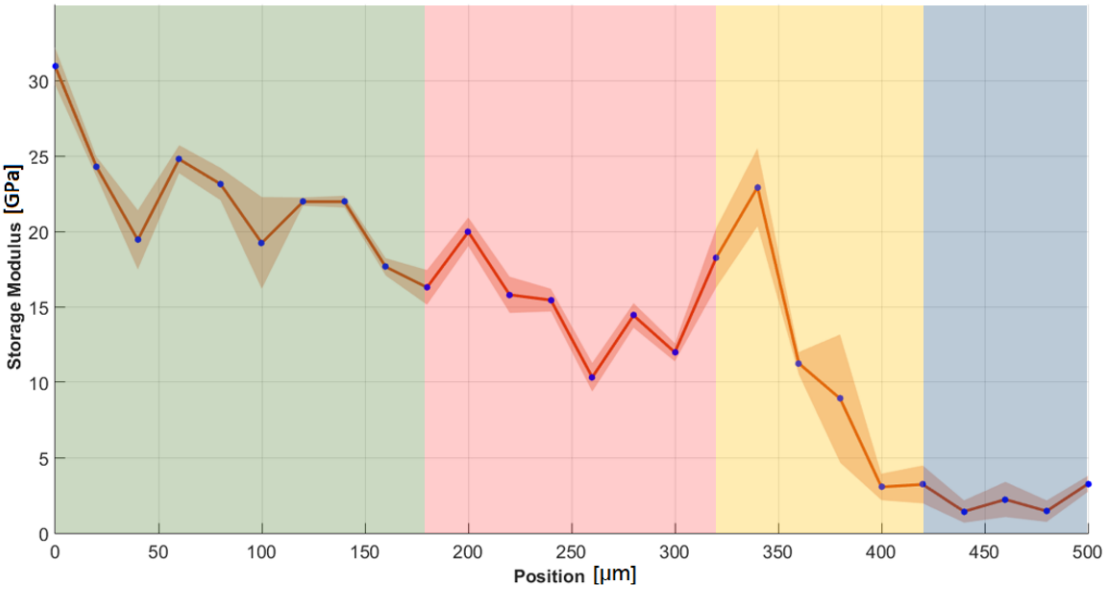

Figure 3.57: Enthesis interface A storage modulus evolution

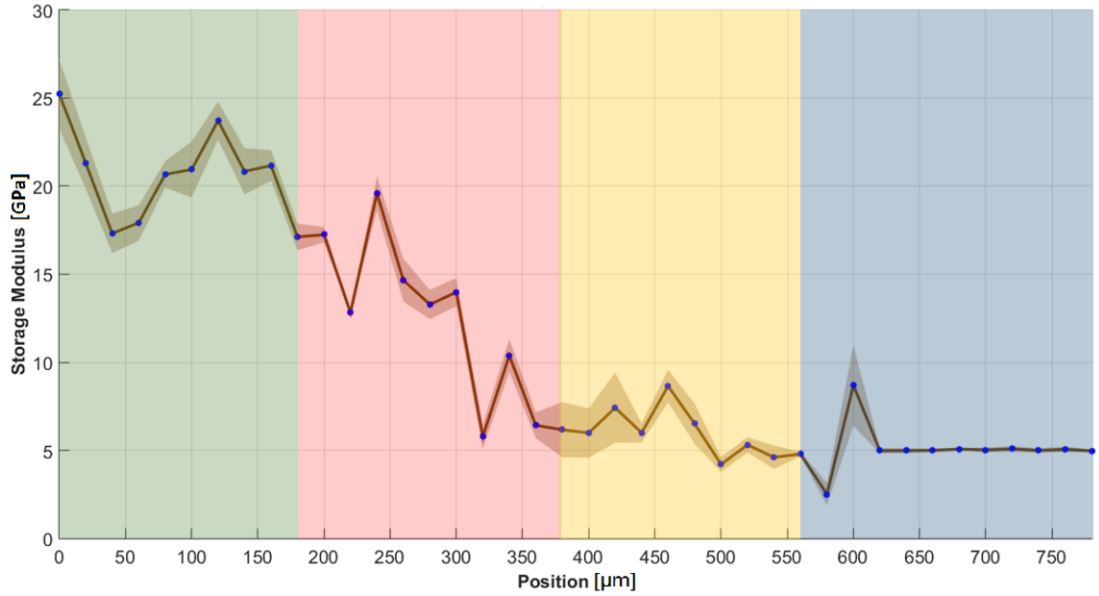

Figure 3.58: Enthesis interface B storage modulus evolution

3.4.6 Periosteal interface DMA

The Periosteal Interface B has better optical pictures and results, we focus only on this sample to present this region.

The mechanical transition between the bone and the cartilage show a sharp storage modulus decline starting at 24 GPa to reach 4 GPa at a distance of 250 μm. The cartilage has constant value at 4 GPa. Tan delta starts at low value (0.04) and reach 0.08 after the same distance. The evolution of the cartilage is not as constant as for the storage modulus, inducing change in the loss modulus. The same trend is followed as in the other regions for the depth dependence.

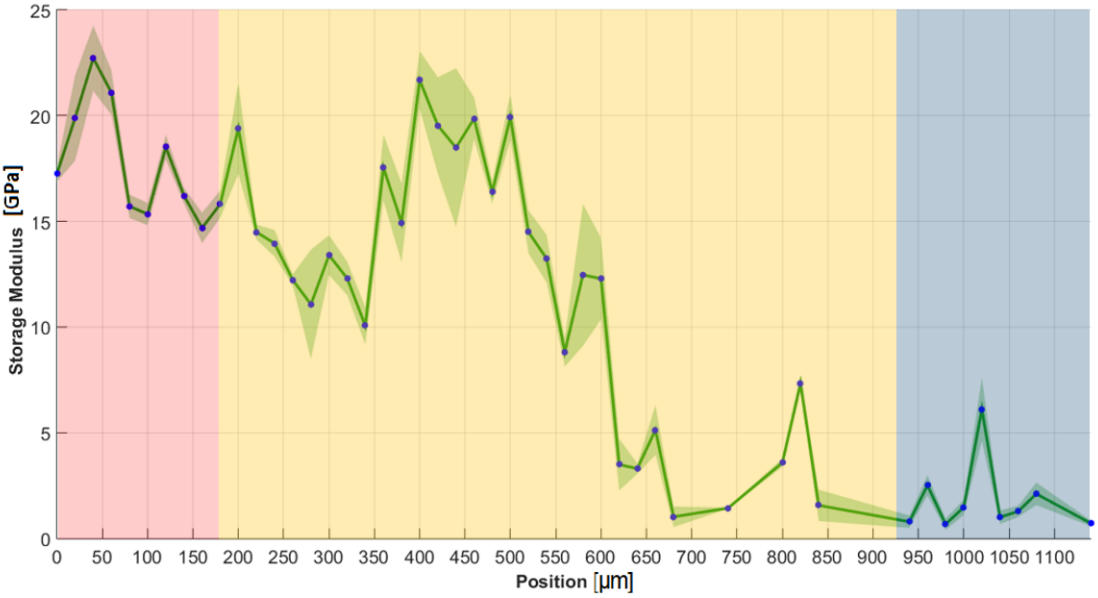

Figure 3.59: Enthesis interface C storage modulus evolution

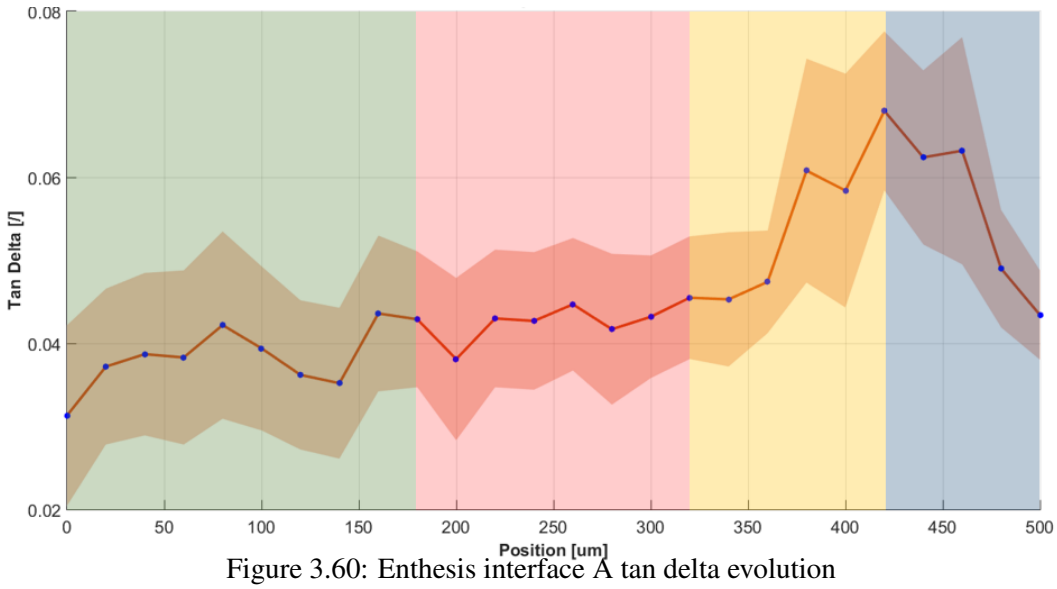

Figure 3.60: Enthesis interface A tan delta evolution

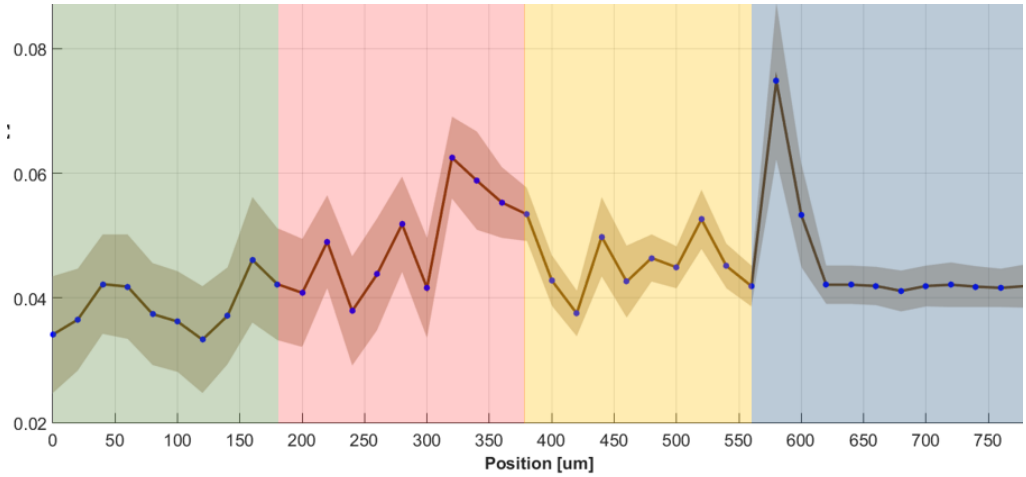

Figure 3.61: Enthesis interface B tan delta evolution

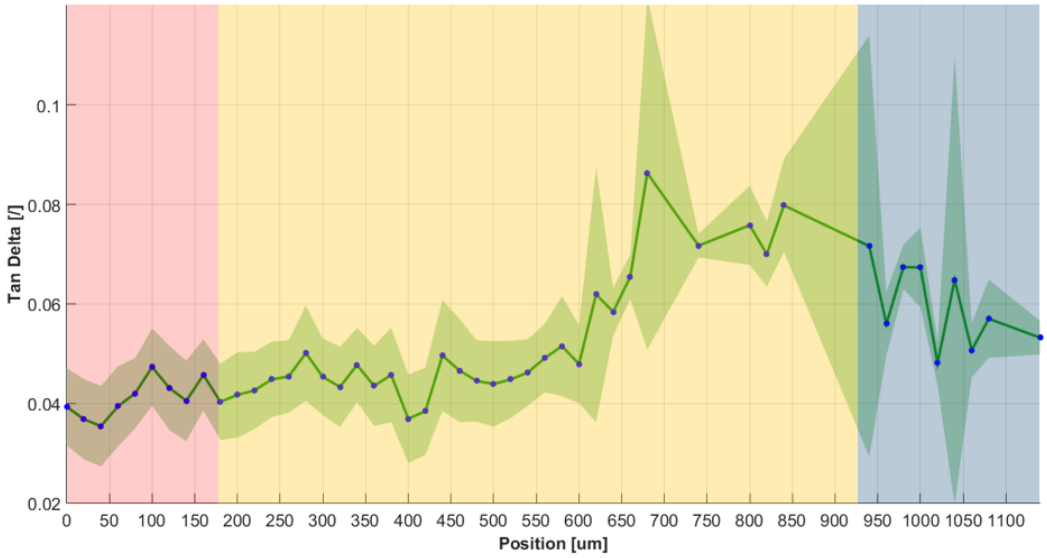

Figure 3.62: Enthesis interface C tan delta evolution

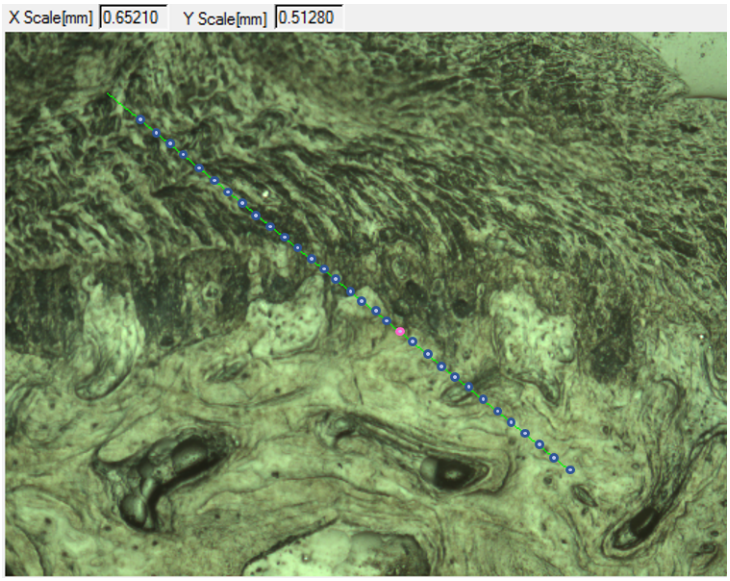

Figure 3.63: Periosteal interface: optical picture

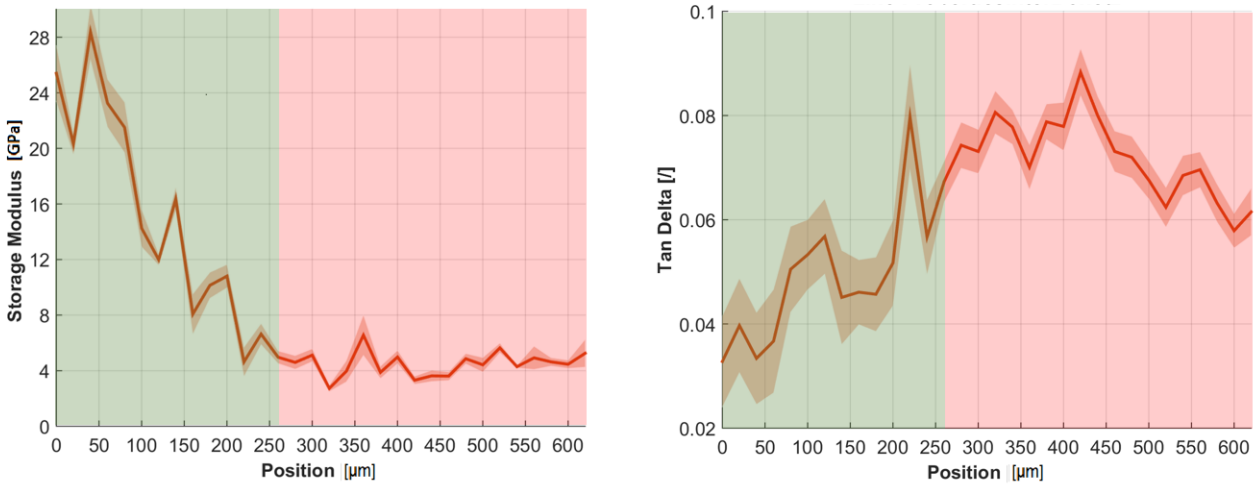

Figure 3.64: Periosteal interface B: storage modulus and tan delta evolution

4. Discussion and conclusions

The purpose of this chapter is to provide a critical review of the results and highlight most relevant findings. Comparison with current literature is not easy as articles on this topic are sparse. Tendons and tendons side interfaces are less investigated in literature and were challenging. The most part of the protocol research was focus on the soft tissue. To our knowledge, dynamic nanoindentation analysis on Achilles' tendon enthesis was not done yet before.

Histology The decalcification protocol was not optimal. Indeed, the bones were tested by pushing a wooden stick into the bone. If the stick sinks in it, the decalcification is complete. For our sample, the stick sank only at the bone surface, not in depth. The decalcification was performed with formic acid. New decalcification protocols need to be trying to obtain depth decalcification. Other products can be used as chromic acid 3%, saturated solution of picric acid with alcoholic washing bath or even nitric acids 1-2% but they might create tissue damages [49].

The most suitable protocol might be neutral EDTA at pH 7. This chelating agent capture the calcium ions from the surface of the apatite crystal. The action is very slow (few weeks) but harmless for the tissues, the stains are unaffected by this process. It works more rapidly at pH 10 but some tissue elements can be damaged by alkaline pH [50].

Even if most of the pictures obtained by this technique were not exploitable, some of them show the different orientations of collagen fibres from the tendon to bone. They are well aligned with the tendon. The alignment degree decline in the interface and the fibres have totally random orientations. This loss of alignment is believed to make the interface even more compliant than tendons to absorb deformation energy [9].

Indentation The nanoindentation of tendons and entheses are not common, and thus there is no sample preparation standardise protocol. The first step was to extract the samples from the rats. Fresh rats were easier to scalp than frozen rats and had fewer adipose tissues stick to the tendon. Then, the dehydration and embedding protocol must include impregnation step to diminish the surface deterioration during the SPM. This step was not optimal. Indeed, the SPM in soft tissues did not show similar forward and reverse scanning lines. changing the resin did not improve much this issue. However, soft tissues are naturally compliant, new embedding protocols may not change this.

Then, the polishing step was performed with several grids and suspensions. To validate our polishing protocol, we have done depth analysis. The protocol suits perfectly for bones and cartilage but a bit less for tendons and interfaces, having higher fluctuations in roughness, even after tilt correction. More than that, this analysis shows that the bone seems to have been removed by the polishing at the resin contact. The same behaviour has been seen with cartilage - resin interfaces.

We accepted the quasistatitic nanoindentation results of the sample S4. The reduced modulus measured had similar values as in bulk materials [2]. The enthesis interface roughness analysis showed that almost all the points had acceptable roughness. The reduced modulus evolution shows a clear decrease through the interface. This behaviour was also observed by [32]. Since we had SPM issues, we consider using DMA to minimise the influence of high roughness.

DMA shows a depth influence in all the pure tissues for the storage modulus. The values recorded decrease in depth till around 350 nm. The decrease is about 10 $\%$ in bone, 12 $\%$ in cartilage and 30 $\%$ in tendons. The behaviour is in opposition to the conclusion given by Mittra and al. saying that there is no depth influence in trabecular bone elastic modulus [51]. Tan delta dependence is less pronounced.

In bone, the average storage modulus is at 19-20 GPa on sample D1 and 16-18 GPa on sample D2, with very low standard deviation. The second sample was prepared months ago by Cristina Gatti, Erasmus student of Prof. *D. Ruffoni*. Gibson and al. shows that this delay influence the recorded data. In fact, nanoindentation studies should be done within 6 months after embedding [51] [21]. The loss modulus is very close to 0.039 for all the indentation points.

In mineralized cartilage, the storage modulus is included in a large range of value with sharp variations along the indentation lines varying from 9 to 21 GPa. This may be due to the local mineral contents. The viscoelastic behaviour described by the tan delta measurements is slightly more important than in bone being at $\sim$ 0.043 in pure cartilage. Tendon shows even more viscoelastic behaviour with tan delta higher than 0.05 and storage modulus lower than 10 GPa. Tendon had higher values of material properties than described in literature. This might be due to several reasons. Firstly, tendon and cartilages are tissues characterized by large amounts of water, the dehydration may influence the properties [35, 52]. Secondly, the mechanical properties of tendon and cartilage depend on the collagen fibres orientation, they are anisotropic materials. The collagen orientations were not known prior each indentation points. Indentation study on single fibrils of collagen by AFM reported values of Young's modulus between 5GPa – 11.5 GPa [53].

Comparing the results obtained on these three tissue types, the viscoelastic behaviour is more seen in tendon than in bone, tendon have more tendency to dissipate than to store energy. This observation is in agreement with tendon composition. Indeed, tendons, containing elastin and proteoglycan which interacting with water, are flexible to transmit the muscle forces. Bones are more elastic with low viscoelastic behaviour to support the body weight.

As hypothesised, periosteal interface has abrupt storage modulus transition in opposition to enthesis interface having gradual transition. This two closed but distinct regions have different functions. Periosteal fibrocartilage facilitates the sliding of the tendon on the bone surface. Enthesis allows a proper load transfer from the tendon to bone, and so gradual mechanical properties transition to reduce stress concentration and failure risks. Transition occurs in thicker area for entheses ($\sim$ 350 μm) than for periosteal interface ($\sim$ 100 μm).

5. Conclusion

This master thesis study the interface between Achilles' tendon and calcaneus bone at nano-scale. This insertion zone is a complex structure linking two dissimilar tissues with Young's modulus mismatch of two orders of magnitude. Bone is a stiff and tough material having a Young's modulus of 20 GPa and tendon is a soft connective tissue with Young's modulus of 0.5-2 GPa. Such properties dissimilarity is known to induce stress concentration. However, the specific structure of entheses create a gradient of mechanical stiffness that avoids traumatic injury, reducing the concentration of stress at the interface.

The aim of this master thesis was to better understand the mechanical properties of the entheses, connecting soft tissue to bone, to reach their efficiency. New approach is proposed to investigate this tissue consisting of dynamic mechanical analysis.

First, we have been able to develop a protocol for sample preparation and nanoDMA on soft tissues, bones and interfaces. Improvement can still be done by changing the resin and increasing the curing time. The results obtained on bone, cartilage and tendon are in agreement with current literature. The mechanical gradient comparison between periosteal cartilage and fibrocartilage show different behaviour as expected. The fibrocartilage contained at the enthesis present gradual decrease of stiffness from bone to the tendon to reduce stress concentration and failure risks in opposition to the periosteal interface which has abrupt transition because no force transmission is done in this area. The main function of the periosteal cartilage is to facilitate sliding of the tendon on the calcaneus bones surface.

Second, the histological investigation protocol need some improvements to decalcify the tendon - bone complex properly in order to reduce the tendon tearing from the bone during microtome cut.

Further research are needed to complete this introductory study, using more samples. Also, to have a global understanding of this area, using hydrated sample and composition investigations with Raman spectroscopy.

A. Surface properties

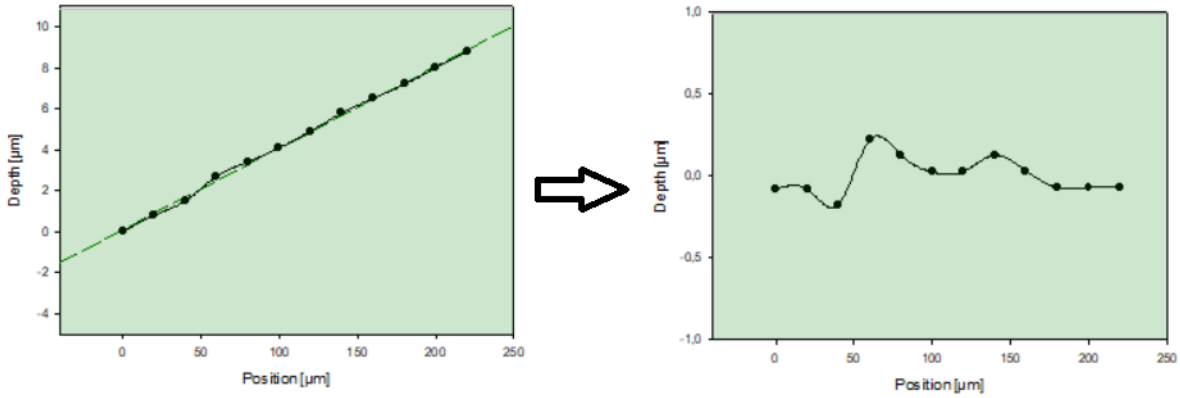

Figure A.1: Depth evolution and correction on the sample S4, bone region

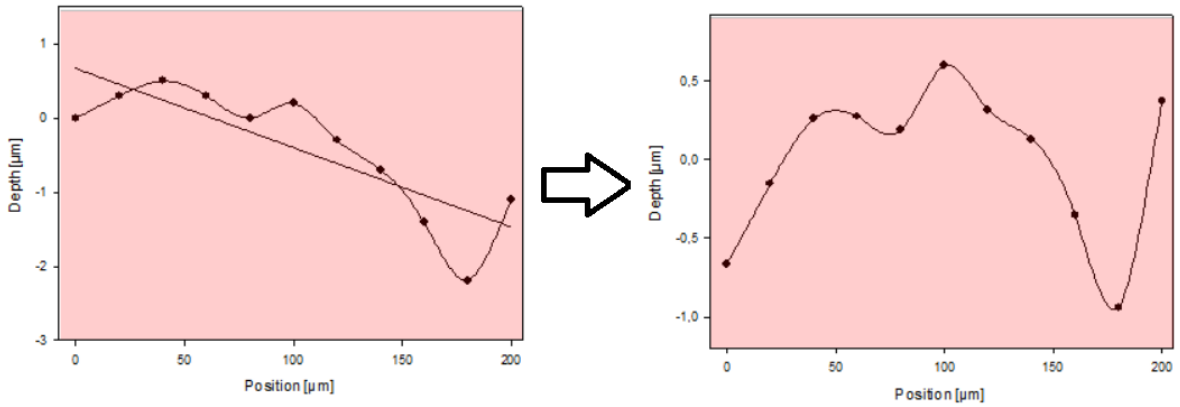

Figure A.2: Depth evolution and correction on the sample D2, cartilage region

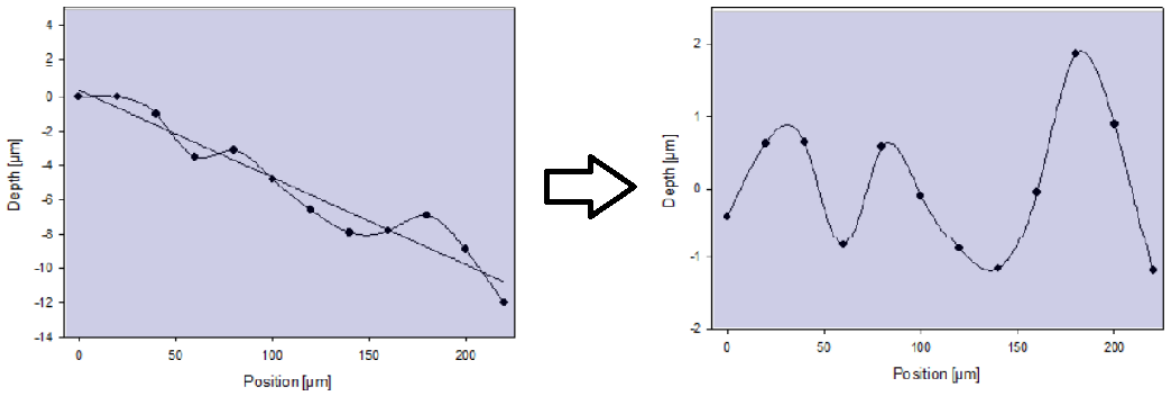

Figure A.3: Depth evolution and correction on the sample D2, tendon region

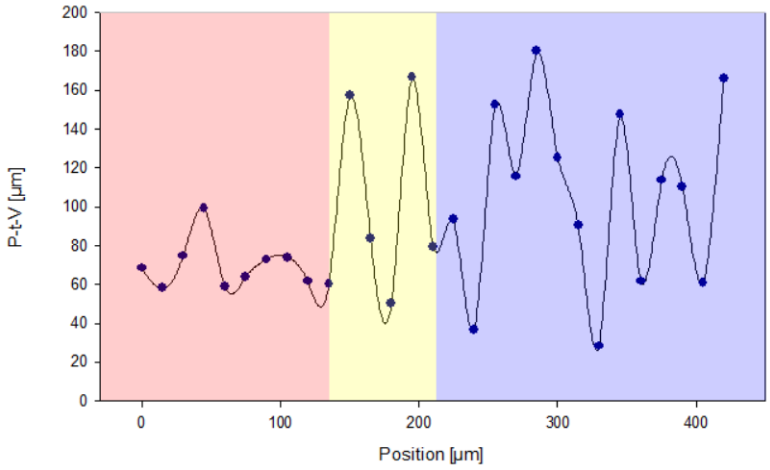

Figure A.5: Sample S4 Peak-to-Valley measurement on the fibrocartilage interface

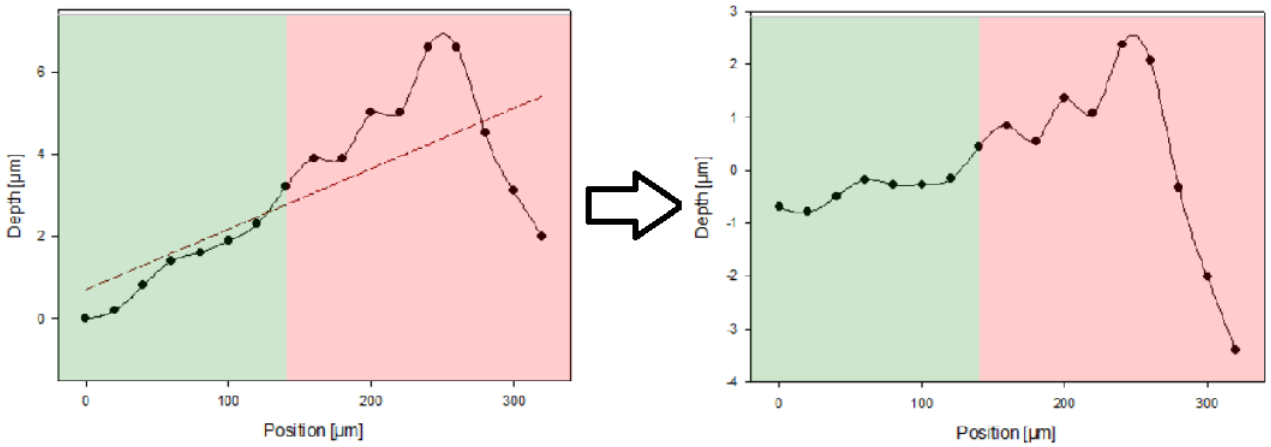

Figure A.4: Depth evolution and correction on the sample D2, interface between periosteal fibrocartilage and bone

B. Raman Spectroscopy

Raman spectroscopy is a non-contact and non-destructive observation and characterization technique based on the Raman effect, namely inelastic light scattering process. It is commonly used to provide a structural fingerprint by which molecules can be identified. Components distribution maps can be made by Raman spectroscopy analysis. Using monochromatic incident light exciting the molecules, data are collected from the scattered light having different wavelengths from the incident light, providing information on the molecular vibration and crystal structure. Indeed, the photon energy gain or loss during the process is seen as an energy change, and so wavelength change, of the irradiating photon. The amount of energy corresponds to a particular bond in the molecule. Most of the diffusive photons do not have energy change, this is the Rayleigh scattering. The small number of photons having energy change are registered to form the Raman spectrum of emission. This spectrum is noised by fluorescence, which can be very intense. Background baseline must be subtracted in order to extract the proper Raman signal. Optimized precision instruments must be used to detect the weak Raman signal. Raman spectrum gives qualitative measurement. Quantitative measurement cannot be obtained without baseline correction, known reference samples and spectrum normalization.

Raman spectroscopy analysis is influenced by the laser type and the associated wavelength λ, regarding the sensitivity, the spatial resolution and the result optimization. Raman scattering intensity is proportional to λ^{-4}. Green lasers have greater scattering intensity than infrared lasers. Spite of green lasers have intense Raman signal, the fluorescence is also at high intensity [54]. A filter is used to remove the incident light wavelength from the Raman spectrum.

This technique is useful for the study of composite material, either organic and inorganic sample. Study of dead cells is as possible as living cells or in vivo [55, 56].Nonetheless, metals and alloys cannot be analysed with Raman spectroscopy because the reflected light intensity obstruct the detector and, more than that, it is really difficult to see their molecules vibration resulting in a change in the polarizability of the molecules [57] although organic samples are much studied by Raman, vascular tissues bring a lot of undesirable fluorescence, which can make difficult the background subtraction under 532 nm excitation. Raman spectroscopy allows the analysis of samples that can be in different states such as liquid or solid and which do not need preparation, except maybe being a glass or transparent polymer mounted. Also, this technique is compatible with water (in opposition to Fourier Transform InfraRed spectroscopy), allowing the investigation of hydrated samples. Despite the non-specific preparation needs, the surface roughness influence the spectrum, it must be controlled to be lower than 1 μm [**?**].

The Raman spectrum is presented as light intensity versus Raman wavelength shift expressed in δcm^{-1} and it is normalized. Raman spectra can be recorded over a range of 4000 to 10 cm^1. Positions and intensities of the several pics allow the identification of the components. Some components, as collagen or bone, have specific bands of identification and can be easily recognized by the spectrum i.e. bone has

specific band a 960 cm^{-1} for P-O stretching band of hydroxyapatite. However, sometimes no specific band can be recognized because of overlapping. In this case, the spectrum is decomposed into a sum of spectra to identify several components.

Regarding entheses investigations, Raman spectroscopy shows a mineral concentration across the tendon-to-bone interface. The study of Schwartz and al. focus on the degree of mineralization and the spatial distribution of minerals in the tissue of murine supraspinatus. They said that no spectral differences were observed between fibrocartilage and tendon in the non-mineralized tissue but there is an increase in mineral content across the tendon-to-bone interface. However, the results seem contradictory to the histologic analyses, maybe due the sensitivity of the two techniques [58].

C. Matlab Codes

Listing C.1: main.m

```
clear all;close all;clc

%%%%%%%%%%%%%%%%% BEGIN PARAMETERS %%%%%%%%%%%%%%%%%

nbins=20; %Number of bin in histogram
Number_Set=[4;2;3;3;2]; %Total number of Set by Region
%PARAMETERS IN filtred_data.m !!!

%%%%%%%%%%%%%%%%% END PARAMETERS % %%%%%%%%%%%%%%%%%

Region={'Bone';'Cartilage';'Tendon';'Interface';'InterBone'}; %Region
    of indentation
s1='C:\Users\Une petite bretzelle\Dropbox (ChaBen)\TFE\5-NANO\
    DMA_Text_Files+Matlab\'; %begin of access path
%%%%%%%%%%%%%%%%% EXTRACT DATA %%%%%%%%%%%%%%%%%
%value = [Set,Properties,data, if X=1 Height X=2 Centers]
Values_Bone      = Get_Data_By_Region(Region{1},Number_Set(1),nbins,
    s1);
Values_Cartilage = Get_Data_By_Region(Region{2},Number_Set(2),nbins,
    s1);
Values_Tendon    = Get_Data_By_Region(Region{3},Number_Set(3),nbins,
    s1);
Values_Interface = Get_Data_By_Region(Region{4},Number_Set(4),nbins,
    s1);
Values_InterBone = Get_Data_By_Region(Region{5},Number_Set(5),nbins,
    s1);
%%
%%%%%%% GRAPH TO PLOT %%%%%%%%%%%%%%%%%
%%%s1,num_figure,Values_X,Region{},num_set,num_propertie,save,dim,
    setfinal

%Region: 1=BONE 2=CARTILAGE, 3=TENDON, 4=INTERFACE
%num_set: # of chosen set. If combinaison of all set, num_set=
    Number_set +1
%num_propertie: 1=StorM 2=LossM 3=Hard 4=Tan
%save: 'y'=yes 'n'=n
```

```
28 %setfinal: 1=yes 0=no (to change graph title) and save location
29 % S=1;
30 % T=0;
31 % dim = [0.65 0.55 0.4 0.3];      %dimension to display mean in
       histograms dim = [x y w h]
32 % PlotHisto(s1,1,Values_Bone,Region{1},S,1,'n',dim,T);
33 % saveas(gcf,strcat(s4,'\BoneSet',num2str(S),'StorM350','.png'))
34 % dim = [0.65 0.55 0.4 0.3];
35 % PlotHisto(s1,4,Values_Bone,Region{1},S,4,'n',dim,T);
36 % saveas(gcf,strcat(s4,'\BoneSet',num2str(S),'Tan350','.png'))
37 % dim = [0.65 0.55 0.4 0.3];
38 % PlotHisto(s1,2,Values_Bone,Region{1},S,2,'n',dim,T);
39 % dim = [0.28 0.55 0.4 0.3];
40 % PlotHisto(s1,3,Values_Bone,Region{1},S,3,'n',dim,T);
41
42 %%
43 %%figure,valuer,Region,num_set,num_propertie,save,setfinal
44 % p=4;
45 % PlotLine(1,Values_Bone,Region{1},1,p,0,0)
46 % hold on
47 % PlotLine(1,Values_Bone,Region{1},2,p,0,0)
48 % hold on
49 % PlotLine(1,Values_Bone,Region{1},3,p,0,0)
50 % hold on
51 % PlotLine(1,Values_Bone,Region{1},4,p,0,0)
52 % hold on
53 % PlotLine(1,Values_Cartilage,Region{2},1,p,0,0)
54 % hold on
55 % PlotLine(1,Values_Cartilage,Region{2},2,p,0,0)
56 % hold on
57 % PlotLine(1,Values_Cartilage,Region{2},3,p,0,0)
58 % hold on
59 % PlotLine(1,Values_Tendon,Region{3},1,p,0,0)
60 % hold on
61 % PlotLine(1,Values_Tendon,Region{3},2,p,0,0)
62 % hold on
63 % PlotLine(1,Values_Tendon,Region{3},3,p,0,0)
64 % title('Storage Modulus')
65 % title('Tan Delta')
66 % legend('Bone','Cartilage','Tendon', 'Location','NorthWest' )
```

Listing C.2: Get-Data-By-Region.m

```
1 function [ Values ] = Get_Data_By_Region( Region,Number_Set,nbins,s1
```

```
    )
%Get_Data_By_Region Summary
%   Put every Histogram data in Values by set and with TotalSet
%
%   1) For all Sets, take data from fct filtred_data and create
    histograms
%   values (height and center).
%   2) These data are put into Values Matrix (out of the loop)
%   3) The combinaison of all is put in Number_Set+1
if Number_Set>0
    for i=1:Number_Set
        Data_byset = filtred_data(Region,i,s1);
        Values(i,:,:,:)=getHistdata(Data_byset,nbins);
        if i>1
            Data=cat(2,Data,Data_byset);
        else
            Data=Data_byset;
        end
    end
    Values(Number_Set+1,:,:,:)=getHistdata(Data,nbins);
else
    Values=0;
end
end

function V=getHistdata(Data,nbins)
for i=1:size(Data,1)
    [V(i,:,1),Edges(i,:)] = histcounts(Data(i,:),nbins);
    V(i,:,2) = (Edges(i,1:end-1) + Edges(i,2:end))/2;
end
end
```

Listing C.3: filtred-data.m

```
function [ WorkData] = filtred_data( Region,Set,s1)
%Filtred_data Summary
%   Extract data from Txt files by Set of sample with the right
    parameters
%
%   1)Case by set of data: Bone, Cartilage, Tendon then Interface
%   case EXAMPLE
%         Number=11; Total number of files in this set
%         Check_all_file=0; 1=all data 0=some of the data
%         Fichier=[2;4;6;7;10]; If Not all data, these ones
```

```
10 %          BeginTime = [4;4;4;4;4]; %[s] Beginning time for each file
11 %          MinContDepth=80; %[nm] Minimum contact depth to keep
12 %          s2 = '\Bone';      s2 and s4 to have the right path access
13 %          s4 = '_000_DYN.txt';
14 %
15 %    2)Open and read the complete data
16 %    3)Filter the data with BeginTime and MinContDepth
17 %    4)Extract the wanted data (the Properties)
18
19
20 Sample= strcat(Region,'\',num2str(Set));
21
22 switch Sample
23     %%%%%%%%%%%%%%%%%%%%%%%%%%%%%%%% PARAMETERS TO SET
           %%%%%%%%%%%%%%%%%%%%%%%%%%%%%%%%
24
25     %%%%%%%%%%% BONE %%%%%%%%%%%
26     case 'Bone\1'
27         Check_all_file=1;
28         Number=11;
29         BeginTime = [4;4;4;4;4;4;4;4;4;4;4]; %[s] Beginning time for
               each file
30         MinContDepth=70; %[nm] Minimum contact depth to keep
31         s2 = '\ba';
32         s4 = '_000_DYN.txt';
33
34     case 'Bone\2'
35         Check_all_file=1;
36         Number=11;
37         BeginTime = [4;4;4;4;4;4;4;4;4;4;4]; %[s] Beginning time for
               each file
38         MinContDepth=70; %[nm] Minimum contact depth to keep
39         s2 = '\bb';
40         s4 = '_000_DYN.txt';
41
42     case 'Bone\3'
43         Check_all_file=1;
44         Number=12;
45         BeginTime = [4;4;4;4;4;4;4;4;4;4;4;4] ; %[s] Beginning time
               for each file
46         MinContDepth=60; %[nm] Minimum contact depth to keep
47         s2 = '\ba';
```

```
48          s4 = '_000_DYN.txt';
49
50      case 'Bone\4'
51          Check_all_file=1;
52          Number=12;
53          BeginTime = [4;4;4;4;4;4;4;4;4;4;4;4]; %[s] Beginning time
                for each file
54          MinContDepth=80; %[nm] Minimum contact depth to keep
55          s2 = '\bb';
56          s4 = '_000_DYN.txt';
57
58
59          %%%%%%%%%%%% CARTILAGE %%%%%%%%%%%%
60  %     case 'Cartilage\1'
61  %         Check_all_file=1;
62  %         Number=11;
63  %         BeginTime = [4;4;4;4;4;4;4;4;4;4;4];
64  %         MinContDepth=80;
65  %         s2 = '\ca';
66  %         s4 = '_000_DYN.txt';
67  %
68      case 'Cartilage\1'
69          Check_all_file=0;
70          Fichier=[1,2,3,4,5,6,8,9,10];
71          Number=11;
72          BeginTime = [4;4;4;4;4;4;4;4;4;4;4];
73          MinContDepth=80;
74          s2 = '\cb';
75          s4 = '_000_DYN.txt';
76
77      case 'Cartilage\2'
78          Check_all_file=1;
79          Number=11;
80          BeginTime = [4;4;4;4;4;4;4;4;4;4;4];
81          MinContDepth=100;
82          s2 = '\ca';
83          s4 = '_000.tdm_DYN.txt';
84
85
86          %%%%%%%%%%%% TENDON %%%%%%%%%%%%
87      case 'Tendon\1'
88          Check_all_file=0;
```

```
89          Fichier=[1,2,3,4,8,9,10,11];
90          Number=11;
91          BeginTime = [20;4;4;4;13;4;4;4];
92          MinContDepth=120;
93          s2 = '\ta'; s4 = '_000_DYN.txt';
94
95      case 'Tendon\2'
96          Check_all_file=0;
97          Fichier=[1,2,3,4,5,6,7,8,9,10];
98          Number=11;
99          BeginTime = [4;23;4;4;4;4;25;4;4;14] ;
100         MinContDepth=200;
101         s2 = '\tb'; s4 = '_000_DYN.txt';
102
103     case 'Tendon\3'
104         Check_all_file=1;
105         Number=12;
106         BeginTime = [4;4;4;4;4;4;4;4;4;4;4;4] ;
107         MinContDepth=115;
108         s2 = '\ta'; s4 = '_000.tdm_DYN.txt';
109
110         %%%%%%%%%% INTERFACE %%%%%%%%%%
111     case 'Interface\1'
112         Check_all_file=0;
113         Fichier=[1,2,3,4,5,6,7,8,9,10, 11,12,13,14,15,16,17,18,19,20,
                21,22,23,24,25,26];
114         Number=29;
115         BeginTime = [4;4;4;4;4;4;4;4;4;4; 4;4;4;4;4;4;4;4;4;4;
                4;12;22;22;20;4];
116         MinContDepth=100;
117         s2 = '\Ia';
118         s4 = '_000_DYN.txt';
119
120     case 'Interface\2'
121         Check_all_file=1;
122         Number=40;
123         BeginTime = [4;4;4;4;4; 4;4;4;4;4; 4;4;4;4;4; 4;4;4;4;4;
                4;4;4;4;4; 4;4;4;4;4; 4;4;4;4;4; 4;4;4;4;4;] ;
124         MinContDepth=100;
125         %except 24/140 27/120
126         s2 = '\ia';
127         s4 = '_000_DYN.txt';
```

```
128
129     case 'Interface\3'
130         Check_all_file=0;
131         Number=65;
132         Fichier=[1,2,3,4,5,6,7,8,9,10, 11,12,13,14,15,16,17,18,19,20,
                21,22,23,24,25,26,27,28,29,30, 31,32,33,34,35,38,
               41,42,43,48,49,50, 51,52,53,54,55,58] ;
133         BeginTime =
               [4;4;4;4;4;4;4;4;4;4;4;4;4;4;4;4;4;4;4;4;4;4;4;4;4;4;4;4;4;4;
                4;18;4;4;20; 14; 4;4;20; 22;14;24; 13;4;24;22;4; 26];
134         MinContDepth=100;
135         %except 15/115 23/105 29/140 30/150 31/140 33/185 41/150
               55/200
136         s2 = '\Ib';
137         s4 = '_000_DYN.txt';
138
139
140         %%%%%%%%%%% INTERBONE %%%%%%%%%%%
141     case 'InterBone\1'
142         Check_all_file=1;
143         Number=17;
144         BeginTime = [4; 4; 4; 4; 4;  4; 4; 4; 4; 4;  4; 4; 4; 24; 6;
                26; 4] ;
145         MinContDepth=80;
146         s2 = '\ib';
147         s4 = '_000_DYN.txt';
148
149     case 'InterBone\2'
150         Check_all_file=1;
151         Number=32;
152         BeginTime = [4;4;4;4;4; 4;4;4;4;4; 4;4;4;4;4; 4;4;4;4;4;
               4;4;4;4;4; 4;4;4;4;4; 4;4;4;4;4; 4;4;4;4;4; 4;4;4;4;4;
               4;4;4;4;4; 4;4;4;4;4; 4;4;4;4;4; 4;4;4;4;4; 4;4;4;4;4;
               4;4;4;4;4; 4;4;4;4;4; 4;4;4;4;4; 4;4;4;4;4; 4;4;4;4;4;
               4;4;4;4;4; 4;4;4;4;4; 4;4;4;4;4; 4;4;4;4;4; 4;4;4;4;4;
               4;4;4;4;4;];
153         MinContDepth=100;
154         %except 9/130 10/120 11/110 12/160 13/130 14/115 15/160
               16/140
155         %17/140 20/130 21/125 22/130 23/130 24/130 25/140 28/120
               30&31/115
156         s2 = '\Ic';
```

```
157         s4 = '_000_DYN.txt';
158
159 end
160 %%%%%%%%%%%%%%%%%%%%%%%%%%%%%%%% END PARAMETERS TO SET
        %%%%%%%%%%%%%%%%%%%%%%%%%%%%%%%%
161
162 b=1; % Variable to create new matrix of filtered data
163 if (Check_all_file==1)
164     Fichier=1:Number;
165 end
166 for j=1:size(Fichier,2)
167     Num_Fichier=Fichier(j);
168     %%%%%%%%%%%%%%%%%%%%%%%%%%%%%%%% OPEN FILE
            %%%%%%%%%%%%%%%%%%%%%%%%%%%%%%%%
169     input_file = strcat(s1,Sample,s2,num2str(Num_Fichier),s4);
170     fid=fopen(input_file,'r');
171     fgetl(fid);fgetl(fid);fgetl(fid);
172     data = fscanf(fid,'%f',[25 inf]);
173     fclose(fid);
174
175     %%%%%%%%%%%%%%%% Remove data of wrong time & contact depth
            %%%%%%%%%%%%%%%%
176     for i = 1:size(data,2)
177         %if(data(25,i)>=MinContDepth && data(1,i)>BeginTime(j))
178         if(data(25,i)>=MinContDepth && data(1,i)>BeginTime(j))
179             if( strcmp(Region,'Interface') && strcmp(Set,'\2') &&
                    Num_Fichier==24 && data(25,i)>=140)
180                 continue
181             elseif ( strcmp(Region,'Interface') && strcmp(Set,'\2')
                    && Num_Fichier==27 && data(25,i)>=120)
182                 continue
183             elseif ( strcmp(Region,'Interface') && strcmp(Set,'\3')
                    && Num_Fichier==15 && data(25,i)>=115)
184                 continue
185             elseif ( strcmp(Region,'Interface') && strcmp(Set,'\3')
                    && Num_Fichier==23 && data(25,i)>=105)
186                 continue
187             elseif ( strcmp(Region,'Interface') && strcmp(Set,'\3')
                    && Num_Fichier==29 && data(25,i)>=140)
188                 continue
189             elseif ( strcmp(Region,'Interface') && strcmp(Set,'\3')
                    && Num_Fichier==30 && data(25,i)>=150)
```

```
190                 continue
191             elseif ( strcmp(Region,'Interface') && strcmp(Set,'\3')
                    && Num_Fichier==31 && data(25,i)>=140)
192                 continue
193             elseif ( strcmp(Region,'Interface') && strcmp(Set,'\3')
                    && Num_Fichier==33 && data(25,i)>=185)
194                 continue
195             elseif ( strcmp(Region,'Interface') && strcmp(Set,'\3')
                    && Num_Fichier==41 && data(25,i)>=150)
196                 continue
197             elseif ( strcmp(Region,'Interface') && strcmp(Set,'\3')
                    && Num_Fichier==55 && data(25,i)>=200)
198                 continue
199             elseif ( strcmp(Region,'InterBone') && strcmp(Set,'\2')
                    && Num_Fichier==9 && data(25,i)>=130)
200                 continue
201             elseif ( strcmp(Region,'InterBone') && strcmp(Set,'\2')
                    && Num_Fichier==10 && data(25,i)>=120)
202                 continue
203             elseif ( strcmp(Region,'InterBone') && strcmp(Set,'\2')
                    && Num_Fichier==11 && data(25,i)>=110)
204                 continue
205             elseif ( strcmp(Region,'InterBone') && strcmp(Set,'\2')
                    && Num_Fichier==12 && data(25,i)>=160)
206                 continue
207             elseif ( strcmp(Region,'InterBone') && strcmp(Set,'\2')
                    && Num_Fichier==13 && data(25,i)>=130)
208                 continue
209             elseif ( strcmp(Region,'InterBone') && strcmp(Set,'\2')
                    && Num_Fichier==14 && data(25,i)>=115)
210                 continue
211             elseif ( strcmp(Region,'InterBone') && strcmp(Set,'\2')
                    && Num_Fichier==15 && data(25,i)>=160)
212                 continue
213             elseif ( strcmp(Region,'InterBone') && strcmp(Set,'\2')
                    && Num_Fichier==16 && data(25,i)>=140)
214                 continue
215             elseif ( strcmp(Region,'InterBone') && strcmp(Set,'\2')
                    && Num_Fichier==17 && data(25,i)>=140)
216                 continue
217             elseif ( strcmp(Region,'InterBone') && strcmp(Set,'\2')
                    && Num_Fichier==20 && data(25,i)>=130)
```

```
218                     continue
219                 elseif ( strcmp(Region,'InterBone') && strcmp(Set,'\2')
                       && Num_Fichier==21 && data(25,i)>=125)
220                     continue
221                 elseif ( strcmp(Region,'InterBone') && strcmp(Set,'\2')
                       && Num_Fichier==22 && data(25,i)>=130)
222                     continue
223                 elseif ( strcmp(Region,'InterBone') && strcmp(Set,'\2')
                       && Num_Fichier==23 && data(25,i)>=130)
224                     continue
225                 elseif ( strcmp(Region,'InterBone') && strcmp(Set,'\2')
                       && Num_Fichier==24 && data(25,i)>=130)
226                     continue
227                 elseif ( strcmp(Region,'InterBone') && strcmp(Set,'\2')
                       && Num_Fichier==25 && data(25,i)>=140)
228                     continue
229                 elseif ( strcmp(Region,'InterBone') && strcmp(Set,'\2')
                       && Num_Fichier==28 && data(25,i)>=120)
230                     continue
231                 elseif ( strcmp(Region,'InterBone') && strcmp(Set,'\2')
                       && Num_Fichier==30 && data(25,i)>=115)
232                     continue
233                 elseif ( strcmp(Region,'InterBone') && strcmp(Set,'\2')
                       && Num_Fichier==31 && data(25,i)>=115)
234                     continue
235                 else
236                     datafiltred(:,b)=data(:,i);
237                     b = b+1;
238                 end
239             end
240         end
241     end
242
243
244 %%%%%%%%%%%%%%%%%%%%%%%%%%%%%%%% WANTED DATA %%%%%%%%%%%%%%%%%%%%%%%%%%%%%%%%
245 WorkData(1,:) = datafiltred(15,:); %Storage Modulus[Gpa]
246 WorkData(2,:) = datafiltred(16,:); %Loss Modulus[Gpa]
247 WorkData(3,:) = datafiltred(17,:); %Hardness{Gpa]
248 WorkData(4,:) = datafiltred(19,:); %TanDelta[/]
249 WorkData(5,:) = datafiltred(25,:); %ContactDepth[nm]
250
251 end
```

Listing C.4: PlotHisto.m

```
function PlotHisto( s1,Number_Figure,Values,Region,num_set,
    num_propertie,Save,dim,set_tot)
%PlotHisto Summary
%   Return values to plot histograms and means with option to save
    them
%
%   1)names for the title and save
%   2)Values for histogram
%   3)Values for mean + legend for it
%   4)Title (Title change if plot for 1 set or combinaison of all set
    )
%   5)Save

Properties={'Storage Modulus [GPA]';'Loss Modulus [GPA]';'Hardeness [
    GPA]';'Tan-\delta [/]'};
File_Properties={'StorM';'LossM';'Hard';'Tan'};

figure(Number_Figure)
Center=squeeze(Values(num_set,num_propertie,:,2));
N=squeeze(Values(num_set,num_propertie,:,1))/sum(Values(num_set,
    num_propertie,:,1));
bar(Center, N)
S=std(N.*Center);
hold on
m1 = sum(N.*Center);
plot([m1 m1],ylim)
an = strcat('mean =',{' '},num2str(m1));
no = strcat('std =',{' '},num2str(S));
anno={char(an),char(no)};
annotation('textbox',dim,'String',anno,'FitBoxToText','on');

% if (set_tot)
% title(strcat(Properties{num_propertie},{' '},'set total',{' '},
    Region))
% else
% title(strcat(Properties{num_propertie},{' '},'set',{' '},num2str(
    num_set),{' '},Region))
% end
xlabel(Properties{num_propertie})
ylabel('Frequency [%]')
set(gca,'FontSize',16);
```

```
35
36 if (Save=='y')
37     if(set_tot)
38     saveas(gcf,strcat(s1,Region,'\',File_Properties{num_propertie},'_
           ', Region,'_TotalSet.png'))
39     else
40     saveas(gcf,strcat(s1,Region,'\',num2str(num_set),'\',
           File_Properties{num_propertie},'_', Region,'.png'))
41     end
42 end
43 end
```

Listing C.5: PlotLine.m

```
1 function PlotLine( Number_Figure,Values,Region,num_set,num_propertie,
      Save,set_tot )
2 %PlotLine Summary
3 %   Return values to plot Linear histogram with option to save them
4 %
5 %   1)names for the title and save
6 %   2)Values for graph
7 %   3)Title
8 %   4)Save
9
10 Properties={'Storage Modulus [GPA]';'Loss Modulus [GPA]';'Hardeness [
      GPA]';'Tan-\delta [/]'};
11 File_Properties={'StorM';'LossM';'Hard';'Tan'};
12
13 figure(Number_Figure)
14 Center=squeeze(Values(num_set,num_propertie,:,2));
15 N=squeeze(Values(num_set,num_propertie,:,1))/sum(Values(num_set,
      num_propertie,:,1));
16 plot(Center,N)
17
18 if (set_tot)
19 title(strcat(Properties{num_propertie},{' '},'set total',{' '},Region
      ))
20 else
21 title(strcat(Properties{num_propertie},{' '},'set',{' '},num2str(
      num_set),{' '},Region))
22 end
23 xlabel(Properties{num_propertie})
24 ylabel('Frequency [%]')
25 set(gca,'FontSize',16);
```

```
26 if (Save)
27     if(set_tot)
28     saveas(gcf,strcat(s1,Region{1},'\Linear_',File_Properties{
           num_properties},'_', Region,'.png'))
29     else
30     saveas(gcf,strcat(s1,Region{1},'\Linear_',num_set,'\',
           File_Properties{num_properties},'_', Region,'.png'))
31     end
32 end
33
34 end
```

Listing C.6: SinglePoint.m

```
1  clear all;
2  close all;
3  clc;
4
5  %Filtred_data Summary
6  %   Extract data from Txt files by Set of sample with the right
       parameters
7  %
8  %   1)Case by set of data: Bone, Cartilage, Tendon then Interface
9  %   case EXAMPLE
10 %         Number=11; Total number of files in this set
11 %         Check_all_file=0; 1=all data 0=some of the data
12 %         Fichier=[2;4;6;7;10]; If Not all data, these ones
13 %         BeginTime = [4;4;4;4;4]; %[s] Beginning time for each file
14 %         MinContDepth=80; %[nm] Minimum contact depth to keep
15 %         s2 = '\Bone';      s2 and s4 to have the right path access
16 %         s4 = '_000_DYN.txt';
17 %
18 %   2)Open and read a single point
19 %   3)Filter the data with BeginTime and MinContDepth
20 %   4)plot the wanted data
21
22 Region='Bone'; %Region of indentation
23 Set='\1'; %Set of samples of Interest
24 S=1;
25 nbins=20;
26 Sample= strcat(Region,Set)
27 s1='C:\Users\Une petite bretzelle\Dropbox (ChaBen)\TFE\5-NANO\
       DMA_Text_Files+Matlab\'; %begin of access path
28 NT=11;
```

```
29 legend_string = cell(NT,1);
30
31 %%
32     %%%%%%%%%%%%%%%%%%%%%%%%%%%%%%%% PARAMETERS TO SET
           %%%%%%%%%%%%%%%%%%%%%%%%%%%%%%%%
33 switch Sample
34     %%%%%%%%%%% BONE %%%%%%%%%%%
35     case 'Bone\1'
36         Check_all_file=1;
37         Number=11;
38         BeginTime = [4;4;4;4;4;4;4;4;4;4;4]; %[s] Beginning time for
               each file
39         MinContDepth=70; %[nm] Minimum contact depth to keep
40         s2 = '\ba';
41         s4 = '_000_DYN.txt';
42
43     case 'Bone\2'
44         Check_all_file=1;
45         Number=11;
46         BeginTime = [4;4;4;4;4;4;4;4;4;4;4]; %[s] Beginning time for
               each file
47         MinContDepth=70; %[nm] Minimum contact depth to keep
48         s2 = '\bb';
49         s4 = '_000_DYN.txt';
50
51     case 'Bone\3'
52         Check_all_file=1;
53         Number=12;
54         BeginTime = [4;4;4;4;4;4;4;4;4;4;4;4] ; %[s] Beginning time
               for each file
55         MinContDepth=60; %[nm] Minimum contact depth to keep
56         s2 = '\ba';
57         s4 = '_000_DYN.txt';
58
59     case 'Bone\4'
60         Check_all_file=1;
61         Number=12;
62         BeginTime = [4;4;4;4;4;4;4;4;4;4;4;4]; %[s] Beginning time
               for each file
63         MinContDepth=80; %[nm] Minimum contact depth to keep
64         s2 = '\bb';
65         s4 = '_000_DYN.txt';
```

```
66
67
68          %%%%%%%%%%% CARTILAGE %%%%%%%%%%%
69      case 'Cartilage\1'
70          Check_all_file=1;
71          Number=11;
72          BeginTime = [4;4;4;4;4;4;4;4;4;4;4];
73          MinContDepth=80;
74          s2 = '\ca';
75          s4 = '_000_DYN.txt';
76
77      case 'Cartilage\2'
78          Check_all_file=0;
79          Fichier=[1,2,3,4,5,6,8,9,10];
80          Number=11;
81          BeginTime = [4;4;4;4;4;4;4;4;4;4;4];
82          MinContDepth=80;
83          s2 = '\cb';
84          s4 = '_000_DYN.txt';
85
86      case 'Cartilage\3'
87          Check_all_file=1;
88          Number=11;
89          BeginTime = [4;4;4;4;4;4;4;4;4;4;4];
90          MinContDepth=100;
91          s2 = '\ca';
92          s4 = '_000.tdm_DYN.txt';
93
94
95          %%%%%%%%%%% TENDON %%%%%%%%%%%
96      case 'Tendon\1'
97          %           Check_all_file=1;
98          %           Number=11;
99          %           BeginTime = [20;4;4;4;30;33;30;13;4;4;4];
100         %           MinContDepth=120;
101         %           s2 = '\ta'; s4 = '_000_DYN.txt';
102
103         Check_all_file=0;
104         Fichier=[1,2,3,4,8,9,10,11];
105         Number=11;
106         BeginTime = [20;4;4;4;13;4;4;4];
107         MinContDepth=120;
```

```
108         s2 = '\ta'; s4 = '_000_DYN.txt';
109         %
110     case 'Tendon\2'
111         %           Check_all_file=1;
112         %           Number=11;
113         %           BeginTime = [4;23;4;4;4;4;25;4;4;14;26] ;
114         %           MinContDepth=200;
115         %           s2 = '\tb'; s4 = '_000_DYN.txt';
116
117         Check_all_file=0;
118         Fichier=[1,2,3,4,5,6,7,8,9,10];
119         Number=11;
120         BeginTime = [4;23;4;4;4;4;25;4;4;14] ;
121         MinContDepth=200;
122         s2 = '\tb'; s4 = '_000_DYN.txt';
123
124     case 'Tendon\3'
125         Check_all_file=1;
126         Number=12;
127         BeginTime = [4;4;4;4;4;4;4;4;4;4;4;4] ;
128         MinContDepth=115;
129         s2 = '\ta'; s4 = '_000.tdm_DYN.txt';
130
131
132         %%%%%%%%%%% INTERFACE %%%%%%%%%%%
133     case 'Interface\1'
134         %           Check_all_file=1;
135         %           Number=29;
136         %           BeginTime = [4;4;4;4;4;4;4;4;4;4;
                4;4;4;4;4;4;4;4;4;4; 4;12;22;22;20;4;26;26;26];
137         %           MinContDepth=100;
138         %           s2 = '\Ia';
139         %           s4 = '_000_DYN.txt';
140
141         Check_all_file=0;
142         Fichier=[1,2,3,4,5,6,7,8,9,10, 11,12,13,14,15,16,17,18,19,20,
                21,22,23,24,25,26];
143         Number=29;
144         BeginTime = [4;4;4;4;4;4;4;4;4;4; 4;4;4;4;4;4;4;4;4;4;
                4;12;22;22;20;4];
145         MinContDepth=100;
146         s2 = '\Ia';
```

```
147         s4 = '_000_DYN.txt';
148
149     case 'Interface\2'
150         Check_all_file=1;
151         Number=40;
152         BeginTime = [4;4;4;4;4; 4;4;4;4;4; 4;4;4;4;4; 4;4;4;4;4;
                4;4;4;4;4; 4;4;4;4;4; 4;4;4;4;4; 4;4;4;4;4;] ;
153         MinContDepth=100;
154         %except 24/140 27/120
155         s2 = '\ia';
156         s4 = '_000_DYN.txt';
157
158     case 'Interface\3'
159
160         Check_all_file=0;
161         Number=65;
162         %BeginTime =
                [4;4;4;4;4;4;4;4;4;4;4;4;4;4;4;4;4;4;4;4;4;4;4;4;4;4;4;4;4;
                 4;18;4;4;20; 26;32;14;26;26; 4;4;20;26;26;
                26;26;22;14;24; 13;4;24;22;4; 26;26;25;26;26;
                26;26;26;26;30];
163         %if check=0
164         Fichier=[1,2,3,4,5,6,7,8,9,10, 11,12,13,14,15,16,17,18,19,20,
                 21,22,23,24,25,26,27,28,29,30, 31,32,33,34,35,38,
                41,42,43,48,49,50, 51,52,53,54,55,58] ;
165         BeginTime =
                [4;4;4;4;4;4;4;4;4;4;4;4;4;4;4;4;4;4;4;4;4;4;4;4;4;4;4;4;4;
                 4;18;4;4;20; 14; 4;4;20; 22;14;24; 13;4;24;22;4; 26];
166         MinContDepth=100;
167         %except 15/115 23/105 29/140 30/150 31/140 33/185 41/150
                55/200
168         s2 = '\Ib';
169         s4 = '_000_DYN.txt';
170
171         %%%%%%%%%%% INTERBONE %%%%%%%%%%%
172     case 'InterBone\1'
173         Check_all_file=1;
174         Number=17;
175         BeginTime = [4; 4; 4; 4; 4;  4; 4; 4; 4; 4;  4; 4; 4; 24; 6;
                 26; 4] ;
176         MinContDepth=80;
177         s2 = '\ib';
```

```
178         s4 = '_000_DYN.txt';
179
180     case 'InterBone\2'
181         Check_all_file=1;
182         Number=32;
183         BeginTime = [4;4;4;4;4; 4;4;4;4;4; 4;4;4;4;4; 4;4;4;4;4;
                4;4;4;4;4; 4;4;4;4;4; 4;4;4;4;4; 4;4;4;4;4; 4;4;4;4;4;
                4;4;4;4;4; 4;4;4;4;4; 4;4;4;4;4; 4;4;4;4;4; 4;4;4;4;4;
                4;4;4;4;4; 4;4;4;4;4; 4;4;4;4;4; 4;4;4;4;4; 4;4;4;4;4;
                4;4;4;4;4; 4;4;4;4;4; 4;4;4;4;4; 4;4;4;4;4; 4;4;4;4;4;
                4;4;4;4;4;];
184         MinContDepth=100;
185         %except 9/130 10/120 11/110 12/160 13/130 14/115 15/160
                16/140
186         %17/140 20/130 21/125 22/130 23/130 24/130 25/140 28/120
                30&31/115
187         s2 = '\Ic';
188         s4 = '_000_DYN.txt';
189
190 end
191 %%
192 if (Check_all_file==1)
193     Fichier=1:Number;
194 end
195 for j=1:size(Fichier,2)
196     Num_Fichier=Fichier(j);
197     for f=1:1:NT
198         b=1;% Variable to create new matrix of filtered data
199         datafiltred=[];
200         if(Num_Fichier==f) %%%%%%%%%%%% OUVRIR 1 FICHIER %%%%%%%%%%%%
201             f
202             %%%%%%%%%%%%%%%%%%%%%%%%%%%%%%%%%% OPEN FILE
                    %%%%%%%%%%%%%%%%%%%%%%%%%%%%%%%%%%
203             s3 = num2str(Num_Fichier);
204             input_file = strcat(s1,Sample,s2,s3,s4);
205             fid=fopen(input_file,'r');
206             fgetl(fid);fgetl(fid);fgetl(fid);
207             data = fscanf(fid,'%f',[25 inf]);
208             fclose(fid);
209
210             %%%%%%%%%%%%%%%% Remove data of wrong time & contact depth
                    %%%%%%%%%%%%%%%%%%
```

```
211             for i = 1:size(data,2)
212                 if(data(25,i)>=MinContDepth && data(1,i)>BeginTime(j)
                        )
213                     if( strcmp(Region,'Interface') && strcmp(Set,'\2'
                            ) && Num_Fichier==24 && data(25,i)<=140)
214                         continue %sort de la boucle!!
215                     elseif ( strcmp(Region,'Interface') && strcmp(Set
                            ,'\2') && Num_Fichier==27 && data(25,i)<=120)
216                         continue
217                     elseif ( strcmp(Region,'Interface') && strcmp(Set
                            ,'\3') && Num_Fichier==15 && data(25,i)<=115)
218                         continue
219                     elseif ( strcmp(Region,'Interface') && strcmp(Set
                            ,'\3') && Num_Fichier==23 && data(25,i)<=105)
220                         continue
221                     elseif ( strcmp(Region,'Interface') && strcmp(Set
                            ,'\3') && Num_Fichier==29 && data(25,i)<=140)
222                         continue
223                     elseif ( strcmp(Region,'Interface') && strcmp(Set
                            ,'\3') && Num_Fichier==30 && data(25,i)<=150)
224                         continue
225                     elseif ( strcmp(Region,'Interface') && strcmp(Set
                            ,'\3') && Num_Fichier==31 && data(25,i)<=140)
226                         continue
227                     elseif ( strcmp(Region,'Interface') && strcmp(Set
                            ,'\3') && Num_Fichier==33 && data(25,i)<=185)
228                         continue
229                     elseif ( strcmp(Region,'Interface') && strcmp(Set
                            ,'\3') && Num_Fichier==41 && data(25,i)<=150)
230                         continue
231                     elseif ( strcmp(Region,'Interface') && strcmp(Set
                            ,'\3') && Num_Fichier==55 && data(25,i)<=200)
232                         continue
233                     elseif ( strcmp(Region,'InterBone') && strcmp(Set
                            ,'\2') && Num_Fichier==9 && data(25,i)<=130)
234                         continue
235                     elseif ( strcmp(Region,'InterBone') && strcmp(Set
                            ,'\2') && Num_Fichier==10 && data(25,i)<=120)
236                         continue
237                     elseif ( strcmp(Region,'InterBone') && strcmp(Set
                            ,'\2') && Num_Fichier==11 && data(25,i)<=110)
238                         continue
```

```
239                 elseif ( strcmp(Region,'InterBone') && strcmp(Set
                        ,'\2') && Num_Fichier==12 && data(25,i)<=160)
240                     continue
241                 elseif ( strcmp(Region,'InterBone') && strcmp(Set
                        ,'\2') && Num_Fichier==13 && data(25,i)<=130)
242                     continue
243                 elseif ( strcmp(Region,'InterBone') && strcmp(Set
                        ,'\2') && Num_Fichier==14 && data(25,i)<=115)
244                     continue
245                 elseif ( strcmp(Region,'InterBone') && strcmp(Set
                        ,'\2') && Num_Fichier==15 && data(25,i)<=160)
246                     continue
247                 elseif ( strcmp(Region,'InterBone') && strcmp(Set
                        ,'\2') && Num_Fichier==16 && data(25,i)<=140)
248                     continue
249                 elseif ( strcmp(Region,'InterBone') && strcmp(Set
                        ,'\2') && Num_Fichier==17 && data(25,i)<=140)
250                     continue
251                 elseif ( strcmp(Region,'InterBone') && strcmp(Set
                        ,'\2') && Num_Fichier==20 && data(25,i)<=130)
252                     continue
253                 elseif ( strcmp(Region,'InterBone') && strcmp(Set
                        ,'\2') && Num_Fichier==21 && data(25,i)<=125)
254                     continue
255                 elseif ( strcmp(Region,'InterBone') && strcmp(Set
                        ,'\2') && Num_Fichier==22 && data(25,i)<=130)
256                     continue
257                 elseif ( strcmp(Region,'InterBone') && strcmp(Set
                        ,'\2') && Num_Fichier==23 && data(25,i)<=130)
258                     continue
259                 elseif ( strcmp(Region,'InterBone') && strcmp(Set
                        ,'\2') && Num_Fichier==24 && data(25,i)<=130)
260                     continue
261                 elseif ( strcmp(Region,'InterBone') && strcmp(Set
                        ,'\2') && Num_Fichier==25 && data(25,i)<=140)
262                     continue
263                 elseif ( strcmp(Region,'InterBone') && strcmp(Set
                        ,'\2') && Num_Fichier==28 && data(25,i)<=120)
264                     continue
265                 elseif ( strcmp(Region,'InterBone') && strcmp(Set
                        ,'\2') && Num_Fichier==30 && data(25,i)<=115)
266                     continue
```

```
267                         elseif ( strcmp(Region,'InterBone') && strcmp(Set
                                ,'\2') && Num_Fichier==31 && data(25,i)<=115)
268                             continue
269                         else
270                             datafiltred(:,b)=data(:,i);
271                             b = b+1;
272                         end
273                     end
274                 end
275             else continue
276             end
277
278
279             %%%%%%%%%%%%%%%%%%%%%%%%%%%%%%%% WANTED DATA
                    %%%%%%%%%%%%%%%%%%%%%%%%%%%%%%%%
280             Time = datafiltred(1,:); %[s]
281             Depth = datafiltred(25,:); %Contact Depth [nm]
282             StorMod = datafiltred(15,:); %Storage Modulus[Gpa]
283             LossMod = datafiltred(16,:); %Loss Modulus[Gpa]
284             Hardness = datafiltred(17,:); %[Gpa]
285             TanDelta = datafiltred(19,:); %[/]
286             DisplAmp = datafiltred(9,:); %[nm]
287
288 %%
289 % figure(1)
290 %
291 % %hold on
292 % plot(Depth,StorMod);
293 % ylabel('Storage Modulus [GPa]')
294 % xlabel('Depth penetration [nm]')
295 % grid on
296 % % axis([0 3100 0 12]);
297 % % set(gca, 'xtick', [0000:400:2000],'ytick', [0:4:32],'FontSize
        ',16);
298 % set(gca, 'FontSize',16);
299 % %legend_string{f}=num2str(f);
300 % saveas(gcf,strcat(s1,Sample,'\Depth\',Region,num2str(S),'StorM','F
        ',s3,'.png'))
301
302 % figure(2)
303 % %hold on
304 % plot(Depth,TanDelta);
```

```
% ylabel('Tan Delta [\]')
% xlabel('Depth penetration [nm]')
% grid on
% axis([0 650 0 0.1]);
%%       %axis([0 2000 0.02 0.08]);
%%       %   set(gca, 'xtick', [00:400:2000],'ytick',
    [0.02:0.02:0.08],'FontSize',16);
% set(gca, 'FontSize',16);
% saveas(gcf,strcat(s1,Sample,'\Depth\',Region,num2str(S),'Tan','F',
    s3,'.png'))
%%
% figure(1)
%
% dim = [0.15 0.6 0.3 0.3];
% StorM_h = histogram(StorMod,nbins,'Normalization','probability');
% Std1=std(StorMod);
% hold on
% m1 = mean(StorMod);
% plot([m1 m1], ylim)
% an = strcat('mean =',{' '},num2str(m1));
% no = strcat('std =',{' '},num2str(Std1));
% anno={char(an),char(no)};
% annotation('textbox',dim,'String',anno,'FitBoxToText','on');
% xlabel('Storage Modulus [GPa]')
% ylabel('Frequency [%]')
% set(gca,'FontSize',16);
%
% saveas(gcf,strcat(s1,Sample,'\PrByFile\',Region,num2str(S),'ST-F',
    s3,'.png'))
%
% figure(2)
% dim = [0.8 0.6 0.3 0.3];
% TanDelta_h = histogram(TanDelta,nbins,'Normalization','probability
    ');
% %ylim([0 0.15]);
% hold on
% m4 = mean(TanDelta);
% plot([m4 m4], ylim)
% Std4=std(TanDelta);
% an = strcat('mean =',{' '},num2str(m4));
% no = strcat('std =',{' '},num2str(Std4));
% anno={char(an),char(no)};
```

```
343 % annotation('textbox',dim,'String',anno,'FitBoxToText','on');title(
    strcat('Tan-\delta',{' '},Region))
344 % xlabel('Tan-\delta [/]')
345 % ylabel('Frequency [%]')
346 % set(gca,'FontSize',16);
347 %
348 % saveas(gcf,strcat(s1,Sample,'\PrByFile\',Region,num2str(S),'T-F',s3
    ,'.png'))
349
350  %%
351 %           figure(1)
352 %           subplot(2,2,1)
353 %           dim = [0.15  0.6  0.3  0.3];
354 %           StorM_h = histogram(StorMod,nbins,'Normalization','
    probability');
355 %           Std1=std(StorMod);
356 %           hold on
357 %           m1 = mean(StorMod);
358 %           plot([m1 m1], ylim)
359 %
360 %           an = strcat('mean =',{' '},num2str(m1));
361 %           no = strcat('std =',{' '},num2str(Std1));
362 %           anno={char(an),char(no)};
363 %           annotation('textbox',dim,'String',anno,'FitBoxToText','on')
    ;
364 %
365 %           MeanStorM(f)=round(m1,4);
366 %           STD1StorM(f)=round(Std1,4);
367 %
368 %          %annotation('textbox',dim,'String',strcat('mean =',{' '},
    num2str(m1)),'FitBoxToText','on');
369 %           title(strcat('Storage Modulus',{' '},Region,Set,{' '},
    num2str(f)))
370 %           xlabel('Storage Modulus [GPa]')
371 %           ylabel('Frequency [%]')
372 %
373 %           subplot(2,2,2)
374 %           dim = [0.8  0.6  0.3  0.3];
375 %           TanDelta_h = histogram(TanDelta,nbins,'Normalization','
    probability');
376 %          %ylim([0  0.15]);
377 %           hold on
```

```
378 %           m4 = mean(TanDelta);
379 %           plot([m4 m4], ylim)
380 %           Std4=std(TanDelta);
381 %           an = strcat('mean =',{' '},num2str(m4));
382 %           no = strcat('std =',{' '},num2str(Std4));
383 %           anno={char(an),char(no)};
384 %           annotation('textbox',dim,'String',anno,'FitBoxToText','on')
    ;title(strcat('Tan-\delta',{' '},Region))
385 %           xlabel('Tan-\delta [/]')
386 %           ylabel('Frequency [%]')
387 %
388 %           MeanTan(f)=round(m4,4);
389 %           STDTan(f)=round(Std4,4);
390 %
391 %           subplot(2,2,3)
392 %           dim = [0.15 0.12 0.3 0.3];
393 %           LossMod_h = histogram(LossMod,nbins,'Normalization','
    probability');
394 %           %ylim([0 0.15]);
395 %           hold on
396 %           m2 = mean(LossMod);
397 %           plot([m2 m2], ylim)
398 %           Std2=std(LossMod);
399 %           an = strcat('mean =',{' '},num2str(m2));
400 %           no = strcat('std =',{' '},num2str(Std2));
401 %           anno={char(an),char(no)};
402 %           annotation('textbox',dim,'String',anno,'FitBoxToText','on')
    ;
403 %           title(strcat('Loss Modulus',{' '},Region))
404 %           xlabel('Loss Modulus [GPa]')
405 %           ylabel('Frequency [%]')
406 %
407 %           subplot(2,2,4)
408 %           dim = [0.8 0.12 0.3 0.3];
409 %           Hardness_h = histogram(Hardness,nbins,'Normalization','
    probability');
410 %           %xlim([0.7 1.2]);
411 %           hold on
412 %           m3 = mean(Hardness);
413 %           plot([m3 m3], ylim)
414 %           Std3=std(Hardness);
415 %           an = strcat('mean =',{' '},num2str(m3));
```

```
416 %           no = strcat('std =',{' '},num2str(Std3));
417 %           anno={char(an),char(no)};
418 %           annotation('textbox',dim,'String',anno,'FitBoxToText','on')
    ;
419 %           title(strcat('Hardeness',{' '}, Region))
420 %           xlabel('Hardeness [GPa]')
421 %           ylabel('Frequency [%]')
422 %
423           %saveas(gcf,strcat(s1,Sample,'\PrByFile\',Region,'Set',
                num2str(S),'F',s3,'.png'))
424
425       end
426     close all
427 end
428 %legend(legend_string(~cellfun('isempty',legend_string)));
```

Surgical kit and microscope used in histology

Figure C.1: Surgical Kit

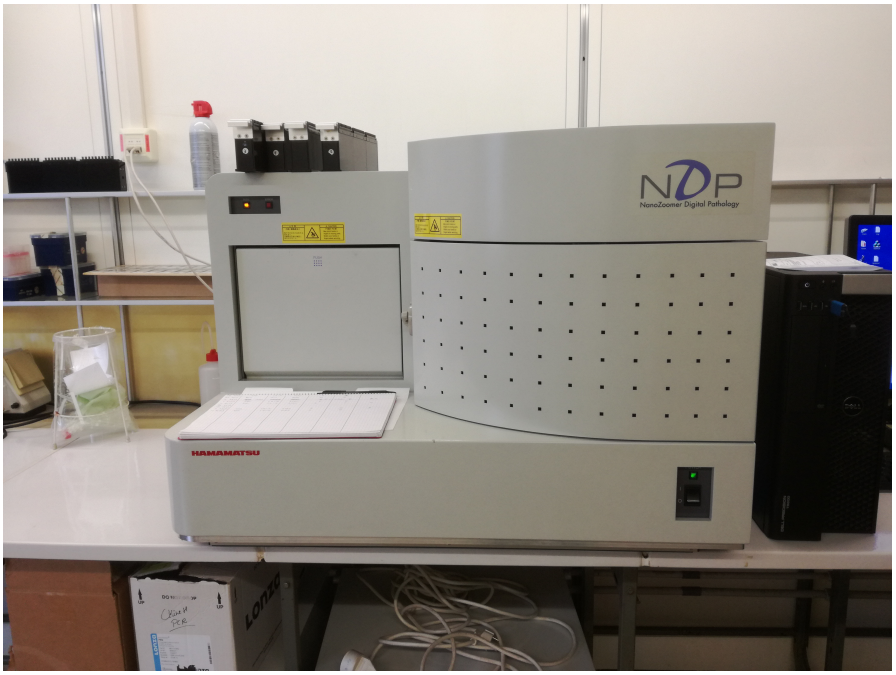

Figure C.2: microscope

Bibliography

[1] L. Rossetti. The microstructure and micromechanics of the tendon–bone insertion. *Nature Materials*, Feb 2017.

[2] D. Ruffoni. Biomechanics. University of Liège, 2016.

[3] Xiaojian Wang, Shanqing Xu, Shiwei Zhou, Wei Xu, M Leary, Peter Choong, Ma Qian, Milan Brandt, and Yi Xie. Topological design and additive manufacturing of porous metals for bone scaffolds and orthopaedic implants: A review. 83:127–141, Jan 2016.

[4] Ann Harvey, Mark Thompson, L E Cochlin, P A Raju, Z Cui, H R Cornell, Philippa Hulley, and Michael Brady. Functional imaging of tendon. 2009:1–11, Jan 2009.

[5] Csaba Matta and Róza Zákány. Calcium signalling in chondrogenesis: Implications for cartilage repair. S5:305–324, Jan 2013.

[6] Neri Thomas. Cartilage: Classification et histoire naturelle des lésions. Feb 2016. `http://orthopedie-lyon.fr/wp-content/uploads/2012/02/DIU-GENOU-2016-CARTILAGE-NERI.pdf`.

[7] M. Benjamin. The skeletal attachment of tendons—tendon 'entheses'. *Elsevier*, May 2022.

[8] Helen H. Lu. Functional attachment of soft tissues to bone: Development, healing, and tissue engineering. *Annu. Rev. Biomed. Eng. 2013*, Apr 2013.

[9] S Font Tellado. Strategies to engineer tendon/ligament-to-bone interface: Biomaterials, cells and growth factors. *Advances in pediatrics.*, Nov 2015.

[10] Yizhong Hu. Stochastic interdigitation as a toughening mechanism at the interface between tendon and bone. *Biophysical Journal*, 108:431–437, Jan 2015.

[11] Healthline Medical Team. Achilles tendon anatomy, origin function | body maps, Apr 2015. `https://www.healthline.com/human-body-maps/achilles-tendon#1`.

[12] M. Benjamin. The anatomy of the achilles tendon.

[13] Matthew Hoffman. Picture of the achilles tendon.

[14] S Milz. Three-dimensional reconstructions of the achilles tendon insertion in man. *Advances in pediatrics.*, Feb 2002.

[15] S.H.Chang. Comparison of mouse and human ankles and establishment of mouse ankle osteoarthritis models by surgically-induced instability. *ScienceDirect*, Nov 2015.

[16] Yusuke Hashimoto. Generation of tendon-to-bone interface "enthesis" with use of recombinant bmp-2 in a rabbit model. *Wiley InterScience*, jun 2047.

[17] Gillian Johnson Ming Zhang. A comparison between epoxy resin slices and histology sections in the study of spinal connective tissue structure. *J Int Soc Plastination*, 15(1), 2000.

[18] Emilie Velot, Nadia Messaddecq, Jean-Luc Weickert, Arnaud Bianchi, and Lydie Ventéo. Evaluation de différentes solutions de décalcification pour l'étude du cartilage : compatibilité avec les techniques d'histologie, d'immunohistochimie et d'hybridation in situ. *Rev Fr Histotechnol.*, pages 82–94, January 2011.

[19] Elvira Eivazova. Histology: Study of human tissue. *Encyclopedia of Applied Science*, pages 964–969, May 2012.

[20] Introduction to histology.

[21] Ronald F. Gibson. A review of recent research on nanoindentation of polymer composites and their constituents. *ScienceDirect*, Oct 2014. https://www.sciencedirect.com/science/article/pii/S0266353814003492?via=ihub.

[22] Christopher A.Schuh. Nanoindentation studies of materials. *ScienceDirect*, Apr 2006.

[23] L'équipe sf composites. Petit brief sur la resine epoxy. *Le blog de l'équipe SF*, Jun 2010. http://materiaux-composites.over-blog.com/article-petit-brief-sur-la-resine-epoxy-52709137.html.

[24] H S Gupta. Two different correlations between nanoindentation modulus and mineral content in the bone-cartilage interface. *Journal of structural biology.*, Feb 2005.

[25] H Isaksson. Precision of nanoindentation protocols for measurement of viscoelasticity in cortical and trabecular bone. *National Center for Biotechnology Information*, Aug 2010.

[26] J Y Rho. Mechanical properties and the hierarchical structure of bone. *National Center for Biotechnology Information*, Mar 1998.

[27] Eve Donnelly. Effects of surface roughness and maximum load on the mechanical properties of cancellous bone measured by nanoindentation. *National Center for Biotechnology Information*, May 2006.

[28] J Xu. Atomic force microscopy and nanoindentation characterization of human lamellar bone prepared by microtome sectioning and mechanical polishing technique. *National Center for Biotechnology Information*, Dec 2003.

[29] Werner A. Hofer. Theories of scanning probe microscopes at the atomic scale. *Reviews of Modern Physics*, Volume 75, 2003.

[30] Ondřej Jiroušek. Nanoindentation of human trabecular bone – tissue mechanical properties compared to standard engineering test methods. *Semantic Scholar*, 2012.

[31] W.C. Oliver. Measurement of hardness and elastic modulus by instrumented indentation: Advances in understanding and refinements to methodology. *Materials Research*, 19(1), Jan 2004.

[32] K.N. Hauch, M.L. Oyen, G.M. Odegard, and T. L. Haut Donahue. *National Center for Biotechnology Information*, Aug 2009.

[33] Igor Zlotnikov. Nano-scale modulus mapping of biological composite materials: Theory and practice. *ScienceDirect*, Mar 2017.

[34] Michele Casanova, Anna Balmelli, Davide Carnelli, Diana Courty, Philipp Schneider, and Ralph Müller. *National Center for Biotechnology Information*, Feb 2017.

[35] Siddhartha Pathak. Measuring the dynamic mechanical response of hydrated mouse bone by nanoindentation. *Journal of the Mechanical Behavior of Biomedical Materials*, Jan 2011.

[36] Dynamic mechanical analysis (dma), chapter 6 , note=`http://files.hanser.de/hanser/docs/20041012_2411215439-82_3-446-22673-7.pdf`.

[37] Sandrine Bec Jean-Luc Loubet Gaylord Guillonneau, Guillaume Kermouche. Determination of mechanical properties by nanoindentation independently of indentation depth measurement. *Journal of Materials Research, Cambridge University Press (CUP)*, 27(2551-2560), 2012.

[38] Jennifer Hay. Dynamic mechanical analysis (dma) of polymers by oscillatory indentation. *Nanomechanics, Inc*. http://nanomechanicsinc.com/wp/wp-content/uploads/2015/10/Report-01-2015-09-031.pdf.

[39] Erik Herbert, Warren Oliver, and G M Pharr. Nanoindentation and the dynamic characterization of viscoelastic solids. 41:074021, Mar 2008.

[40] Naiara Rodriguez-Florez. Insight into differences in nanoindentation properties of bone. *Journal of Mechanical Behavior and Biomedical Materials*, Sep 2012.

[41] Jiyu Sun. Quasi-static and dynamic nanoindentation of some selected biomaterials. *Journal of Bionic Engineering*, (11):144–150, 2014.

[42] Zaifeng Fan. Effects of viscoelasticity and time-dependent plasticity on nanoindentation measurements of human cortical bone. *Wiley Periodicals, Inc. J Biomed Mater Res*, (67), 2013.

[43] Junro Yamashita. The use of dynamic mechanical analysis to assess the viscoelastic properties of human cortical bone. *John Wiley Sons, Inc.*, 2000.

[44] C. C. WHITE. Viscoelastic characterization of polymers using instrumented indentation. ii. dynamic testing. *Journal of Polymer Science: Part B: Polymer Physics,*.

[45] A.K. Bembey. Hydration effects on the micro-mechanical properties of bone. *Materials Research*, 21(8):1962–1968, Aug 2006.

[46] Harrison Electropolishing. Ra rms:calculating surface roughness. http://www.harrisonep.com/electropolishing-ra.html.

[47] Unremodeled endochondral bone is a major architectural component of the cortical bone of the rat (rattus norvegicus). *Journal of Structural Biology*, (183):132–140, Apr 2013.

[48] Sebastián Jaramillo Isaza. Characterization of the mechanical and morphological properties of cortical bones by nanoindentation and atomic force microscopy. *Université de Technologie de Compiègne*, pages 126–137, 2014.

[49] Techniques de fixation et de décalcification en histologie. *iMedecin.com*. http://imedecin.com/Histologie/techniques-de-fixation-et-de-decalcification-en-histologie.htmlh2-decalcification.

[50] Geoffrey Rolls. An introduction to decalcification. *Leica Biosystems*, Apr 2013.

[51] Erik Mittra. The effects of embedding material, loading rate and magnitude, and penetration depth in nanoindentation of trabecular bone. *Wiley InterScience*, 2006.

[52] The role of water compartments in the material properties of cortical bone.

[53] Bozec L. Horton-M. A. Mesquidaz P. Wenger, M. P. E. Mechanical properties of collagen fibrils. *Biophys. J*, 2007.

[54] Raman faqs - what laser wavelengths are used for raman spectroscopy? http://www.horiba.com/scientific/products/raman-spectroscopy/raman-academy/raman-faqs/what-laser-wavelengths-are-used-for-raman-spectroscopy/.

[55] Is raman spectroscopy a reliable technique for cell death (structural damage)? 2015. `https://www.researchgate.net/post/Is_Raman_spectroscopy_a_reliable_technique_for_cell_death_structural_damage`.

[56] Paul I. Okagbare, Francis W. L. Esmonde-White, Steven A. Goldstein, and Michael D. Morris. Development of non-invasive raman spectroscopy for in-vivo evaluation of bone graft osseointegration in a rat model, Dec 2010.

[57] Jrobin. The raman spectra of metals. *Physics Forums - The Fusion of Science and Community*, May 2011.

[58] Andrea G. Schwartz, Jill D. Pasteris, Guy M. Genin, Tyrone L. Daulton, and Stavros Thomopoulos. Mineral distributions at the developing tendon enthesis. *PLOS Medicine*.